

An Experimental and Finite Element Study of the Fatigue Behaviors of Welded Armor Plate Joints

by

Daniel J. Sinnott II

A dissertation submitted in partial fulfillment
of the requirements for the degree of
Doctor of Philosophy
(Naval Architecture and Marine Engineering)
in The University of Michigan
2022

Doctoral Committee:

Professor Pingsha Dong, Co-Chair

Professor Nickolas Vlahopoulos, Co-Chair

Associate Professor Matthew Collette

Associate Professor Ann Jeffers

Daniel J. Sinnott II

sinnottd@umich.edu

ORCID iD: 0000-0002-7156-8504

© Daniel J. Sinnott II 2022

To my family, thank you for everything.

Acknowledgements

I would like to thank the Department of Defense SMART Scholarship for supporting this research for several years. SMART was especially supportive during the coronavirus pandemic, having been very considerate of not only my situation but also other scholars' situations by continuing to offer help and financial aid as necessary during 2020-2021. I'd also like to thank Naval Surface Warfare Center Philadelphia Division for the sponsorship, as well as Brandon Weiss, Branch Manager of Code 337 at NSWC PD for finding my SMART application and reaching out to me personally to discuss sponsorship at Philadelphia Division.

I would also like to personally thank my research advisors and dissertation committee co-chairs, Professor Pingsha Dong and Professor Nickolas Vlahopoulos. I am incredibly grateful for the opportunity to pursue this research, and I could not have accomplished anything without their frequent advice, guidance, and input. I'd also like to thank committee members Professor Matthew Collette and Professor Ann Jeffers, who have both been excellent references for some of the more specialized topics I've needed to cover during this research.

I would like to acknowledge the important role that the Automotive Research Center played in this research between the University of Michigan and the Ground Vehicle Systems Center. I'd also like to thank Martin McDonnell, Matthew Rogers, David Ostberg, and Ian Toppler for their direct assistance with working and testing at GVSC. All four of them likely become sick of seeing my emails, so I appreciate their patience and assistance over the past few years. Special thanks goes out to the other members of the Welded Structures Lab who

I've had the pleasure of working with at Michigan. Thanks to Shaopin Song, Fengchao Liu, Xianjun Pei, Sandipp Krishnan Ravi, Wenqing Zhou, Shizhu Xing, and Zetao Jin for their assistance and expertise over the years.

I also would like to thank my family, who have been supportive of all of my university studies for the nearly nine years I was in college. Whether I was fooling around overseas, moving across the country multiple times, burning through their grocery budget, living at their home(s), or making them watch my dog, my family has been fully supportive every step of my academic journey. Thank you very much, and I love you all dearly. I would also like to give a thank you to my friends in grad school at Michigan. Thanks to James Coller, Sam Edwards, Carly Mayhood, Sammi Meister, Matt Schirmann, Sam Taylordean, and Claire Wincott for the years of wonderful friendship, great advice, and much-needed support.

Table of Contents

Dedication	ii
Acknowledgements	iii
List of Figures	viii
List of Tables	xi
List of Abbreviations	xii
Abstract	xiii
CHAPTER 1 Introduction	1
CHAPTER 2 Background	3
2.1 Fatigue of Welded Joints	3
2.1.1 Crack Initiation vs. Crack Propagation	5
2.2 Cold-cracking in Armor Steel Welds	6
2.3 Effect of Material Selection	7
2.4 Stress Determination	7
2.5 Mesh Insensitive Structural Stress Method	8
2.5.1 Mesh Insensitive Structural Stress Method - Example	9
2.6 Master S-N Curve Applications	13
2.7 Research Approach	14
CHAPTER 3 Welded Armor Specimen Testing	16
3.1 Weld Wire Characterization	16
3.2 Equipment	17
3.3 Welded Specimens	18
3.4 Procedure	22
3.5 Test Plan	24
3.6 Completed Tests	26
CHAPTER 4 Finite Element Analysis	27
4.1 Strip Specimen Sketch Geometry	27
4.2 Nonlinear Analysis	28
4.3 Finite Element Modeling	30

4.4	Master S-N Curve Formulation	33
4.4.1	Stress Concentration Effect	33
4.4.2	Loading Mode Effect	35
4.4.3	Thickness Effect	35
CHAPTER 5 Analysis of Fatigue Test Strip Data		37
5.1	Applicability of Master S-N Curve Definition	37
5.2	Faulty Test Data	38
5.3	Strip Specimen S-N Curve	40
5.4	Trends	41
CHAPTER 6 Remote Research and Parametric Analysis of Test Strip Data		47
6.1	Analytic Methods	48
6.1.1	Linear Analytic Method	48
6.1.2	Nonlinear Analytic Method	52
6.2	Finite Element Model Refinement	55
6.2.1	Forced-Displacement Misalignment Test	59
6.2.2	Rigid Body Contact-to-Contact Clamping Method	61
6.3	Residual Stress Effects	64
6.4	Statistical Methods	67
6.4.1	Regression Analysis	68
6.4.2	Cox Proportional Hazards Model	70
6.4.3	Cox Proportional Hazards Model Results	71
6.5	Remote Research Conclusions	79
CHAPTER 7 Welded Armor Plate Testing		81
7.1	Plate Specimen Test Plan	81
7.2	Plate Specimen Procedure Adjustments	83
7.3	Finite Element Model Adjustments	87
7.3.1	Root-cracking Revisited	90
CHAPTER 8 Analysis of Fatigue Test Plate Data		98
8.1	Updated Master S-N Curve	98
8.2	Trends and Cox PH Results	100
8.2.1	Angular Deformation	100
8.2.2	Mismatch Ratio	100
8.2.3	Stainless vs. Non-stainless Weld Filament	102
8.2.4	Weld Filament Yield Strength	109
8.2.5	Base Material Yield Strength	112
CHAPTER 9 Observations and Conclusions		114
CHAPTER 10 Future Work		116
Appendix		118
A.1	Cox Proportional Hazards Model - Script	118

A.2	Cox Proportional Hazards Model - Function	121
A.3	Kruskal-Wallis - Script	140
A.4	Kruskal-Wallis - Function	144
	Bibliography	147

List of Figures

2.1	Examples of welded joint (a) heterogeneity, (b) residual stresses, (c) global discontinuity, (d) local discontinuity	4
2.2	Borrowed from [17] with permission: Through-thickness structural stress definition: (a) actual nonlinear stress distribution at weld toe; (b) structural stress or far-field stress in terms of through-thickness membrane and bending; (c) self-equilibrating notch stresses	10
2.3	Borrowed from [17] with permission: Structural stress calculation procedure in the mesh-insensitive method for an arbitrary curved weld using plate/shell element models	11
2.4	Borrow from [19] with permission: (a) T-joint geometry (b) four different meshes (c) Comparison of stress results between the four meshes	12
2.5	From [19]: Demonstration of effectiveness of equivalent structural stress parameter given in Equation 3	13
2.6	From [20]: (a) Comparison of fatigue lives for various joints based on weld material selection. (b) Finite element model used for the mesh-insensitive stress calculations	14
3.1	(a) Plan view of strip specimen; (b) Plan view of plate specimen; (c) Elevation view of both strip and plate specimen	20
3.2	(a) Strip specimen clamping area; (b) 2 1/2" Plate specimen clamping area; (c) 5" Plate clamping area; Note, the 5" plate has less than 50% contact area over the grip length. This is insufficient for fatigue testing.	21
3.3	Photograph of sketched strip geometry pre-testing	23
4.1	Angular deformation and eccentricity measurements in AutoCAD for two strips	28
4.2	Test D: Linear structural stresses vs nonlinear structural stresses	30
4.3	Clamping and Loading Conditions on a strip sample. Boundary conditions are in orange and blue while concentrated loads conditions are in yellow. . .	32
4.4	Abaqus screenshots showing one method of pulling nodal force outputs from the weld partition	34
5.1	Master S-N Curve Basis	38
5.2	Plotted Ferritic and Stainless Steel Mean and +/- 2 σ curves	38
5.3	Example of toe-cracking (a) vs. root-cracking (c). Note in (b) how the root-cracking case leads to an increased through-thickness fracture zone	39
5.4	The tested strip specimens plotted against the ferritic and stainless steel Master S-N Curve	41

5.5	Comparison of mismatch ratios	42
5.6	Comparison of angular deformation	43
5.7	Left: Stainless vs. non-stainless filler metals. Right: 46100 base metal with ER316LSi stainless and ER70S-6 non-stainless fillers	44
5.8	Left: Base metals of the fatigue tests. Right: 46100 and 12560 base metal tests both with ER70S-6 filler	45
6.1	Figure borrowed with permission from Dr. Xing’s paper [23] detailing an axially misaligned cruciform clamped joint. (a) dimensions and shape before clamping; (b) deformed shape after clamping.	49
6.2	Figure borrowed with permission from Dr. Xing’s paper [23] detailing an angularly deformed cruciform clamped joint. (a) dimensions and shape before clamping; (b) deformed shape after clamping.	49
6.3	Analytic results vs. the Master S-N curve results	51
6.4	AutoCAD sketches of various test strips before clamping and testing, note the lack of curvature on either side of the weld	52
6.5	Imaged borrowed from [24] with Dr. Zhou’s permission: Decomposition of complex angular deformations in butt-welded plate. (a) a general distortion shape; (b) global angular deformation component; (c) local angular deformation component	53
6.6	The linear analytic, nonlinear analytic, and Master S-N curve method results	54
6.7	Photograph of a clamped test specimen prior to testing. The red lines indicate vertical planes of the upper and lower (outer) edges while the cyan line indicates a midsection. Note how the sample appear to be clamped more than straight.	56
6.8	Top: A screenshot of the original clamping method using boundary conditions to displace the right (loaded) end. Bottom: A screenshot of the new rigid body clamping method, which forcibly displaces a simulated tester grip into the right end of the deformable strip model.	58
6.9	A screenshot of a two rigid clamp finite element model. The rigid body grips only need to exist as a surface, so they are modeled as just a line.	58
6.10	Upper left: Straight-alignment, single rigid grip. Upper right: Straight-alignment, double rigid grip. Lower left: 50% thickness misalignment, single rigid grip. Lower right: 50% thickness misalignment, double rigid grip. . . .	62
6.11	Welding residual stresses of an differing width 8mm thick steel cruciform joints at (a) the weld groove and (b) the weld root from Liang et al. [30] Note how the residual stresses continue to relax as the specimen width is reduced. . . .	65
6.12	Estimate of where the 2 1/2” wide plate specimens would fall on the Master S-N curve if they were fatigue tested at the same loads as the strip specimens.	66
6.13	Regression lines of best fit plotted against the logarithmic scatterplot data of the test strips.	68
6.14	MATLAB Scatterplot of Input Loads vs. Cycles to Failure for the Fatigue Tests	78
7.1	Flattening a plate specimen with a hydraulic press	85
7.2	A successfully flattened specimen	86

7.3	Screenshot of the simplified clamping condition. The left end is fixed in all three degrees of freedom on its grip contact surfaces. The right end does not need to be fixed, it only needs to be loaded at its contact surfaces.	88
7.4	AutoCAD screenshots showing examples of: (a) equivalent OAL between deformed and straightened sketch, (b) equivalent weld cap radius and identical root radius of deformed and straightened sketch	89
7.5	Root cracking in a plate specimen	91
7.6	Test Group H specimen fracture surface. There does not appear to be any evidence of rust	92
7.7	Dye penetrant testing for Test G before (left) and after (right) letting the developer sit. Note that there does not appear to be any obvious cracks at the root in either photo as expected for dye penetrant tests.	93
7.8	Test 6G, which was dye penetrant tested before fatiguing. (a) small amount of dye in the unstable fracture zone from after fatigue testing; (b) a small amount of dye is present on the external part of root. Neither (a) nor (b) are indicative of penetrant seeping through a pre-crack	94
7.9	Test G dye penetrant fracture surface. Note the narrow band at the root. The lack of dye penetrant in the band suggests sufficient fusion and thus not a pre-existing crack.	94
7.10	(a) Strip specimen being clamped in fatigue tester. (b) Strip specimen while clamped to straight, with tension at its weld cap and compression at weld root. (c) Strip specimen after loading with tension at the cap being significantly higher than at the root, leading to fatigue crack initiation.	95
7.11	(a) Plate specimen experiences four-point bending beyond straight alignment. Four-point bending load is removed, allowing residual stresses to resolve and plate elastically deforms to straight. (b) Plate specimen after being clamped in fatigue tester, with no additional bending stresses due to plate being straight. (c) Plate specimen after loading, weld cap tension being equivalent to weld root tension. In this case, the relative weakness of the brazen root ("kissing bond") leads to fatigue crack initiation.	96
8.1	The updated Master S-N curve with both strip tests (circles) and plate tests (triangles). Test groups with the same color are of the same combination. . .	99
8.2	Comparison of mismatch ratios	101
8.3	Updated comparison of stainless vs. non-stainless weld wires	103
8.4	Left: The original Master S-N curve plate data. Right: The plate data if each test was shifted along the $-h = -0.3195$ slope to be standardized at an equivalent structural stress of 425MPa.	107
8.5	Left: Kruskal-Wallis boxplots and outputs for tests G, H, and I. Right: Kruskal-Wallis boxplots and outputs for just tests H and I.	108
8.6	Comparison of filler materials	110
8.7	Updated comparison of base metals	112

List of Tables

3.1	Available base and filler metals	19
3.2	Selected base-filler combinations for initial testing	25
3.3	Completed strip specimen fatigue tests	26
4.1	The seven geometric sketch groups for Abaqus	28
4.2	Test group FE material properties. Note: 46100 and 12560 have identical properties	31
5.1	Test strip specimens with root-cracking	40
6.1	Original Straight Clamp Structural Stress vs. 50% Overclamp Structural Stress	60
6.2	Regression Analysis of Strip Test Data	68
6.3	Cox Model Outputs and Uses	72
6.4	MATLAB outputs from the Cox PH models and calculated statistics for the first two Cox models	73
6.5	MATLAB Cox outputs for Model #3	75
6.6	MATLAB Cox outputs for Model #4	77
7.1	Selected base-filler combinations for plate testing	83
8.1	Outputs from the 5th Cox PH Model, which took in mismatch ratio as the predictor	102
8.2	Cox PH Model #6 and #7, which both use the presence of stainless steel filler as a predictor.	104
8.3	Outputs of Cox PH Model #8 with filler yield strength is passed in as the predictor.	111
8.4	Outputs of Cox PH Model #9 with base material yield strength is passed in as the predictor.	113

List of Abbreviations

ASME American Society of Mechanical Engineers.

ASTM American Society of Testing and Materials.

BM Base metal.

CAD Computer-aided design.

CSCAR Center for Statistics, Consulting, and Analytics Research.

CVN Charpy “V” Notch.

FEA Finite element analysis.

GVSC Ground Vehicle Systems Center.

HAZ Heat-affected zone.

K-W Kruskal-Wallis.

PH Proportional hazards.

SCF Stress concentration factor.

SS Structural stresses.

TARDEC Tank Automotive Research, Development and Engineering Center.

TE Thickness effect.

WM Weld metal.

Abstract

Readiness is a key area of focus for the U.S. Army. The Ground Vehicles Systems Center (GVSC) in Warren, Michigan has been investigating various performance parameters of welded structures in armored vehicles. Of these parameters, the fatigue of welded vehicle structures is of unique interest. Cyclic fatigue damage incurred during normal operation can lead to additional maintenance or structural failure, severely limiting vehicle availability. A better understanding of the fatigue parameters of welded armored vehicle structures is of great value to the U.S. Army in order to maintain readiness.

This research was proposed to directly study the fatigue parameters of relevant base-filler combinations for GVSC by fatigue testing welded specimens. This approach allows for a comparison between the fatigue characteristics of welded armor steels to common welded ferritic and stainless steels that are seen in civil structures. In addition, the Master S-N curve approach used here provides a better method for analyzing fatigue performance across differing combinations of base metal and weld filament, allowing for a more robust study of the effects of material selection.

The GVSC provided fatigue testing equipment and hundreds of welded armor steel specimens consisting of relevant base metal and weld material combinations for study. These specimens were fatigue tested over a period of several years. Finite element models simulating the test specimens were generated to determine the structural stresses experienced by each welded sample during fatigue testing using a novel mesh-insensitive method. These structural stresses can then be transformed into equivalent structural stresses by including

the relevant bending ratio and thickness effects of the tested specimens themselves. These equivalent structural stresses can be used in conjunction with the experimentally determined fatigue lives of the tested welded specimens to plot fatigue results on the Master S-N curve for ferritic and stainless steels. These results can be compared to the expected mean Master S-N curve to determine agreement with ferritic and stainless steels as well as compared to each other to examine what effect, if any, base or filler selection had on fatigue performance.

In total, 47 welded specimens with a 1:1 width-to-thickness ratio and 19 welded specimens with a 5:1 ratio were fatigue tested and analyzed using the Master S-N curve method. Based on the results, it does not appear that welded armor steels behave differently than common ferritic and stainless steels seen in civil structures. Over 92% of the tested specimens were within two standard deviations of the mean Master S-N curve. The 1:1 ratio welded strips had a vertical shift from the mean curve due to the lack of residual stresses from their small width-to-thickness ratio. The 5:1 ratio specimens had excellent alignment with the mean Master S-N curve, showing the importance of ensuring residual stresses for fatigue analysis.

It was found that the selection of base metal or weld filament had very little effect on the fatigue life of the welded test specimens when using survival statistics to examine the test data results. Rather, the presence of welding-induced distortion was the only variable that was shown to have a significant effect on the fatigue behaviors of welded armor joints. Ensuring sufficient weld quality is therefore more valuable for improving the fatigue parameters of welded armor plate joints than the choice of base metal or weld filament for armored vehicle structures.

CHAPTER 1

Introduction

The U.S. Army's Ground Vehicles Systems Center (GVSC) has been supporting Army readiness with a specific focus on system sustainment and lightweighting of vehicle structures. Producing vehicles that reliably meet structural design lives will reduce the need for repairs and increase their availability for combat operations. In armored vehicles, structures' fatigue life is often dominated by their welded joints. These joints typically have complex geometric configurations with varying material combinations due to ballistic performance, structural lightweighting, and load requirements. While the weld category approach of the American Welding Society and American Association of State Highway and Transportation Officials has been around for several decades, GVSC has only used metal fatigue approaches with smooth bar specimen tests for investigating the fatigue life of armored vehicle structures. Because of this, the GVSC has been unable to take advantage of rapid advances in finite element structural modeling methods, which would help to eliminate a significant number of uncertainties in estimating structural lives for armored vehicles in operation. With advances in mesh-insensitive structural stress methods [1, 2] and the Master S-N curve approach adopted by ASME Codes and Standards [3, 4], a quantitative evaluation of armored vehicle structural life becomes possible once fatigue behaviors in thick armor plate weldments are understood in the context of relevant material combinations and welding conditions. Then, a

relevant Master S-N curve using this mesh-insensitive structural stress method can be formulated for implementation in structural optimization algorithms to evaluate design scenarios and meet both required structural life and lightweighting goals. Such modeling capabilities also represent a significant advancement over the methods used in conventional automotive applications.

The purpose of the original proposal to GVSC (at the time TARDEC) was to achieve the following research objectives:

- Develop a fundamental understanding of unique fatigue behaviors associated with thick plate joints used in armored vehicle structures through computational modeling and selected laboratory testing.
- Establish a theoretical framework for transferability of fatigue test data from different joint types, loading modes, thicknesses, and material combinations into a Master S-N curve representation of joint fatigue life.
- Develop computational algorithms for incorporating the Master S-N curve structural life evaluation and weight optimization for armored vehicle structures. The new algorithms will consider the candidate materials, the panel thicknesses, the layout of the welds, and the type of the welds as design variables. Improvement in performance metrics associated with lightweighting and reducing the manufacturing cost will be pursued, while meeting expectations for the fatigue life, and the survivability to loads from blast and ballistic impact.

This doctoral dissertation is focused primarily with the first two objectives, with the third being investigated more thoroughly by another graduate student.

CHAPTER 2

Background

Research into the fatigue of welded structures is fairly expansive, however when considering the welded structures of armored vehicles specifically, there is not as much literature. This lack of armored structure fatigue life information led GVSC to originally include a fatigue study in their weld wire research efforts. This chapter details relevant literature reviews of typical armor steel weld research, the uniqueness of welded armor steel joints in this research, prior publications on fatigue and stress analysis methods, and the theoretical framework that was used for testing and analysis of this topic.

2.1 Fatigue of Welded Joints

The fatigue of welded joints is unique compared to typical non-welded metal fatigue applications. [4] In metal fatigue, smooth rod specimens are machined from solid metal bars and fatigue tested to failure at various loads. This process determines the metal's fatigue resistance for a variety of loading ranges, but is not very useful for understanding the fatigue resistance of welded joints, which have three key differences: property heterogeneity, presence of residual stresses, and geometric discontinuities. Figure 2.1 below provides examples of these differences. [5]

In typical metal fatigue analysis, only the metal of interest is present in a smooth bar

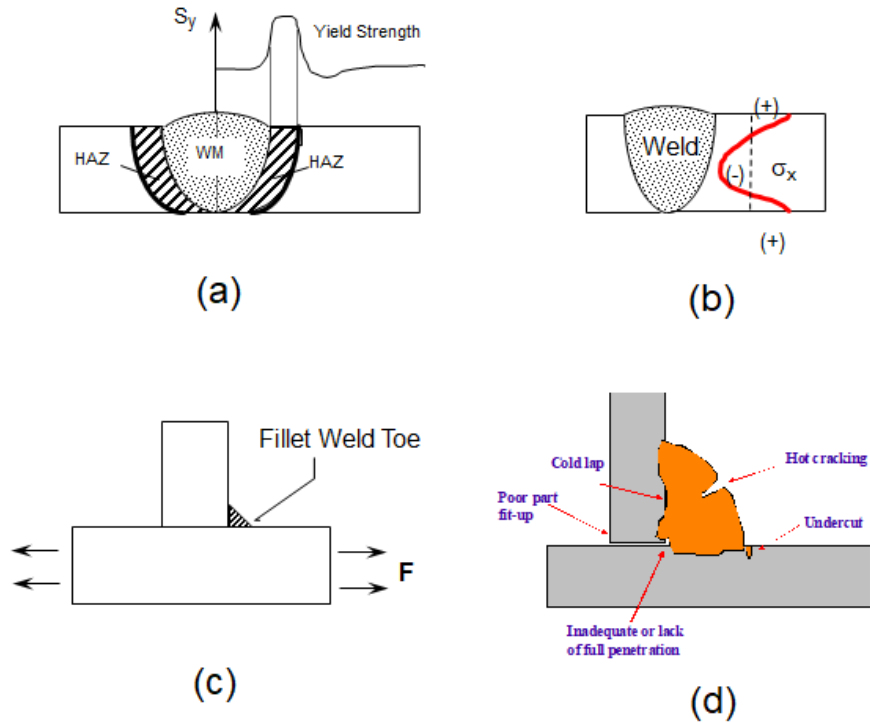


Figure 2.1: Examples of welded joint (a) heterogeneity, (b) residual stresses, (c) global discontinuity, (d) local discontinuity

test specimen consisting of just a base metal. For welded joints, the base metal, weld metal, and heat-affected zone (HAZ) are all present, Each of these zones have different hardness, ductility, and fatigue resistance behavior. This makes welded joint fatigue more complicated to study, as fatigue cracking could occur in any of these distinct zones of the welded component.

Very little heat is generated during the machining of a smooth bar rod specimen for metal fatigue testing, so there is no concern of any residual stresses in the specimen during testing. For welded joints, however, a significant amount of the residual stresses from the welding process are present in the welded structure. These residual stresses often are large enough to affect the total nominal stress experienced by a welded joint during fatigue test loading. In essence, this changes the loading range of the welded specimen during testing, thus affecting fatigue performance significantly. It is important to note, however, that these residual stress effects can be mostly mitigated with sufficiently large specimens, which is usually defined as

their length being at least twice their width, and their width being at least ten times their thickness.

2.1.1 Crack Initiation vs. Crack Propagation

Results from typical non-welded metal fatigue tests are also a poor representation of welded component fatigue due to the fact the smooth base metal fatigue life is dominated by crack initiation. Crack initiation mainly concerns fatigue testing when initial cracks are infinitesimally small due to microscopic material defects. In these cases, the smooth bar or rod specimens used in typical metal fatigue approaches do not contain any geometric discontinuities or non-microscopic deformations present in welded components. This was an issue for a number of years because ASME design guidelines for fatigue lives of boilers and pressure vessels only contained fatigue s-n curves from smooth, non-welded base metal tests. [6]

Welded component fatigue is dominated by crack propagation, not crack initiation. In crack propagation, an initial crack is already assumed either due to the introduction of a pre-crack notch or due to the various geometric discontinuities from welding and joint type. Crack propagation from these initial cracks exhibits two distinct stages of crack growth, depending on the size of the initial or propagated crack. [6] Crack sizes less than 10% of the thickness of the welded plate are typically considered “short cracks” and differ in growth mechanics compared to “long cracks” greater than 10% thickness. Short cracks (notch-dominated) and long cracks (far-field stress dominated) behave differently in terms of crack growth due to the differences in their associated stress intensity factor K . These two distinct behaviors thus necessitate two different stress intensity factor solutions for the notch-dominated and far-field stress dominated components of crack growth in order to characterize full range stress crack growth behavior. [6] This type of two stage approach best encompasses the effect of the short crack growth behavior being overtaken by long crack growth behavior as a fatigue crack propagates and grows in welded components, but is absent in non-welded

metal fatigue testing.

Propagation-dominated crack growth is important to keep in mind for study, as actual welded structures contain discontinuities and minor deformations that act as initial cracks. These discontinuities can be “global” such as a welded joint having a very distinct shape (i.e. T-joint) or “local” such as hot/cold cracking in the weld filament or undercuts at the toe. (Figures 2.1c and 2.1d) Both global and local discontinuities will often lead to higher concentrations of stress. The stress concentrations lead to greater stresses at the discontinuities than the nominal stresses applied during fatigue testing, which significantly affects fatigue life. Therefore it is important to avoid non-welded metal fatigue tests in order to more appropriately approximate actual welded structures. By using “as-welded” structures in fatigue testing, the welding-relevant geometric discontinuities are still present during testing and better represent true welded components.

There are published works on the topic of welded armor joint fatigue, however they typically introduce a pre-crack notch. [7, 8] These pre-crack notches act as a well defined short crack, and allow for the comparison of crack propagation in the different zones (base metal, HAZ, weld material) of the welded joint. The test strips provided by GVSC for use in the fatigue testing of this study were intentionally not pre-cracked; they were left as-welded. The testing in this research therefore is unique from most of the published works on armor steel weldments. While both pre-crack and unaltered welded armor steel joints are crack propagation-dominated, the unaltered weld approach is more appropriate for comparing to actual structures because they both contain initial cracks from geometric discontinuities instead of intentional notches.

2.2 Cold-cracking in Armor Steel Welds

In academia and industry, the topic of armor steel weldments is dominated by the discussion of cold-cracking, which is the biggest issue with the high hardness steels typical in armor

applications. Because of this, there is a lot of interest in investigating the microstructure and weldability of these high hardness armor steels [9, 10, 11].

Cold-cracking can have a significant effect on fatigue life of welded armor steels, so the effects of poor welding may be important to consider when conducting fatigue tests for this portion of the weld wire characterization project. However, the presence of cold-cracking is not anticipated in this study, as the prepared welded strips and plates all passed inspection at GVSC prior to testing.

2.3 Effect of Material Selection

Another unique aspect of this research compared to industry and academia is the deliberate study of differing welded combinations of base material and weld wire in the fatigue of welded joints. There does not appear to be any published works that specifically investigate how differing the weld filament of an armor steel weld can impact fatigue performance.

U.S. Army armored vehicles are typically not built to exact material and design specifications. Rather, military contractors are given the option of using any base metal or filler material they choose so long as required design parameters such as weight, strength, and cost are still met. This leads to a variety of welded combinations consisting of many base armor metals and differing weld wires being present in U.S. military vehicle structures. GVSC expressed deliberate interest in understanding if these different combinations have differing fatigue performance. Given this is a key point of interest for GVSC, this research provides unique opportunity to shed light on what appears to be a less understood aspect of welded armor structures.

2.4 Stress Determination

In fatigue analysis, the cyclic stress of a fatigue test is required in order to plot data an s-n curve. For simple metal fatigue, the applied load divided by the cross-sectional area

of the smooth specimen is appropriate for determining cyclic fatigue stress. This type of approach is not appropriate for use in welded joint fatigue analysis, as it does not consider the different effects of stress concentration, weld joint type, loading mode effect, etc. [6] A different approach that more accurately determines the actual stress present during fatigue testing of a welded joint is important to consider for this type of research.

Originally, early attempts to calculate fatigue cycle stresses using finite element analysis were unsuccessful. This was due to the fact that stresses at weld root and weld toe were ill-defined mathematically, as continuous refining of finite element meshes would see stresses infinitely increase. [4, 6] This “mesh sensitivity,” as it is commonly known, limited the ability to use finite element methods for fatigue evaluation in the 1980s-1990s, and lead to the adoption of using simple nominal stress definitions in the form of fatigue s-n curves. These s-n curves would thus need vary according to welded joint type, as different joints would follow different curves.

Surface-extrapolated hot spot stress (HSS) methods began being proposed in the 1990s-2000s as a means to improve finite element accuracy for fatigue evaluations of welded joints. [12, 13, 14, 15] Since the location of fatigue interest is ill-defined for stress evaluation in FE, it was believed that adjacent well-defined characteristics could be used to extrapolate the stresses at the location of interest. HSS methods were still very sensitive to mesh size and element type, and the variability in the extrapolated hot spot stresses were significant. Ultimately, they could not be viewed as anything more than empirical stress determination procedures and were not very effective for broad fatigue stress analysis application.

2.5 Mesh Insensitive Structural Stress Method

The mesh-insensitive structural stress procedure was a new attempt at dealing with the shortcomings of nominal stress and HSS approaches being used in the 1980s-2000s. [4] Dong and his colleagues’ development of the mesh insensitive method stemmed from four main

observations:

1. Rather than focus on localized stresses at crack notches, a through-thickness stress distribution consisting of membrane and bending terms was more appropriate modeling fatigue behavior over a lifespan.
2. A hypothetical crack plane (Plate A-A) of a welded joint would only have three fatigue-relevant stress components: normal stress σ_x , in-plane shear stress τ_y , and transverse shear stress τ_z
3. These three stress components are directly related to corresponding line forces and line moments of plate theory. By using generalized nodal forces from finite element, these stress components could then be related to their nodal forces and moments in the same plane. This would satisfy equilibrium and displacement conditions
4. The finite element nodal forces could be used to determine the membrane and bending components of stress in a through-thickness cut, allowing finite element to be used to determine fatigue stresses regardless of mesh size and joint type

The mesh-insensitive method was thus an incredible advancement in finite element fatigue analysis, as it provides a consistent stress state measure that can be directly related to the fatigue damage process associated with weldments. The effectiveness of the mesh-insensitive method has been demonstrated in a number of publications. [1, 3, 4, 16, 17, 18]

2.5.1 Mesh Insensitive Structural Stress Method - Example

This mesh insensitive example detailed here is taken from [4, 17, 19]. The mesh-insensitive structural stress parameter is calculated in terms of through-thickness membrane and bending (Figure 2.2), and can be directly related to the statically-equivalent far-field stress or crack face pressure at a hypothetical crack location of interest, such as the weld root or weld toe, in the context of fracture mechanics.

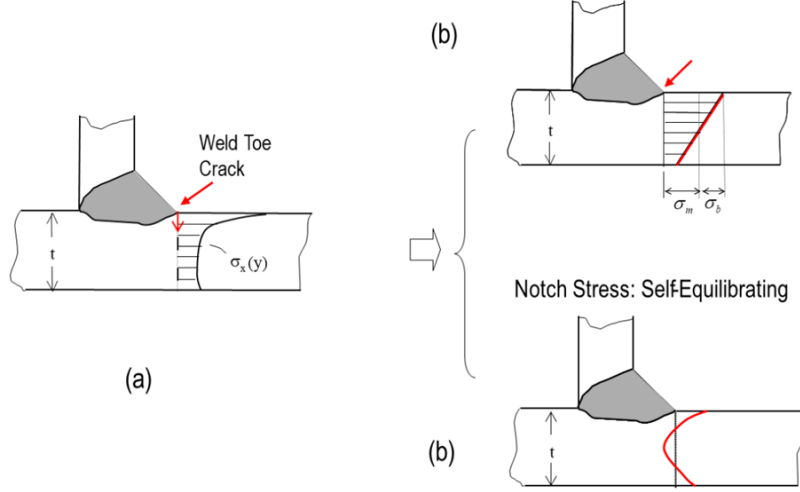


Figure 2.2: Borrowed from [17] with permission: Through-thickness structural stress definition: (a) actual nonlinear stress distribution at weld toe; (b) structural stress or far-field stress in terms of through-thickness membrane and bending; (c) self-equilibrating notch stresses

The equilibrium-equivalent membrane and bending parts of the structural stress can be calculated by means of a system of simultaneous equations by using nodal forces and nodal moments from shell or plate element models as follows in Equation 2.1:

$$\begin{Bmatrix} F_1 \\ F_2 \\ F_3 \\ \dots \\ \dots \\ F_{n-1} \end{Bmatrix} = \begin{bmatrix} \frac{l_1+l_{n-1}}{3} & \frac{l_1}{6} & 0 & \frac{l_{n-1}}{6} \\ \frac{l_1}{3} & \frac{l_1+l_2}{3} & \frac{l_2}{6} & 0 \\ 0 & \frac{l_2}{6} & \frac{l_2+l_3}{3} & \frac{l_3}{6} \\ \dots & \dots & \dots & \dots \\ \dots & \dots & \dots & \dots \\ \frac{l_{n-1}}{6} & 0 & \frac{l_{n-2}}{6} & \frac{l_{n-2}+l_{n-1}}{3} \end{bmatrix} \begin{Bmatrix} f_1 \\ f_2 \\ f_3 \\ \dots \\ \dots \\ f_{n-1} \end{Bmatrix} \quad (2.1)$$

A closed weld line is assumed in the above equation. The lowercase f_1, f_2, \dots, f_{n-1} are line forces along y' . The l_i term element represents the element edge length projected onto the weld toe line from the i th element. The corresponding line moments can be calculated with respect to the center in an identical manner by replacing the balanced nodal forces in the local y' direction with balanced nodal moments M_1, M_2, \dots, M_{n-1} as depicted in Figure 2.2. The nodal force F_i in the above equation represents the summation of the nodal forces at node i from the adjoining weld toe elements situated on the positive side of the y' axis as

shown in Figure 2.3.

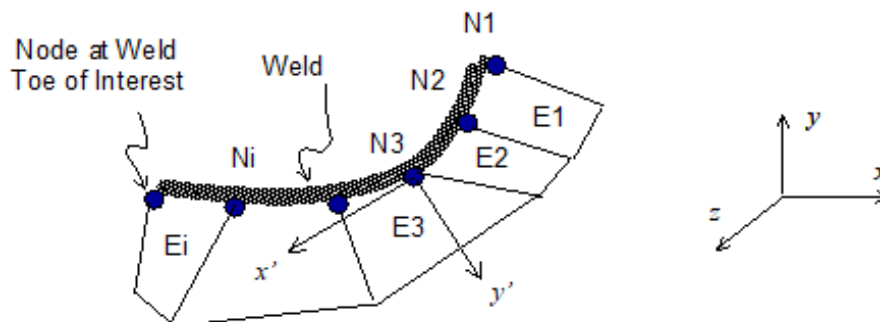


Figure 2.3: Borrowed from [17] with permission: Structural stress calculation procedure in the mesh-insensitive method for an arbitrary curved weld using plate/shell element models

Before Equation 2.1 can be constructed, coordinate transformation for the nodal forces and nodal moments from the global axis to a local axis system must be performed. Here, we define x' as traveling along the weld line and y' as being perpendicular to the weld line. All these calculations have been automated as a structural stress post-processor. The linear system of equations described by Equation 2.1 can be solved simultaneously to obtain line forces for all nodes along the line connected all weld toe nodes. Substituting the corresponding nodal moments into Equation 2.1, one obtains line moments in the same manner. Then, the structural stress shown in Figure 2.3 at each node along the weld (such as the weld toe) can be calculated as:

$$\sigma_s = \sigma_m + \sigma_b = \frac{f_{y'}}{t} + \frac{6m_{x'}}{t^2} \quad (2.2)$$

To demonstrate the effectiveness of the mesh-insensitive stress evaluation method the tube-to-tube weld depicted in Figure 2.4(a) is modeled with four drastically different meshes (Figure 2.4(b)). The results for the stresses at the saddle position of the weld toe obtained by the four different mesh sizes are summarized in Figure 2.4(c).

The saddle position on the weldments has the maximum stress concentrations of the models, so those locations are chosen for comparing stress results. As it can be observed, the structural stresses for each mesh size are all within 2% of each other when the coarsest mesh

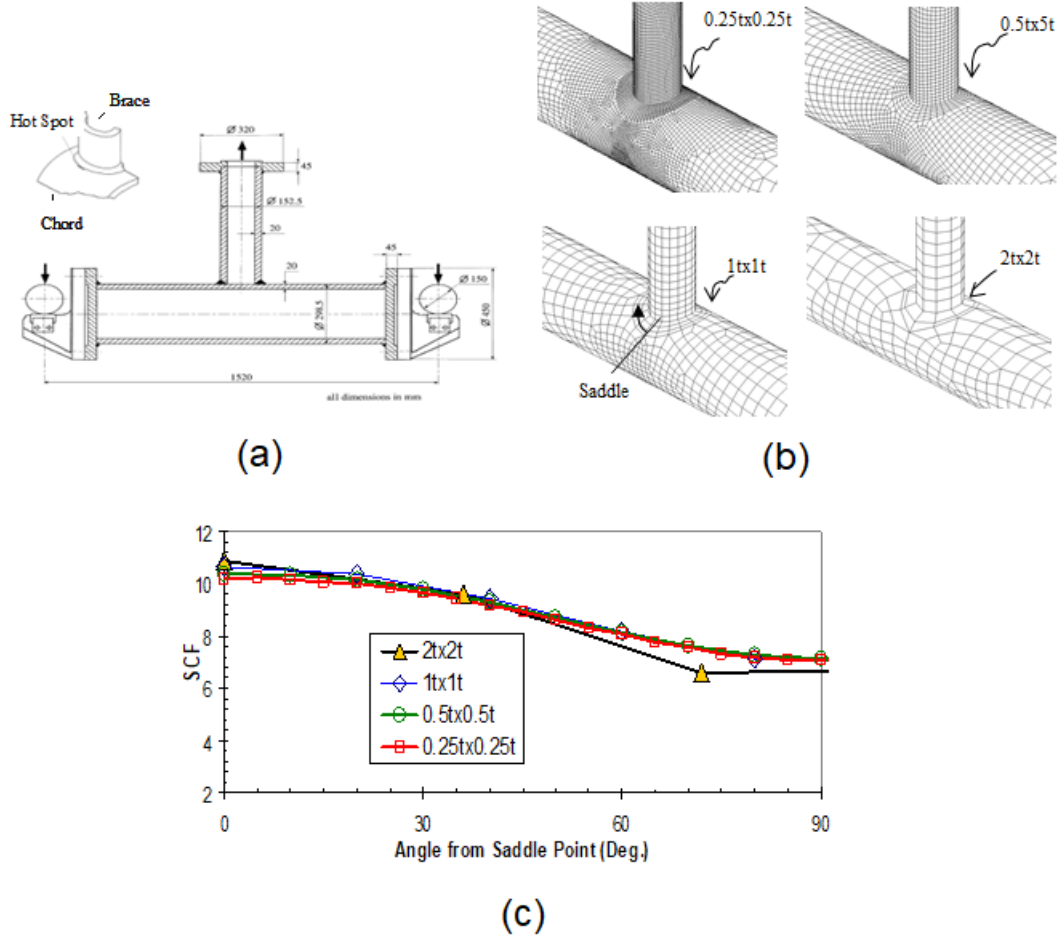


Figure 2.4: Borrow from [19] with permission: (a) T-joint geometry (b) four different meshes (c) Comparison of stress results between the four meshes

is excluded. When considering all four mesh sizes, they are all within 5% of each other. In the proposed research, the mesh-insensitive stress method will be formulated for finite element models made out of solid elements, since such elements are often used for modeling Army vehicle structures.

By applying fracture mechanics principles, an equivalent structural stress range parameter ΔS_s can be formulated as:

$$\Delta S_S = \frac{\Delta \sigma_s}{t^{\frac{2-m}{2m}} I(r)^{\frac{1}{m}}} = CN^{\frac{1}{n}} \quad (2.3)$$

Equation 2.3 collapses the many nominal stress based S-N curves into a single narrow

band regardless of joint types, loading mode, and plate thicknesses. This can be seen in Figure 2.5 below.

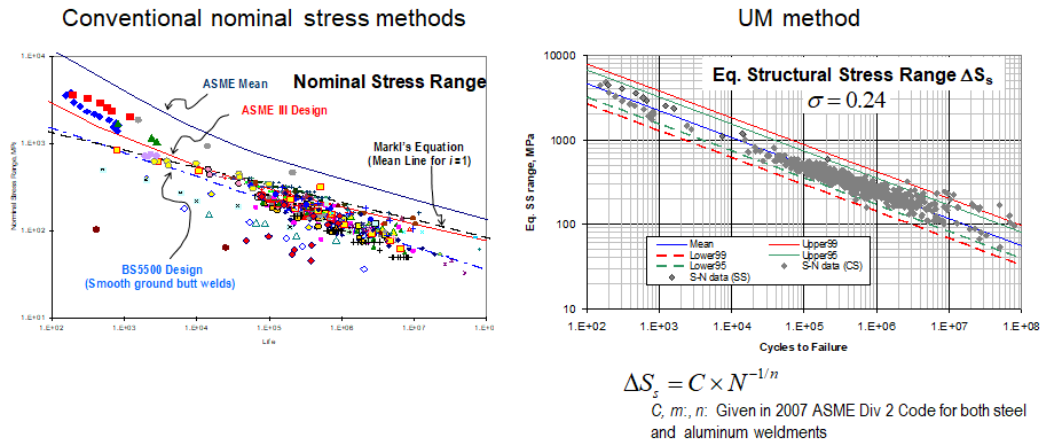


Figure 2.5: From [19]: Demonstration of effectiveness of equivalent structural stress parameter given in Equation 3

2.6 Master S-N Curve Applications

The Master S-N curve method is a state-of-the-art fatigue analysis method that has been used in the past in naval applications for evaluating fatigue lives along weld lines, configuring scantlings, and guiding the material selection for a titanium mid-ship section. [4, 17, 20] Naval structures are constructed by joining thick metal plates. Material selection and weld placement were both based on fatigue life and manufacturing considerations. Figure 2.6(a) shows the comparison of the fatigue lives for different materials and different weld locations which were considered for construction of a mid-ship section.

There are many similarities between the welded armor structures of land-based US military vehicles and welded plate structures of naval vessels and supporting structure, including their use of thick plating, inclusion of both carbon and stainless steels, complex geometric welds, and strict need for strong, effective welds. Given the historic success of using the Master S-N curve method for evaluating fatigue in naval structures, it stands to reason that the method will also be an excellent fit for analyzing armored vehicle structures fatigue. [3, 4, 17]

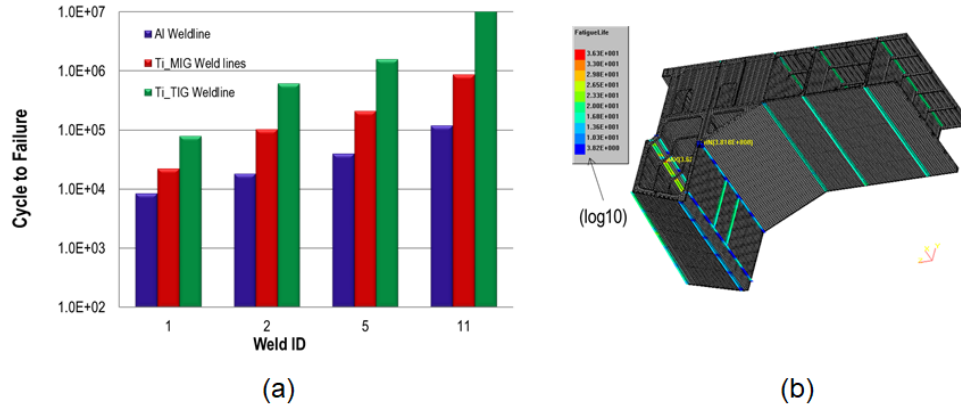


Figure 2.6: From [20]: (a) Comparison of fatigue lives for various joints based on weld material selection. (b) Finite element model used for the mesh-insensitive stress calculations

Not only is the inclusion of the Master S-N curve approach an appropriate fit for use with welded armored vehicle structures analysis, but it does not appear to have yet been used in the field of armored vehicle fatigue analysis. The application of the Master S-N curve to welded armor vehicle structures appears to be wholly unique for purposes of fatigue characterization and life cycle analysis.

2.7 Research Approach

Considering all of the current research on the topic and the relevant theoretical framework for welded joint fatigue testing noted above, there is sufficient foundation to investigate the fatigue performance of armored vehicle structures. The following sequence is a summary of the employed approach:

1. Develop an experimental plan for fatigue testing
2. Conduct fatigue testing of pre-selected specimens in GVSC laboratory
3. Analyze tests using the mesh-insensitive method with finite element software
4. Formulate the Master S-N curve with the analyzed data and check validity
5. Examine Master S-N curve data for any trends or unique patterns

6. Determine what, if any, further testing or developments are needed

CHAPTER 3

Welded Armor Specimen Testing

As mentioned above, this research consists of two main components: fatigue testing of welded specimens and formulation of the Master S-N curve from finite element modeling. This chapter details the previous fatigue project, current equipment, welded specimens, procedure, and plan of the testing phase up until this point.

3.1 Weld Wire Characterization

Several years ago, GVSC set out to determine many characteristics of various weld wire combinations with base metal armor structures. Different contractors will use different weld wires and armor steels for the construction of armored vehicles. Understanding how these different base metal and weld metal combinations behave was of great interest to the U.S. Army, so a project to investigate these combinations started.

This original project, the Weld Wire Characterization Project, involved conducting tests to determine the tensile strength, CVN, macro hardness, face bend, root bend, side bend, hydrogen embrittlement, x-ray, ballistic, and penetration qualities of weld and base metal combinations across four testing phases. The fatigue tests were to be conducted in the final phase, but GVSC was unable to continue testing, leaving Phase 4 of the project incomplete. GVSC researchers reached out to Prof. Dong and Prof. Vlahopoulos at the University

of Michigan through the Automotive Research Center. This led to a joint proposal from Professors Dong and Vlahopoulos to GVSC to complete Phase 4 of the Weld Wire Characterization Project, while also investigating additional modeling performance metrics relevant to armored vehicle structures.

The equipment and welded armor plates that were originally prepared for use in the Weld Wire Characterization project were made available for use in this research.

3.2 Equipment

This Chapter details the equipment necessary to conduct the fatigue testing in this research. This equipment was provided by GVSC on-location at the start of this project in the summer of 2018. Additional equipment was provided on-location for further testing in the fall of 2021. This equipment included:

- Instron Model 1333 fatigue testing system with 8800 controller
- Instron Model 3156 110-kip load cell (tension and compression rated)
- Four 2" x 2" textured wedges
- Two Instron 3,000psi, 22.4kip hydraulic grips
- Blue Hill 3 and WaveMatrix testing software
- Strain gauge extensometers
- Biaxial extensometers
- National Instruments CDAQ computer I/O system
- Instron Model 8802 fatigue testing system with 8800 controller (2021)
- Two Instron 3,000psi, 100kip hydraulic grips (2021)

- Four 4" x 4" textured wedges (2021)

The first fatigue tester (Model 1333) provided by GVSC was rated to operate at loads of 250+ kips and was equipped with a load cell rated for up to 110 kips. The hydraulic grips available for the Model 1333 were only rated for 22.4kips, so no fatigue testing can be done with greater than 22,400 pounds of force. This is not an issue for test specimens with relatively small cross sectional areas, but for larger specimens the maximum stress that can be imparted during a fatigue cycle is very limited. When GVSC purchased and installed a newer fatigue tester (Model 8802), hydraulic grips rated up to 100kips were included. This new tester allowed for testing welded specimens with greater cross sectional areas due to the improved loading capacity.

3.3 Welded Specimens

As part of their Weld Wire Characterization Project, GVSC had already created welded test specimens for fatigue testing. Their selection of base metal-filler metal combinations was chosen based on common armor steels and weld filaments that U.S. Army contractors would use in manufacturing. In total, GVSC prepared fatigue samples for 36 base-filler combinations, consisting of three base metals and twelve weld filaments. A table of these base metals and filler metals can be seen in Table 3.1.

It is worth noting that one of the base metals that GVSC provided welded specimens for, ASTM A514, is not actually an armor steel. A514 steel is a common building steel, and was included in the Weld Wire Characterization Project at the request of another department of the federal government. While the main concern of this research is to investigate the fatigue life of armored vehicle structures build with armor-grade steel, several tests were still conducted with the ASTM A514 steel for reasons which are described later.

For each base-filler welded combination, there are 31 samples with an approximate size of 14" x 1/2" x 1/2" and 4 samples with an approximate size of 14" x 5" x 1/2". Typical

Table 3.1: Available base and filler metals

Base Metal	Filler Metal
MIL-STD-12560	ER70S-6
MIL-STD-46100	ER80S-D2
ASTM A514	ER100S-6
	ER120S-6
	ER347
	ER308LSi
	ER309LSi
	ER316LSi
	E70C-6M H4
	E70C-6M H8
	E90C-G H4
	E110C-G H4

fatigue testing requirements for welded joint specimens require them to be sufficiently sized, which is usually defined as width to thickness being at least 10:1 and length to width being at least 2:1. While the 5” wide specimens are sufficiently sized, the 1/2” specimens with a width to thickness of 1:1 are not. This may lead to issues with a lack of residual stress in the welded joints from waterjet cutting. These “strip” specimens are not completely sufficient for fatigue testing study. Due to their large number and the ease of testing them, however, it was decided that all initial testing would be conducted on the strip specimens first. The ability to detect trends and collect exploratory data on the more plentiful strip specimens is still valuable, and much lower risk compared to the limited number of 5” width “plate” specimens. By testing the strips first, any difficulties or irregularities in testing or modeling could be worked out first, and simple trends could still be observed in post-testing analysis. A diagram of the plate and strip specimens can be seen in Figure 3.1.

The hydraulic grips also presented another limiting factor for fatigue testing. For the strip specimens with a cross section of 0.25sq inches, the grips could be loaded to provide a theoretical maximum stress of 89,600psi, well above the ranges typical for fatigue testing steels. However, the plate specimens, with their larger cross section of 2.5sq inches, could only be loaded to a maximum stress of 8,960psi in the fatigue tester. That low of a stress would

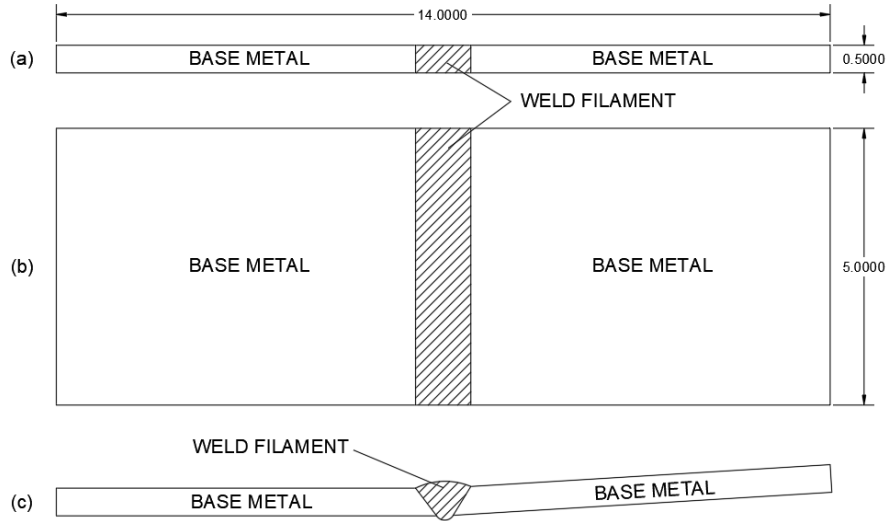


Figure 3.1: (a) Plan view of strip specimen; (b) Plan view of plate specimen; (c) Elevation view of both strip and plate specimen

lead to fatigue tests lasting well over 24 hours, and since testing could only be conducted during normal working hours at GVSC, testing the plate specimens with the originally provided equipment was not a reasonable option. Additionally, the 5" width plate samples likely could not be appropriately clamped in the 2" x 2" wedges in the hydraulic grips. This means that testing the plate samples may not have been possible with the original equipment.

Additional measures were necessary to test the larger welded specimens. Cutting down the 5" width plate samples to instead be 2 1/2" width plate samples provides several advantages, the first being that the decreased width would decrease the cross sectional area by half, thus doubling the maximum stress that could be induced in a fatigue cycle. This also doubles the total number of plates specimens to 8 which allows for more testing per base-filler combination. Additionally, cut-down plates would better fit in the wedge grips. A diagram of the wedge clamping areas for the 5" plate, cut down 2 1/2" plate, and 1/2" strip specimens can be seen in Figure 3.2.

There are other considerations that must be taken into account with the strip and plate specimens. All the welded specimens have angular deformations due to heat transfer effects during the welding process. While the angular deformations are not large enough to make

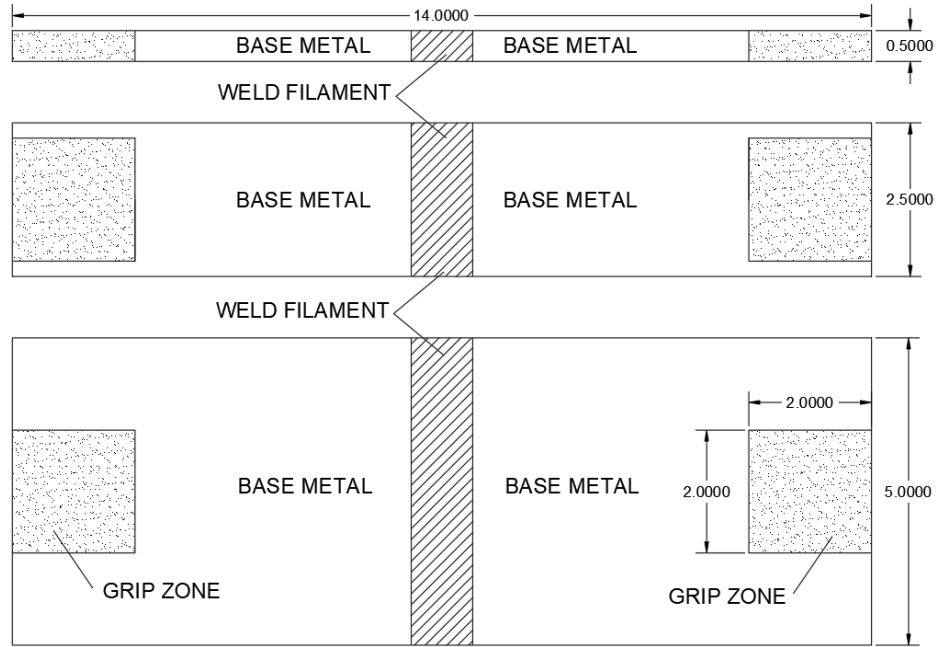


Figure 3.2: (a) Strip specimen clamping area; (b) 2 1/2" Plate specimen clamping area; (c) 5" Plate clamping area; Note, the 5" plate has less than 50% contact area over the grip length. This is insufficient for fatigue testing.

trouble during clamping and testing, they are large enough to be geometrically significant. The additional angularity changes the stress profile both during static clamping and during cyclic loading, so these angles must be noted prior to testing for analysis later on. Additionally, only the strip samples are currently available at GVSC. The plate samples are located at the Pacific Northwest National Laboratory in Richland, Washington. Therefore, in order to test any plate specimens, they must be ordered and shipped from Washington. Because of this, it is vital that only necessary plate specimens are shipped in order to keep shipping costs down for GVSC. Additionally, plate specimens must be queued up for a few weeks to be cut down to their 2 1/2" plate configuration, since getting them waterjet cut requires prior notice. For these two reasons, any plate tests must be decided months ahead of time, and there are additional cost considerations per base-filler combination plate selected for testing. Strip tests can be prepped and executed in a day without additional cost, thus they are much more convenient to test with.

3.4 Procedure

In this research, a standardized testing procedure was developed in order to consistently conduct and document fatigue tests.

First, each specimen to be tested was inspected for cracks, surface defects, significant corrosion, or other issues. If there weren't any issues, specimens were cleaned up to remove soot or other debris. Clean specimens were labeled on both sides of the weld groove with a test ID corresponding to their base-filler combination and a unique number. These ID's and numbers were also recorded in a research logbook, to keep track of how each specimen was tested.

Newly labeled specimens then had their geometries and distortions recorded. This was done by carefully sketching each specimen on an engineering draft paper. By making sketches before the fatigue test, the original geometry could be referenced in analysis. This was important, as original geometry is a key variable in the finite element analysis, and having documentation of angular deformations is vital for analyzing trends. An example of some specimen sketches can be seen in Figure 3.3 below.

Once specimens are sketched, the clamp surfaces of the specimen are measured to be exactly 2" deep. Equal clamping area and clamp distance is important for proper fatigue testing. Once clamp surfaces were measured and marked, specimens can be clamped into the fatigue tester. Both sides of the weld are clamped at the same time in the event that non-symmetric clamping order could have an effect on bending stress. Once clamped, the test parameters are set in the WaveMatrix software and copied into the logbook.

Fatigue tests can then be conducted until failure. After a few exploratory tests, failure conditions were set to be defined as: a 50% reduction in fatigue load maximum, 50% reduction in fatigue position range, or 50% reduction in fatigue load range. These failure conditions were all compared to their measured values that occurred at cycle 5,000, which was experimentally determined to be a good metric of a fully developed fatigue cycle. Dur-

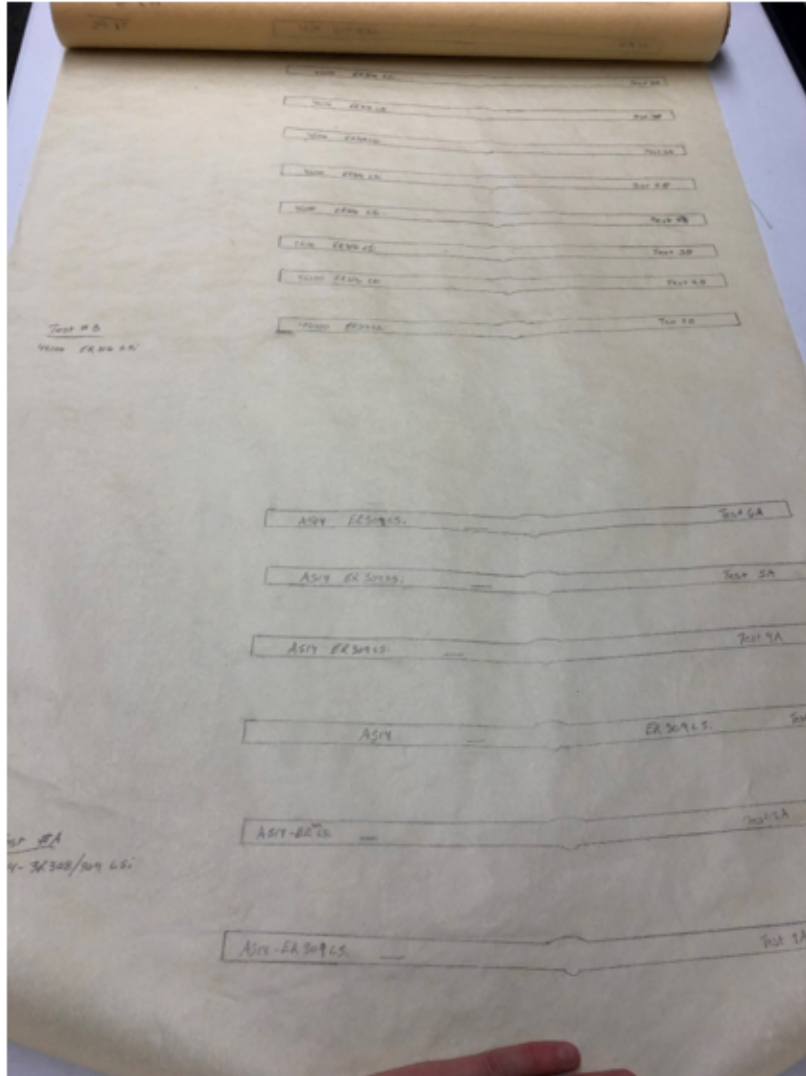


Figure 3.3: Photograph of sketched strip geometry pre-testing

ing testing, these failure conditions usually triggered within a few cycles of the emergency machine safety cut-offs while still getting obvious, through-thickness fatigue failure.

Specimens that were successfully tested to failure were then examined for any irregularities on their fracture surface, covered in WD-40 to prevent oxidation, and collected for storage should they be needed for later analysis.

3.5 Test Plan

The first phase of testing was conducted during the summer of 2019. In order to best take advantage of the limited amount of time available to test at GVSC, a testing plan for the summer was developed based on which base-filler combinations were most important for the research. Initially, three base-filler combinations were selected for the first round of testing, with an additional three added into testing to get more data on emerging trends.

Testing all 36 combinations of base metal and weld filament would be far too time consuming. Instead, if only the extremes of the base and filler combinations were tested and analyzed for their fatigue life, then all other combinations would have fatigue life lying somewhere between them. When considering what extremes to test, the mismatch ratio (R) was determined to be the most relevant. Mismatch ratio is the ratio of the yield strength of the weld metal to the yield strength of the base metal. Each base-filler combination would have a different mismatch ratio, and by testing the combination of interest with the highest R and the combination of interest with the lowest R , the upper and lower bounds of the entire set of data could theoretically be inferred to be between them. 46100 steel with ER316LSi filament has the lowest R of 0.283 and 12560 steel with E110C-G H4 filament has the highest R of 0.665, so they were both selected for initial testing. ASTM A514 steel did have a lower yield than both 12560 and 46100, but because it is not an armor steel it was not selected for setting the upper and lower mismatch ratio bounds.

At the request of GVSC, 12560 steel with ER70S-6 filament was also selected for initial testing. This is because that combination is the most common in armored vehicle joints, and with a R of .415 it sits well between the two extremes.

As testing of these specimens started, it became clear there was time to test other combinations during the summer. Two A514 steel combinations, ER309LSi and ER80S-6, were selected for testing as well. These two combinations both exhibited very high amounts of angular deformation, but one was with a stainless steel filament and the other was not. This

would allow analysis of the effect of stainless vs. non-stainless fillers with roughly similar mismatch ratios, identical base metals, and similar levels of angular deformation. Additionally, 46100 steel with ER80S-6 filament was chosen to undergo testing as well. An employee at GVSC expressed interest in the fatigue capabilities of high strength base metal and high strength filler metal. This combination also had very low angular deformations, and would give more 46100 datapoints for analysis.

In total, six combinations for the first phase of testing were selected. Each combination was assigned a test ID for labeling and documenting purposes. These combinations can be seen in Table 3.2.

Table 3.2: Selected base-filler combinations for initial testing

Test ID	Base-Filler Combination	Mismatch Ratio	Point of Interest
A	A514 with ER309LSi	0.600	High deform, stainless
B	46100 with ER316LSi	0.283	Lowest mismatch ratio
C	12560 with E110C-G H4	0.665	Highest mismatch ratio
D	12560 with ER70S-6	0.415	Most common combo
E	A514 with ER80S-6	0.715	High deform, non-stainless
F	46100 with ER70S-6	0.3195	High strength base and filler

For this first summer of testing, it was decided to only test the 1/2" strip specimens. This was for several reasons. Strip specimens were much more abundant and accessible than their plate specimen counterparts, which were more limited in number, required shipping from out of state, and needed to be cutdown. While not ideal for fatigue data, strip specimens would still provide insight into trends and give rough estimates of fatigue life performance while being significantly quicker to test due to their reduced cross sectional area. Researchers at GVSC also expressed their intent to purchase a new fatigue tester, one that would have higher capacity hydraulic grips and allow for overnight testing. This new fatigue tester would be much more appropriate for testing plate samples, so it was decided to do all strip specimen testing for the first round, then continue testing with the plate samples once the new fatigue tester was operational.

Originally, 10 tests for each strip specimen combination were planned. These tests would

consist of pairs of 5 pre-selected load ranges of 1-17, 1-18, 1-19, 1-20, and 1-21 kips. These load ranges are on the higher end of total testing capability, being close to the maximum 22.4kips grip limit, while maintaining a low load ratio, providing a range of data values, and having repeatability. It was decided to do tensile fatigue tests due to the ease of setting them up, and the low load ratios during cyclic testing were a result of trying to maximize the fatigue load ranges while limiting the possibility of going into compression during the ramp up and failure portions of the fatigue tests. Once a fatigue test was completed, the number of cycles to failure was recorded in the research logbook to be used later for the formulation of the Master S-N curve.

3.6 Completed Tests

Test durations, time constraints, and initial difficulties with running the machine limited the first round of testing to only have 50 tests completed in the summer of 2019. Four additional tests were conducted in the winter of 2019 in order to get some fatigue test data past the 100,000 cycles range, bringing the total number of tests conducted to 54. Table 3.3 below gives each strip specimen combination and the number of successful fatigue tests as of winter 2020.

Table 3.3: Completed strip specimen fatigue tests

Test ID	Base-Filler Combination	# Tests
A	A514 with ER309LSi	6
B	46100 with ER316LSi	10
C	12560 with E110C-G H4	10
D	12560 with ER70S-6	10
E	A514 with ER80S-6	7
F	46100 with ER80S-6	11

With these tests completed, the next step is finite element analysis.

CHAPTER 4

Finite Element Analysis

This chapter details the post processing analysis conducted on the fatigue tests. Specifically, it covers the finite element analysis done on the sketched samples of the tested specimens and their formulation into the Master S-N curve. For simplicity, all input and output units for finite element use inches and psi.

4.1 Strip Specimen Sketch Geometry

In order to formulate the Master S-N curve for the tested specimens, the structural stresses of the specimens at their point of fatigue failure needed to be known. These structural stresses can be determined by use of finite element modeling. In this project, Abaqus was used to determine the structural stresses of the fatigue test specimens using the mesh-insensitive nodal force method.

Using scans of the strip sketches, the geometry of each test specimen was imported into AutoCAD, a computer aided design drafting software. Strip sketches of each combination were then grouped together and compared. If test strips of the same base-filler combination type had negligible differences in angular deformation and eccentricity, then a single sketch could be used to represent all of the strips for the combination in the finite element analysis. If test strips of the same combination were sufficiently different, then each unique

strip sketch would have to be tested separately in FEA. Figure 4.1 shows an example of the angular deformation and eccentricity measurements taken in AutoCAD.

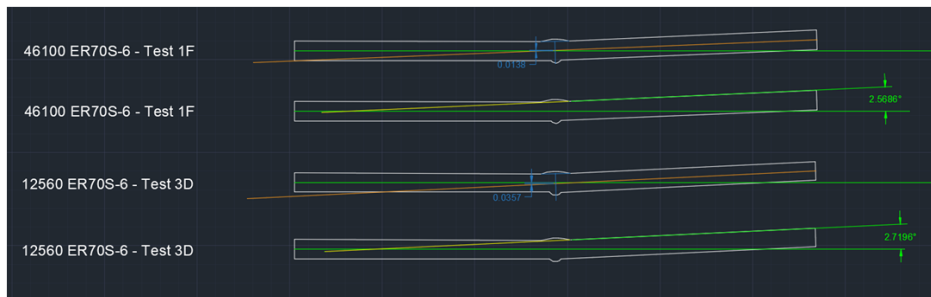


Figure 4.1: Angular deformation and eccentricity measurements in AutoCAD for two strips

Among the six different base-filler combinations tested initially, test groups A, C, D, E, and F all had strip specimen sketches that showed less than 2% variation in geometry. Test group B had two distinct sets of different strip geometry, with each set showing less than 2% variation in geometry within itself. Test group B was then split into these two sets for finite element analysis. The median strip specimen sketch for each of the seven geometric groups was selected for use in Abaqus to represent that group, and their angular deformations and eccentricities are given in Table 4.1.

Table 4.1: The seven geometric sketch groups for Abaqus

Test ID	Angular Deformation [degrees]	Eccentricity [in]
A	6.7595	0.0230
B (set 1)	5.7248	0.0090
B (set 2)	6.2896	0.0200
C	3.3452	0.0053
D	2.7196	0.0357
E	3.7637	0.0173
F	2.5686	0.0138

4.2 Nonlinear Analysis

From the table, it can be seen that nearly all of the specimens have negligible eccentricities, accounting for at most around 4.5% of the specimen’s thickness. The angular deformations, however, are fairly significant, with the largest distortion of 6.29 degrees giving a right end vertical displacement greater than one thickness. This is a very large geometric

nonlinearity, which can skew FEA results. When the finite element modeling and Master S-N curve formulation were initially performed, they were conducted using linear analysis in FEA.

When Abaqus attempts to "clamp" the finite element model into a straight alignment to simulate the fatigue tester's clamping loads before testing, the linear analysis attempts to solve this in a single analysis step. This leads to an inaccurate representation of the bending-induced residual stresses from clamping, as the intricacies of the geometrically nonlinear deformed specimens are not appropriately accounted for in the simpler, single-step linear analysis, which often overestimates their effects.

Additionally, individual terms in the Jacobian matrices of a model during FE calculations are simplified during linear analysis, according to the Abaqus theory manual. [21] In the Jacobian matrix (Equation 4.1), the β_N term defines strain variation of the kinematic variables of the model and is a function of displacement. Since the clamping-induced displacement changes of the geometrically nonlinear specimens do not occur incrementally in linear analysis, the β_N terms in the Jacobian matrix are oversimplified. Thus, the strains are not accurately accounted for in the Jacobian matrix and linear analysis is not accurately determining clamping-induced stresses.

$$\int_{V^0} = \beta_M : H : \beta_N dV^0 \quad (4.1)$$

The load stiffness matrices of an Abaqus model are also not appropriately accounted for in linear analysis. According to the theory manual, the element stiffness calculations that improve convergence behavior contribute significantly to stiffness of the modeled structures. When using linear analysis, certain membrane stiffness terms in the load stiffness matrix are not considered in response to transverse loads. By using nonlinear analysis, these terms are present and update appropriately with every incremental step, which improve convergence behave and more accurately models specimen stiffness.

These differences in Jacobian and load-stiffness matrices lead to massive over-estimates of structural stresses from FEA when using linear analysis. In order to account for the geometric nonlinearities present in these test specimens and avoid the linear overestimates, it was decided to use nonlinear analysis (nlgeom) in Abaqus for the fatigue test models. Fortunately, switching to nonlinear analysis did not drastically increase the amount of processing time in the Abaqus solver, so this not have an associated increase in duration for solver run time. Figure 4.2 gives an example of the differences in structural stress outputs between linear and nonlinear analysis for Test D specimens.

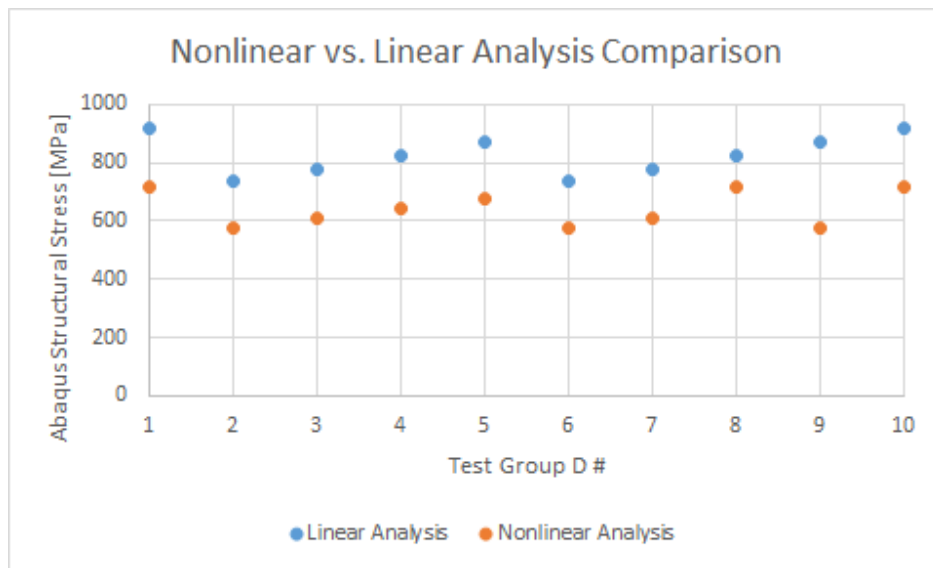


Figure 4.2: Test D: Linear structural stresses vs nonlinear structural stresses

4.3 Finite Element Modeling

Generating the finite element models begins with importing the test group specimen sketches from AutoCAD. These sketches can then be used to create the test strip part in Abaqus as a 2D planar shell. Mesh elements are set to be CPS4R, which is a 4-node bilinear plane stress quadrilateral, reduced integration, hourglass controlled element type. Partitions of the grip extents and toe edges are also drawn into the part. These are necessary to accurately define both the clamping conditions and to ensure that a perpendicular line of element edges exists in the crack location of the weld toe for use in the nodal force method.

Next, material properties are defined for each test group and are assigned to the entire part. A table of these base material properties, and which tests contained these properties, can be seen in Table 4.2. Since we are interested only in the nodal force outputs of these finite element models, it is appropriate to assign the entire part with the base material’s properties. The Young’s Modulus of our base and filler materials are similar enough such that defining a separate weld material property to the weld area of the model will not amount to any difference in the output nodal forces. This means that outputs structural stresses from Abaqus will be nearly identical even when modeling the entire part with the base material’s property.

Table 4.2: Test group FE material properties. Note: 46100 and 12560 have identical properties

Part Material	Young’s Modulus [psi]	Poisson’s Ratio	Tests Assigned
A514 Steel	27,557,000	0.27	A,E
12560 Steel	30,457,000	0.25	C,D
46100 Steel	30,457,000	0.25	B,F

The entire part is sectioned, and an instance is generated on that section. Then, the part is meshed via edge seeding. The nodal force method is insensitive to mesh size, so mesh sizes do not need to be particularly small. For most of the tests, the parts are meshed with 0.125 inch spacing, which gives four elements through thickness of the parts. This is sufficient for the nodal force method, and mesh sensitivity testing shows negligible differences in calculated structural stress for 0.125 inch, 0.0625 inch, and 0.03125 inch edge spacing. The mesh is assigned to have a CPS4R element type. Additionally, the history and field output requests are edited to ensure that the nodal forces are output and propagated through the Abaqus job submission, as these are necessary for the nodal force method. Next, the steps, loading condition, and clamping condition are defined.

The clamping conditions are defined first in Abaqus. In order to simulate the actual clamping of the strip specimen, the “left” half of the strip specimen was given fixed boundary conditions in all three degrees of freedom for two inches from the edge on both the top and bottom model faces. This simulates how the actual clamping occurs in the fatigue tester,

as the wedge grips only grip two inches of the strip while essentially fixing it in translation and rotation. Along its two inch clamping area, the “right” half was instead brought into alignment with the clamped left half using vertical boundary conditions. Due to angularity, the amount of vertical shift necessary to bring the right half into alignment with the left half varies along the clamp area. To account for this, the amount of vertical displacement at each top-bottom node pair was manually changed to ensure the middle of each pair was aligned with the middle of the perfectly level left half. While intensive, this method ensured that the right half of the strip specimen would be clamped into alignment with the left half, as would be expected in a fatigue test. Both of these boundary conditions occur at the same step in the analysis, which has been defined as the “Clamp” step.

For loading, only the right half of the strip specimen is loaded in Abaqus. Two loading steps, “Min” and “Max”, are created to simulate the minimum and maximum load during a fatigue cycle. The minimum load is applied first, then deactivated when the maximum load is applied. The clamping condition propagates throughout both loading steps. These loads are applied by attaching concentrated loads to the clamp nodes on the right half of the model. These concentrated loads act only in the “x” direction to simulate the tensile force of the fatigue tester, and the sum of these concentrated loads equals the total load induced by the tester for whichever test is being modeled. An screenshot of the applied loads and clamping condition can be seen in Figure 4.3.



Figure 4.3: Clamping and Loading Conditions on a strip sample. Boundary conditions are in orange and blue while concentrated loads conditions are in yellow.

Once the steps, loads, and boundary conditions are finished the job can be submitted for analysis in Abaqus. This process is repeated for every fatigue test conducted, with the loads, boundary conditions, and sketches changing as necessary. Since there are only seven geometric sets however, the sketch and boundary conditions only need to be changed for seven instances, leaving only the loads to be changed for each of the 54 tests.

Abaqus outputs the defined output histories for each step in the analysis. This is important, as the loading range between the “Max” and “Min” steps are the values of interest for Master S-N curve formulation. Specifically, just the nodal force outputs from Abaqus along the weld toe partition (i.e. fatigue crack location) are necessary for this type of analysis.

4.4 Master S-N Curve Formulation

In order to formulate the Master S-N curve for the strip specimen data, the equivalent structural stress (Equation 2.3) needs to be calculated. *The Master S-N Curve Approach to Fatigue Evaluation of Offshore and Marine Structures* details the exact methods necessary to determine the three terms that constitute the equivalent structural stress: the stress concentration effect, the loading mode effect, and thickness effect. [17] The calculations for these terms must all be conducted using metric measurements, per the Master S-N curve requirements, so the imperial outputs from the finite element software are converted.

4.4.1 Stress Concentration Effect

The stress concentration effect, also known as the structural stress, can be calculated by using Equation 4.2:

$$\sigma_s = \sigma_m + \sigma_b = \frac{f_{y'}}{t} + \frac{6m_{x'}}{t^2} \quad (4.2)$$

The mesh-insensitive nodal force method can be used in conjunction with the equation above to find the structural stress of each test. The thickness t in Equation 4.2 is the same for all strips at 0.50 inches. The nodal force term $f_{y'}$ and the bending force term $m_{x'}$ are both calculated from the Abaqus outputs. The nodal forces can be found by making a path at the point of fatigue failure (weld toe) through the thickness of the strip. Abaqus then can be used to generate a table of the non-averaged, singular directional nodal forces for each node along the path. The $f_{y'}$ term can then be found by summing these nodal forces along

the path of the weld toe. The $m_{x'}$ term can be found by multiplying the nodal force at each node with the distance between that node and the center of the strip. Once the $f_{y'}$ and $m_{x'}$ terms are calculated, the structural stress for any loading step in the Abaqus model can be determined. Figure 4.4 below shows a few screenshots of using Abaqus to pull the nodal forces of a strip sample.

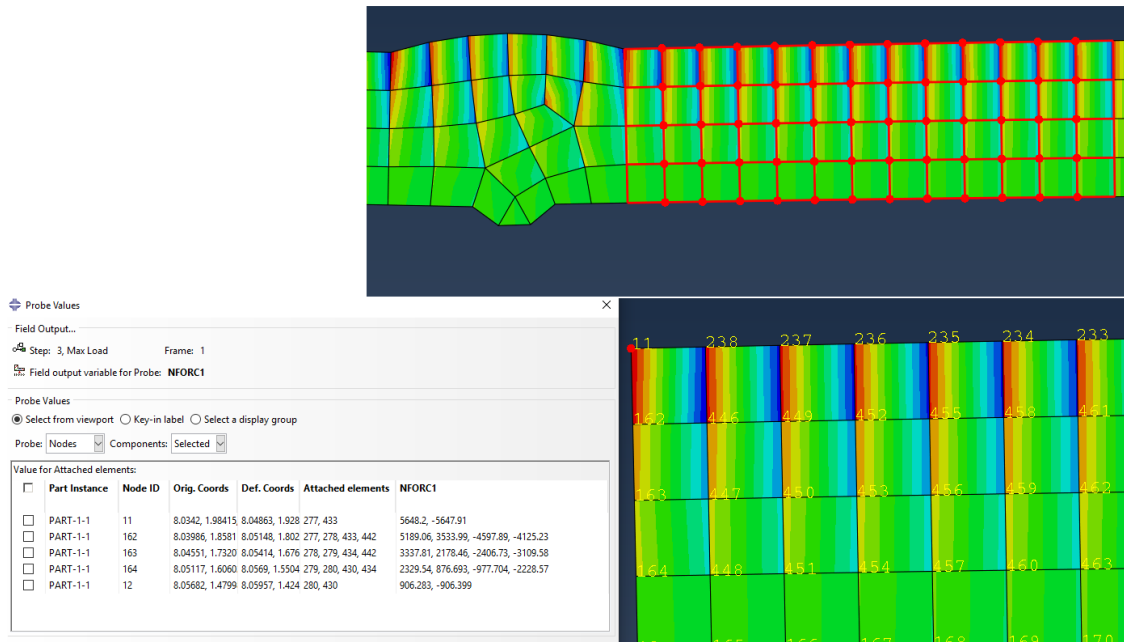


Figure 4.4: Abaqus screenshots showing one method of pulling nodal force outputs from the weld partition

For calculating the equivalent structural stress range, the structural stress range is needed.

$$\Delta\sigma_s = (\sigma_{s,max} - \sigma_{s,clamp}) - (\sigma_{s,min} - \sigma_{s,clamp}) \quad (4.3)$$

Where $\sigma_{s,max}$, $\sigma_{s,min}$, $\sigma_{s,clamp}$ are the calculated structural stresses at the weld toe of the maximum loading step, minimum loading step, and clamping step, respectively. The structural stresses from the clamping step are subtracted from the minimum and maximum steps to ensure that no initial stresses due to clamping are present in the fatigue loading cycle for calculations. In essence, the $\Delta\sigma_s$ simply ends up being $\sigma_{s,max} - \sigma_{s,min}$ for any modeled strip specimen.

4.4.2 Loading Mode Effect

The “loading mode effect” $I(r)^{\frac{1}{m}}$ is an additional term for calculating the equivalent structural stress based on experimentally derived relation between loading type and bending ratios. Since all of the tests in this research were load controlled experiments, the load control equation for loading mode effect is used:

$$I(r)^{\frac{1}{m}} = 1.2223 + 0.014r + 0.0221r^2 + 0.0946r^3 - 0.0988r^4 + 0.0767r^5 + 0.011r^6 \quad (4.4)$$

In Equation 4.4, the r term is the bending ratio, which is equal to the bending stress divided by the sum of the bending and membrane stresses. For this research, the bending ratio for each test strip was calculated as:

$$r = \frac{\sigma_{b,max}}{\sigma_{total,max}} \quad (4.5)$$

Each tested strip has different maximum bending and membrane stresses at its maximum load, so the loading mode effect term needs to be calculated for each strip.

4.4.3 Thickness Effect

The thickness effect “TE” is a dimensionless length parameter present in the equivalent structural stress equation.

$$TE = t^{\frac{2-m}{2m}} \quad (4.6)$$

The t in the above equation is the thickness of the specimen in millimeters, and the m term is an analytically determined slope value of 3.6. Since every test strip has the same thickness, the thickness effects are identical across all tests.

With the structural stress range, loading mode effect, and thickness effects of each test,

the equivalent structural stress ranges can be calculated for all the strip specimens. The equivalent structural stresses from Abaqus and the cycles to failure from testing can then be used to plot the tests on the Master S-N curve plot.

CHAPTER 5

Analysis of Fatigue Test Strip Data

This chapter details the results from testing and analysis for the strip test specimens.

5.1 Applicability of Master S-N Curve Definition

The Master S-N curve is based on thousands of fatigue tests of various joint types, base metals, and weld filaments. The coefficients needed for calculations of the mean curve line and confidence intervals of the Master S-N curve are dependent on whether the testing materials in question are ferritic/stainless steels or aluminum. In this research, all the base metals and weld filaments are either ferritic or stainless steel, therefore they are expected to fit in that set of curves. Figure 5.1 below, which is pulled from the original Master S-N curve documentation [22] with authors' permission, gives the coefficients and equations from ASME div 2 for calculating the mean S-N curve and 95% confidence intervals.

Plotting the $C \cdot N^{-h}$ for the ferritic and stainless steel mean curve and the $\pm 2\sigma$ standard deviation curves over a fatigue life duration of 10,000 to 1,000,000 cycles gives:

The strip specimen tests will be added to the above plot of Master S-N curve for ferritic and stainless steels. This will allow comparison of the test results versus the ferritic/stainless steel Master S-N curve while having a consistent graph for comparison.

Statistical Basis	Ferritic and Stainless Steels		Aluminum	
	C	h	C	h
Mean Curve	19930.2	0.31950	3495.13	0.27712
Upper 95% Prediction Interval (+1σ)	23885.8	0.31950	4293.19	0.27712
Lower 95% Prediction Interval (-1σ)	16629.7	0.31950	2845.42	0.27712
Upper 95% Prediction Interval (+2σ)	28626.5	0.31950	5273.48	0.27712
Lower 95% Prediction Interval (-2σ)	13875.7	0.31950	2316.48	0.27712
Upper 99% Prediction Interval (+3σ)	34308.1	0.31950	6477.60	0.27712
Lower 99% Prediction Interval (-3σ)	11577.9	0.31950	1885.87	0.27712

Note: In SI Units, the equivalent structural stress range parameter, ΔS_{range} , in paragraph 3.F.2.2 and the structural stress effective thickness, t_{ess} , defined in paragraph 5.5.5 are in $MPa/(mm)^{(2-m_{ss})/2m_{ss}}$ and mm , respectively. The parameter m_{ss} is defined in paragraph 5.5.5.

$$\Delta S_{range} = C \cdot N^{-h}$$

$$\Delta S_{range} = \frac{\Delta \sigma_s}{(t_{ess}/t_{ref})^{2m_{ss}} \cdot I(r)^{m_{ss}}}$$

$t_{ref} = 1mm$
 $m = 3.6$

Figure 5.1: Master S-N Curve Basis

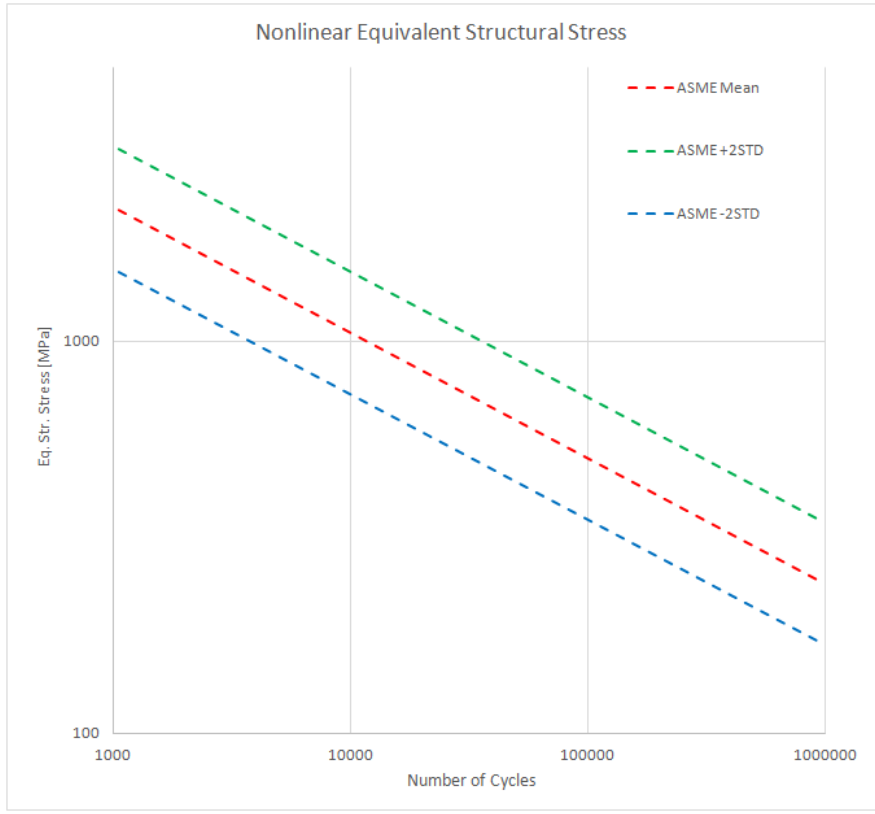


Figure 5.2: Plotted Ferritic and Stainless Steel Mean and +/- 2σ curves

5.2 Faulty Test Data

Not all of the test strip specimens are usable data. Several of the strip specimens did not fail at the FE predicted location of the weld toe, instead exhibiting cracking at the weld root.

These tests cannot be easily analyzed for structural stresses, as the stresses themselves

cannot be easily determined due to the fracture surface having a different cross-sectional area than the weld root cases. In root cracking, the cross-sectional area is simply the specimen width (usually 0.50 inches) multiplied by its thickness (0.50 inches), but toe cracking sees the fracture surface travel through the weld cap. The additional thickness cannot be easily measured after testing, and cannot be predicted before testing, so the cross-sectional areas of the toe cracking tests cannot be determined (Figure 5.3). Additionally, FEA doesn't predict local stress concentrations at root crack locations, so even with an accurate cross section, it is likely impossible to predict a structural stress without exact knowledge of the root conditions before testing.

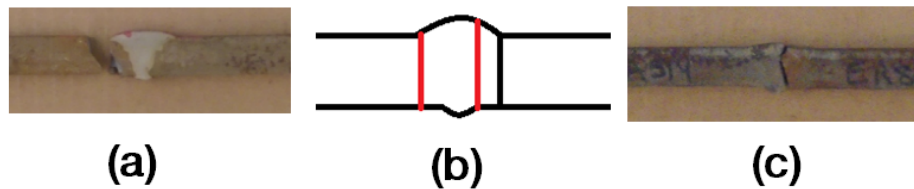


Figure 5.3: Example of toe-cracking (a) vs. root-cracking (c). Note in (b) how the root-cracking case leads to an increased through-thickness fracture zone

For root crack cases, these tests are ignored in the following analysis. At the time of testing, the cause of the root cracking was believed to be a lack of proper fusion during welding. This would lead to a small gap at the weld root. This gap acts as a pre-crack, and causes the weld root to experience a local stress concentration. The finite element models, which are based on tracings of the pre-tested strips, would not contain these gap pre-cracks, thus they would not anticipate a stress concentration at the weld root.

The presence of root-cracking was most prevalent in test group A, which researchers at GVSC warned may have had issues with proper fusion during the welding of the A514 steel and ER309LSi. A table of which base-filler combinations had toe cracking can be seen below.

Table 5.1: Test strip specimens with root-cracking

Test ID	Base-Filler Combination
2A	A514 ER309LSi
3A	A514 ER309LSi
4A	A514 ER309LSi
5A	A514 ER309LSi
6A	A514 ER309LSi
4B	46100 ER316LSi
7E	A514 ER80S-6

Interestingly, of the seven test specimens with root cracking six of them involved A514 steel. Five of them were from the same combination of A514-ER309LSi. After consulting with GVSC, this is likely due to lack of fusion at the root during welding. GVSC suspected that some of the plates were welded poorly, and the failure of five of the six test A specimens seems to confirm this. Test 4B likely had root cracking due to an accident during testing, where someone who was not involved with our research mistakenly changed test parameters in the middle of a test. It is unknown what caused test 7E to experience root cracking.

5.3 Strip Specimen S-N Curve

After ignoring the root-cracking tests, there were 47 remaining test strip specimens available for analysis as of winter 2020. Figure 5.4 gives the results of plotting the cycles to failure from each test with their finite element analyzed equivalent structural stresses.

There are several observations that can be made regarding the current data. The most obvious observation is that a vast majority of the strip tests fall well within two standard deviations of the ASME mean Master S-N curve. Of the 47 total plotted tests, only four lie outside the $+2\sigma$ band, with the rest sitting between the mean line and $+2\sigma$. Statistically, only two tests are expected to lie above $+2\sigma$, but with the relatively smaller sample size four outliers still seems reasonable. Additionally, it can be seen that the overall slope of the tests trends well with the slope of the Master S-N curve.

From the figure it appears that despite the very low width to thickness ratios of the

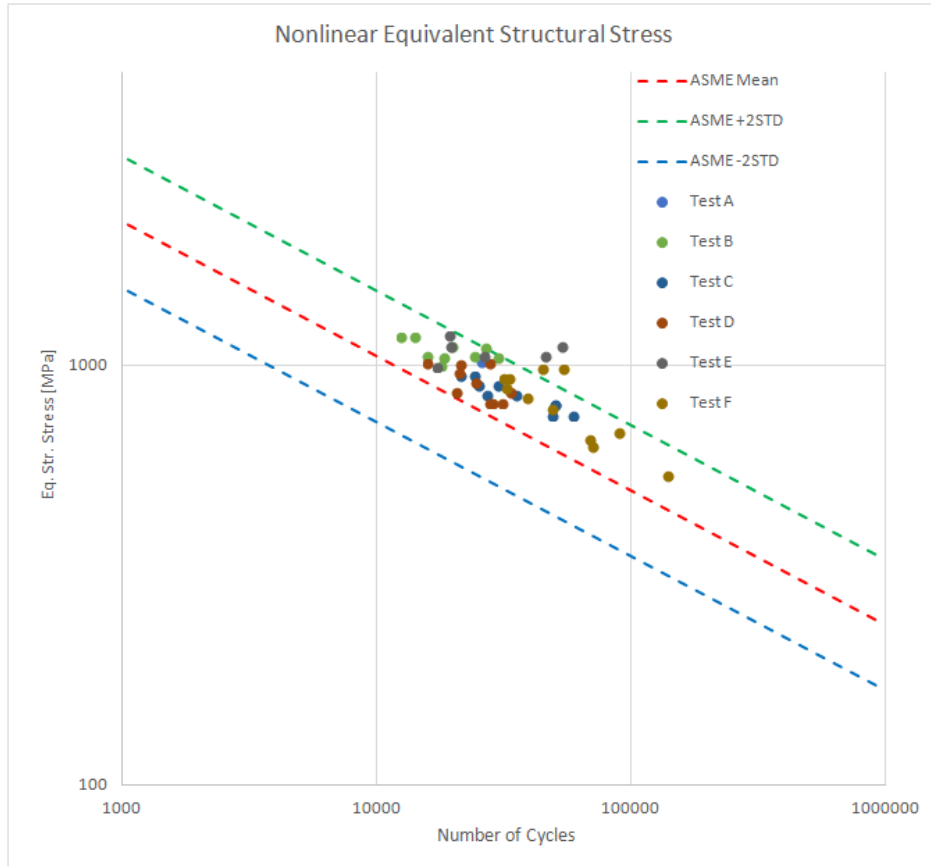


Figure 5.4: The tested strip specimens plotted against the ferritic and stainless steel Master S-N Curve

strip specimen the fatigue tests are all in agreement with the Master S-N curve. This helps show that both the current method for calculating the equivalent structural stresses and the fatigue tests themselves are very reasonable. The strip specimens can also be used to get a rudimentary grasp of any trends among the test data.

5.4 Trends

Trends in the strip test data results can be investigated by categorizing variables of the strip tests together and comparing.

Figure 5.5 shows the strip test data when the tests are categorized by their mismatch ratio (WM_{yield}/BM_{yield}). Tests are group into mismatch ratios less than 0.3, ratios from 0.31 to 0.6, and greater than 0.61. From the plot, it appears that the strips with mismatch ratios

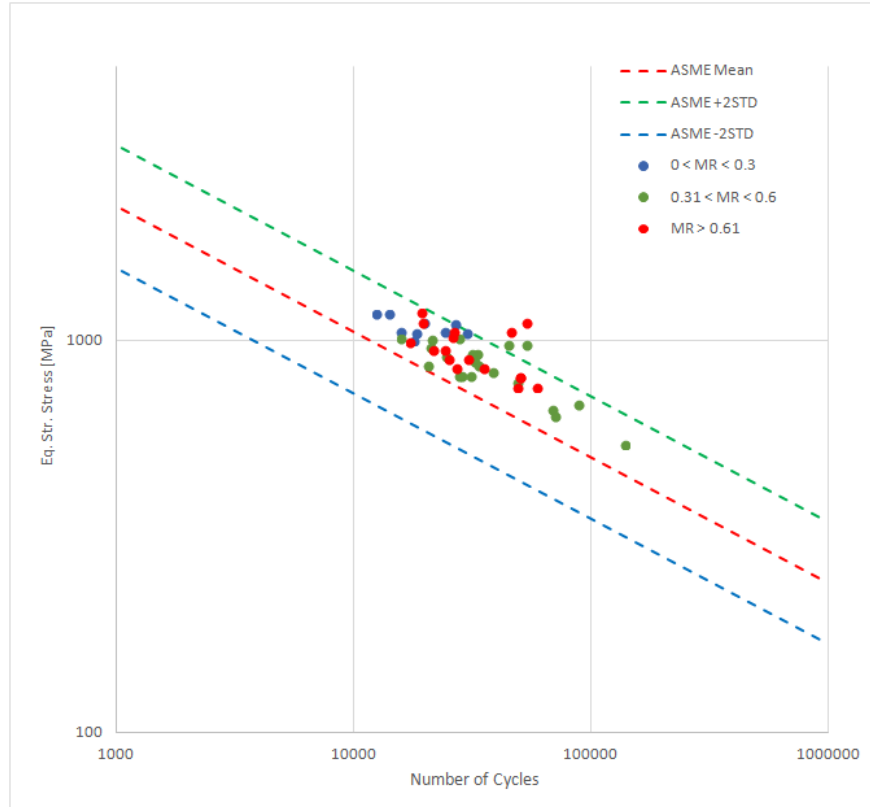


Figure 5.5: Comparison of mismatch ratios

below 0.3 have the shortest fatigue lives. Mismatch ratios greater than 0.3, however, do not appear to have any discernible trend in regards to fatigue life. From this result, it does appear that the selection of weld filament and base metal may have an impact on the fatigue life of a weld depending on the resultant mismatch. However, it is important to look at if the angular deformation of the weld may also explain the reduced fatigue life.

Figure 5.6 shows the test data organized by angular deformation in groups of less than 3 degrees, three to five degrees, and more than five degrees. From the plot, it appears that as the angular deformation increases in the strip specimens, the fatigue life decreases. This makes sense, as larger angular deformations in the weld would lead to additional bending stresses induced during loading. These additional stresses would increase the structural stresses at the weld groove, causing a reduction in fatigue life for strip specimens. The base-filler combinations with the lowest mismatch ratios are the same specimens that have the highest angular deformations. During Winter 2020, when this data was first being analyzed,

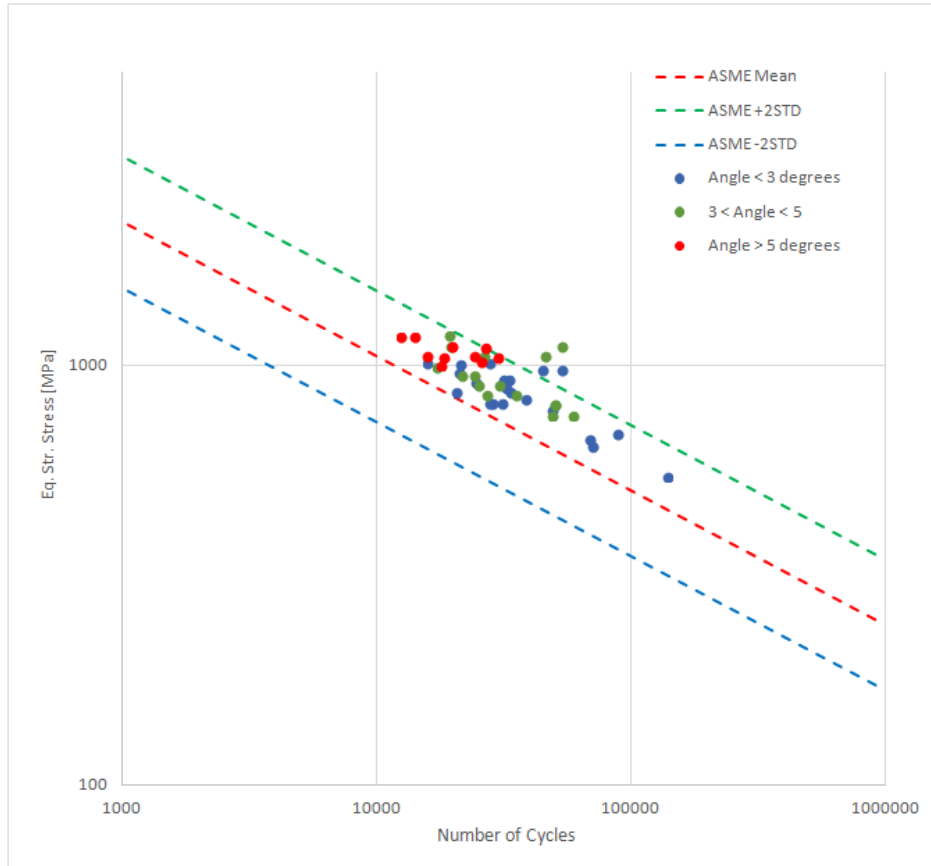


Figure 5.6: Comparison of angular deformation

there was not enough test data to determine which of the two variables is effecting fatigue life. This issue of the two variables being “coupled” is addressed later on.

Using the Master S-N curve data for strip specimens, the effect of stainless steel filler versus non-stainless filler can also be examined. Figure 5.7 gives two plots, one showing all of the data organized by stainless and non-stainless fillers. The second plot shows a constant base metal, 46100, with both a stainless and non-stainless filler.

There are no inherent properties of a stainless steel filler that would be expected to affect fatigue life. However, when looking at all of the strip test data, the stainless steel weld filament generally performs more poorly in fatigue life compared to the non-stainless (carbon-based) weld filament. When comparing the stainless filament ER316LSi with the carbon filament ER70S-6 for the same base metal, there appears to be a significant difference in fatigue performance with the non-stainless having longer fatigue life. In this particular

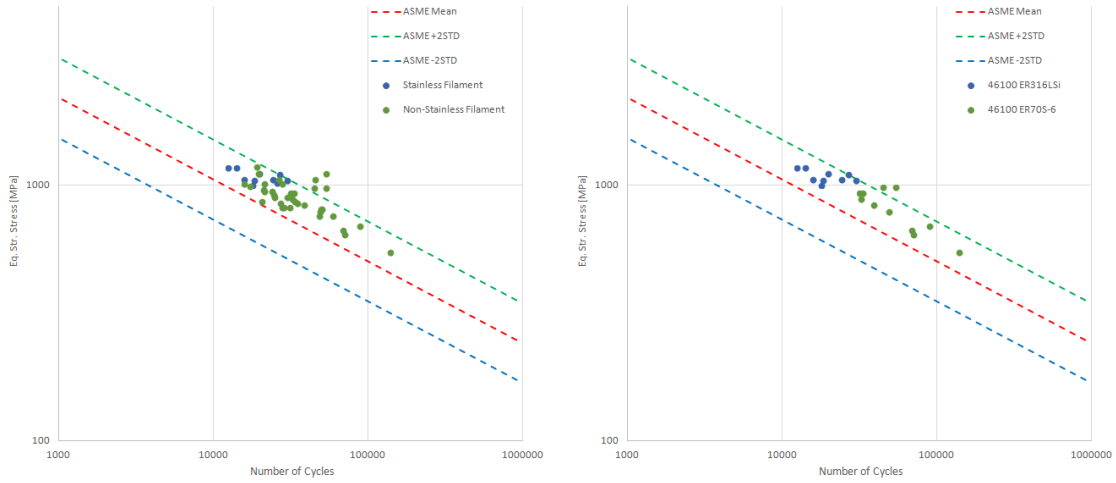


Figure 5.7: Left: Stainless vs. non-stainless filler metals. Right: 46100 base metal with ER316LSi stainless and ER70S-6 non-stainless fillers

example the 46100 with ER316LSi combination has a MR of 0.2829 and angle of 5.7248 degrees while the 46100 with ER70S-6 combination has an MR of 0.3322 and angle of 2.5686 degrees. Considering the difference between mismatch ratios is fairly insignificant as opposed to the difference in angular deformation of these two groups, this lends more credence to the theory that angular deformation has a greater effect on fatigue life than mismatch ratio. Likely, the stainless steel filaments, which are typically more difficult to weld properly, lead to poorer welds and more distortion in the strip samples. Higher amounts of angular deformation would lead to greater structural stresses, and thus lower fatigue lives.

Additionally, we can look at the effect of the different base metals on fatigue life. Figure 5.8 shows one plot with all of the tests organized by base metal type and another plot comparing the two armor steels, 46100 and 12560, with the same filler metal of ER70S-6.

Across all the fatigue tests, there doesn't appear to be a significant difference between 12560 and 46100 in terms of fatigue performance. A514 steel, which is commonly used as a construction steel, does appear to perform a little worse in terms of fatigue due to having higher equivalent structural stresses in this dataset. When comparing 46100 and 12560 specifically with the same weld filament, 46100 appears to have slightly higher fatigue life for the same equivalent structural stresses as 12560. In the finite element software, 12560 and

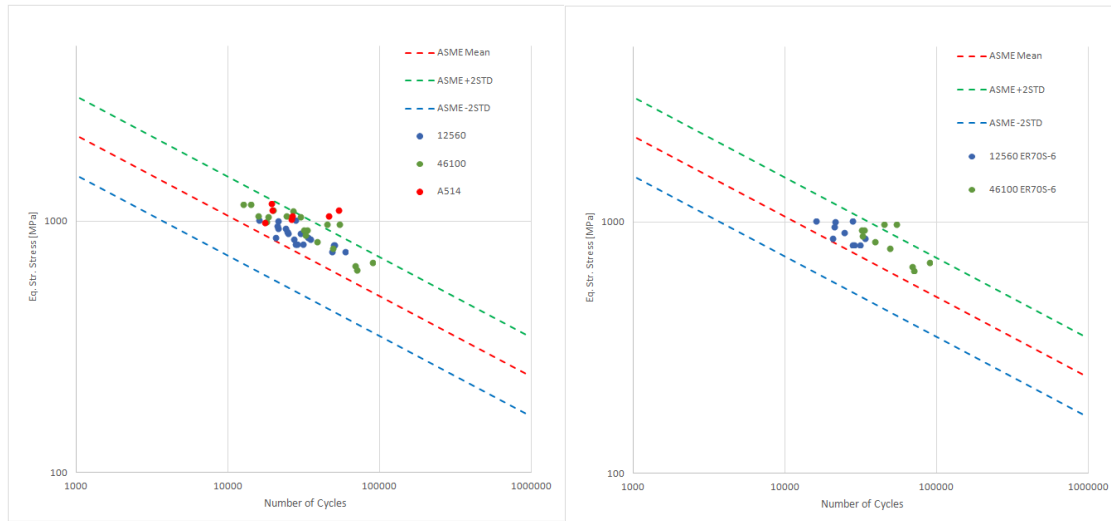


Figure 5.8: Left: Base metals of the fatigue tests. Right: 46100 and 12560 base metal tests both with ER70S-6 filler

46100 were defined to have identical material properties as given by GVSC, however their yield strengths are different at 158ksi and 205ksi respectively. The 12560 with ER70S-6 test group (Test D) has an $MR = 0.4146$ and an angular deformation of 2.7196 degrees while the 46100 with ER70S-6 test group (Test F) has an $MR = 0.3322$ and an angular deformation of 2.5686 degrees. In this case, the angular deformations are nearly identical, while the 12560 has an about 25% greater mismatch ratio. Considering this, it appears mismatch ratio may still have an effect on fatigue life, as the 12560 tests generally appear to have lower fatigue lives for similar equivalent structural stresses compared to 46100. However, considering the 25% difference is driven solely by the 25% difference in yield strength, at the time of analysis it could not be determined which of these two variables is contributing to the clear difference in fatigue performance between 12560 and 46100 with the same filler metal.

By spring of 2020, only the mismatch ratios, angular deformations, base metals, and fillers had been examined for trends. A fuller understanding of the effects of these variables would likely need additional testing or a new method of analysis. Data analysis was halted in April of 2020 due to the uncertainties of the growing coronavirus pandemic, so focus was shifted to preparing for prospectus. After completion of the prospectus in May 2020, it was

not possible to continue testing, so a change it was necessary to change the research focus briefly.

CHAPTER 6

Remote Research and Parametric Analysis of Test Strip Data

This chapter summarizes the steps taken following the completion of the first set of fatigue tests and the prospectus. The COVID-19 pandemic significantly impacted this research, as GVSC did not allow contractors on-base for many months as a health precaution. Additionally, there were issues with the lack of ability to test the larger 2.5” wide plate specimens. GVSC had plans to purchase and install a new fatigue tester with larger grips that could be used to fatigue test the larger plate specimens, however COVID-induced delays complicated the delivery timeline. So even if contractors were allowed back at GVSC, there was no guarantee the new fatigue tester would be available.

Knowing how these issues would delay testing, the research focus was pivoted to analysis that could be conducted remotely. After the prospectus, several issues with the first set of fatigue tests were noticed that could potentially be investigated virtually. In addition, there were a couple alternative analysis methods that could be looked into to better flesh out the existing Master S-N curve. While it would have been preferable to immediately start testing the plate specimens, shifting focus to these other methods which could be done remotely was the only available option until the pandemic situation improved.

6.1 Analytic Methods

The mesh-insensitive Master S-N curve method, while very effective for analyzing fatigue data, is not the only approach that could be used to look at the strip test data. Alternative methods have been developed that use the Master S-N curve approach in conjunction with analytic methods for evaluating the fatigue life of distorted or deformed fatigue specimens. These analytic methods work as a great point of comparison to check the validity of the Master S-N curve while not requiring in-person attendance. Therefore, it was decided to look into analytic methods for fatigue analysis.

6.1.1 Linear Analytic Method

The first analytic method employed on the strip test data was developed by Dr. Shizhu Xing, a former researcher of the Welded Structures Laboratory at the University of Michigan [23]. This method provides a generalized linear analytic method for calculating stress concentration factors for joints with angular or axial misalignments. These stress concentration factors can then be used to calculate equivalent structural stresses, and thus plotted on the Master S-N curve.

This analytic method applies Castigliano's second theorem to allow for a direct calculation of the stress concentration factors (SCFs) at a joint location with respect to both intercostal and continuous members. The paper describes how to calculate an SCF both with an axial joint misalignment and with angular deformation. While the strip test specimens are mostly angularly deformed, they do have a small amount of axial misalignment as well, so both were considered when using this analytic method.

Figure 6.1, which was taken directly from the paper, shows how various measurements of an axially misaligned specimen are defined before and after clamping. Figure 6.2 shows how various measurements of an angularly deformed specimen are defined before and after clamping. Using the definitions from the two figures for axial and angular cases, the paper details how to analytically calculate the stress concentration factors due to axial misalign-

ment (k_e) and angular deformation (k_a). These calculations can be seen in Equations 6.1 and 6.2.

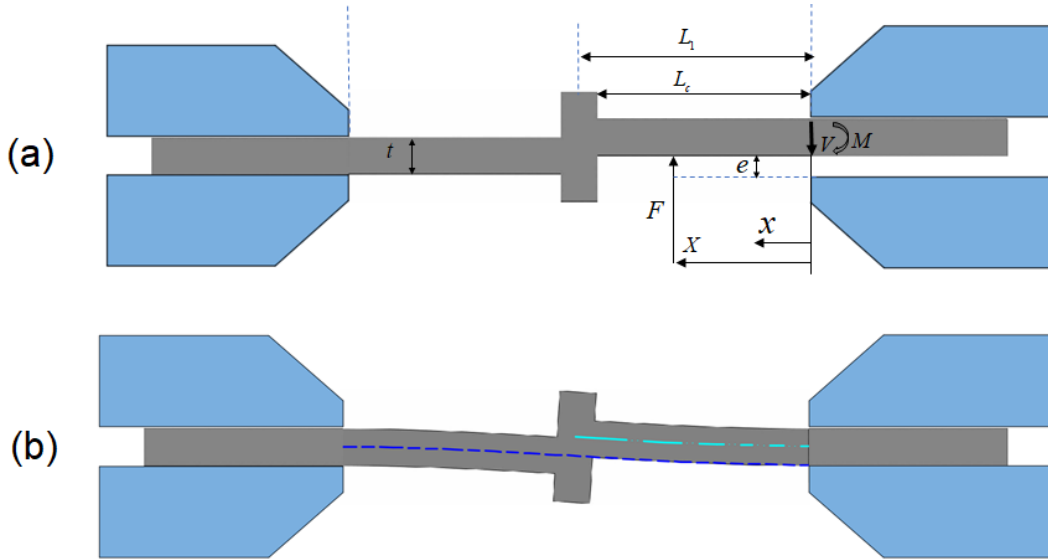


Figure 6.1: Figure borrowed with permission from Dr. Xing’s paper [23] detailing an axially misaligned cruciform clamped joint. (a) dimensions and shape before clamping; (b) deformed shape after clamping.

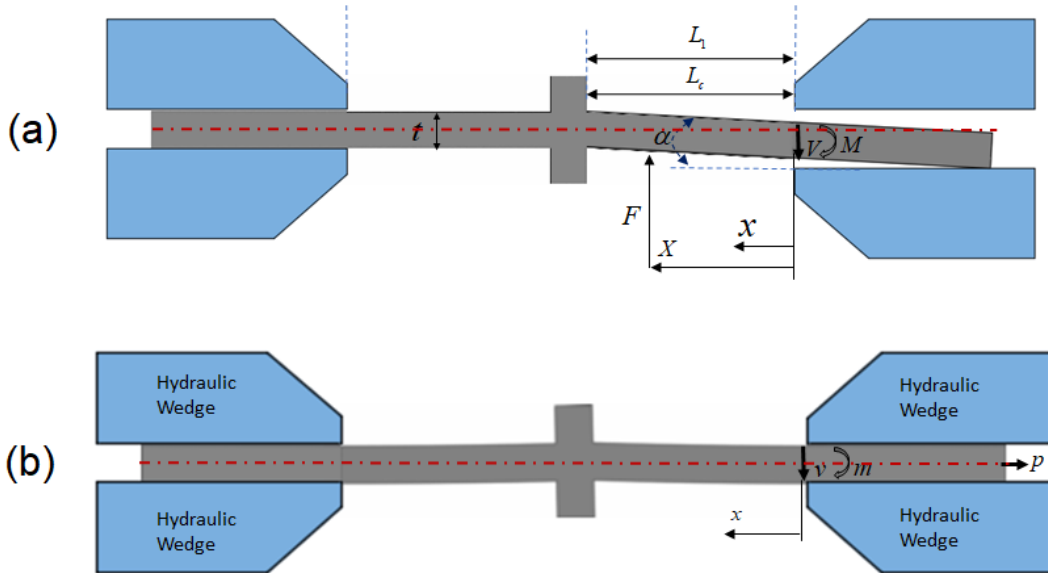


Figure 6.2: Figure borrowed with permission from Dr. Xing’s paper [23] detailing an angularly deformed cruciform clamped joint. (a) dimensions and shape before clamping; (b) deformed shape after clamping.

$$k_e = \frac{3}{10} \left(\frac{(-3L^3 + 6L^2L_c + 60LL_c^2 - 40L_c^4)}{L^3} \right) \frac{e}{t} \quad (6.1)$$

$$k_a = \frac{4}{5} \left(\frac{(L^4 - 9L^3L_c + 39L^2L_c^2 - 60L_c^3L + 30L_c^4)}{L^3t} \right) \alpha \quad (6.2)$$

With k_e and k_a , we can use the following equation to determine the total stress concentration factor at the joint location of interest:

$$SCF = 1.0 + k_m + k_e + k_a \quad (6.3)$$

In the above, the k_m term is the membrane stress concentration factor, which equals 0.05 for simple, non-deformed butt-welded plate specimens. The value of k_m was determined by modeling a perfectly straight welded strip specimen in FE and seeing the effect the geometry the weld cap has on the membrane stress concentration at that location. Because this analytic method does not account for this weld geometry effect of 0.05 or the baseline SCF of 1.0, it is necessary to add both these terms into the total SCF equation.

For each test group, we can analytically determine their k_e and k_a from its measured eccentricity and angular deformation. Then, using Equation 6.3, the stress concentration factor can be calculated for each group. By multiplying the SCF by the nominal stress of each test in the test group, the analytically determined structural stress can be found and then plotted it with the Master S-N curve results to compare. Figure 6.3 is a plot of the analytically calculated structural stresses plotted against the strip specimen Master S-N curve results.

In the the figure, the original Master S-N curve results are plotted in green while the analytically determined results are plotted in light blue. The blue “x” markers indicate a third, simpler analytic method where the nominal stress of each test is simply multiplied by a SCF of 1.05. These values are included to demonstrate what just applying the weld cap stress concentration effect has on the nominal stress of each test. From the figure, it is obvious that this analytic method has predicted a massive increase in structural stresses for each specimen, with a majority of tests being outside of the 2σ upper bound. If we

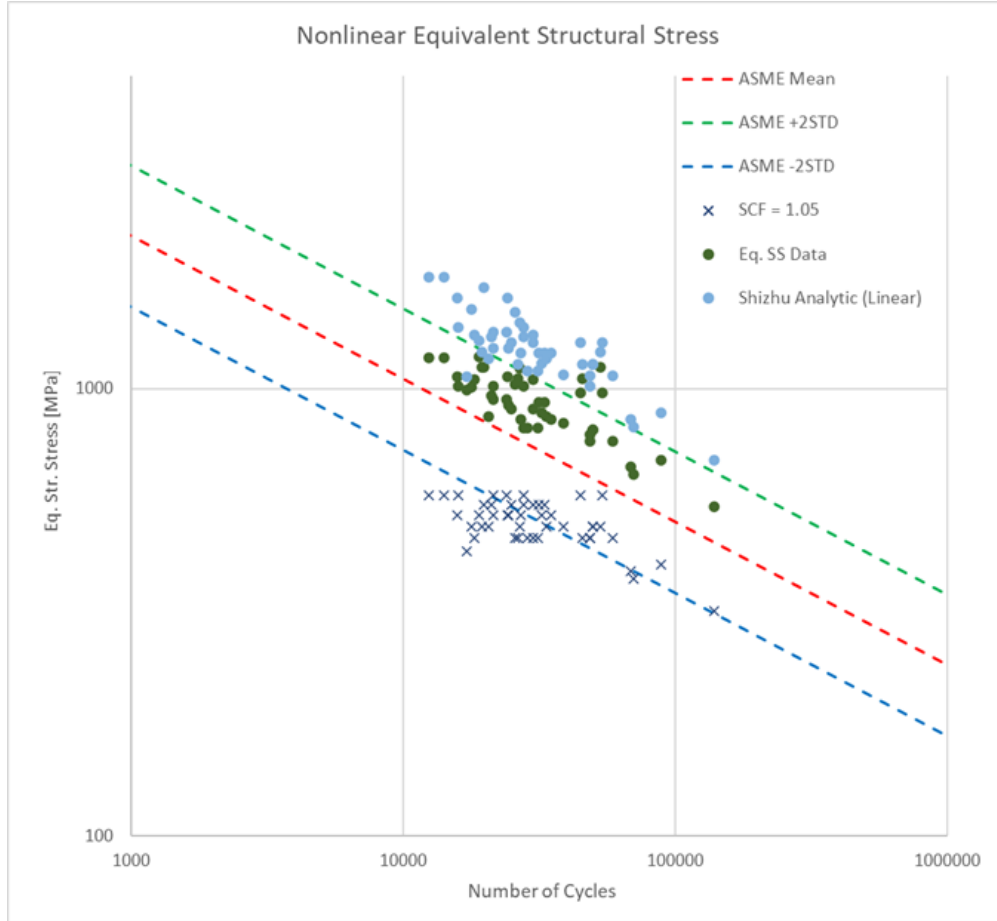


Figure 6.3: Analytic results vs. the Master S-N curve results

take a closer look at Equation 6.2, it becomes clear why this is the case. The α term, which is the angular deformation in radians, has a linear effect on the stress concentration factor. In the paper, only two specimens have an angular deformation greater than 2 degrees, whereas every specimen in the strip tests has more than 2 degrees of angular deformation, with some nearing 7 degrees total. This linear analytic method appears to be accurate for small deformation angles, but the comparatively large distortions of the strip samples are too significant for the linear effect that angle in radians α has on k_a .

While this analytic method would likely work well for less distorted data, for the strips tested a nonlinear analytic method needs is required.

6.1.2 Nonlinear Analytic Method

In order to better account for the large amounts of angular deformation in the strip test specimens, a nonlinear analytic approach is necessary. Dr. Wenqing Zhou et al. developed a more appropriate approach for large-distortion test strips. [24] This nonlinear method focuses on more complex distortion effects on fatigue behaviors of welded structures through a distortion decomposition technique. It better accounts for the nonlinear effects present in highly deformed specimens, making it more appropriate for the welded strips in this research.

This nonlinear analytic method makes note of the difference between global angular deformations and local angular deformations. A photo of sketched strip specimens, as well as a graphic from the paper showing the two distortion types, can be seen in Figures 6.4 and 6.5.

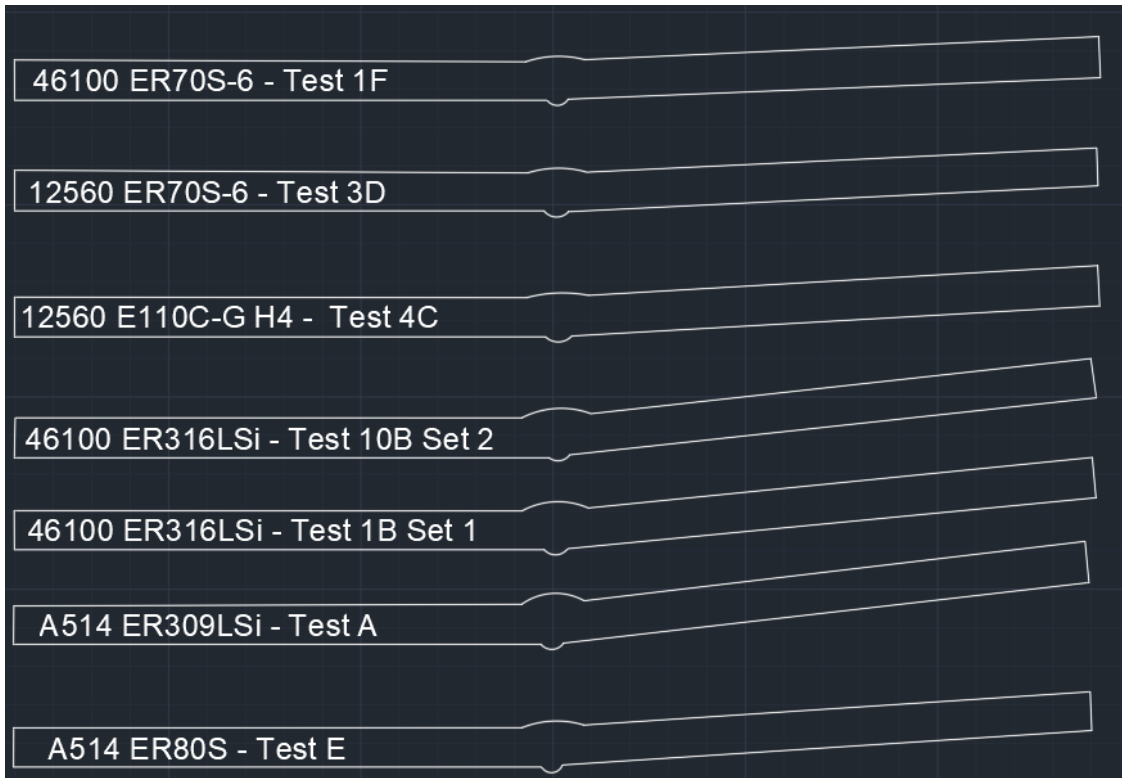


Figure 6.4: AutoCAD sketches of various test strips before clamping and testing, note the lack of curvature on either side of the weld

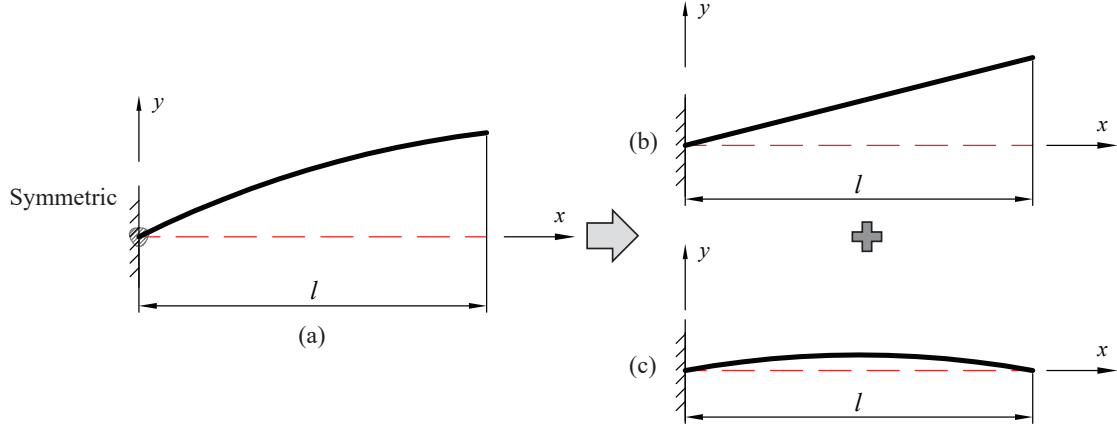


Figure 6.5: Imaged borrowed from [24] with Dr. Zhou’s permission: Decomposition of complex angular deformations in butt-welded plate. (a) a general distortion shape; (b) global angular deformation component; (c) local angular deformation component

With just a quick glance at the figures, it is clear that the distorted strip specimens do not display any localized angular deformation. The distortion in the strip specimens is purely global, as defined in Figure 6.5. While the above shows only a sample of strip specimen sketches, none of the other sketches show any local distortion either. This allows the local angular deformation component of this analytic approach to be ignored and instead focus can be solely on the global angular deformation component.

Fortunately, the calculation to determine the stress concentration factor due to bending, k_b , is fairly simple on its own:

$$SCF_b = k_b = \begin{cases} 6\theta_G \frac{l}{t} \left(\frac{\cosh(\lambda l)}{\lambda l \sinh(\lambda l)} \right), & P > 0 \\ -6\theta_G \frac{l}{t} \left(\frac{\cos(\lambda l)}{\lambda l \sin(\lambda l)} \right), & P < 0 \end{cases} \quad (6.4)$$

In Equation 6.4 above, λ is defined as $\sqrt{\frac{P}{EI}}$, with P being the applied load, E being the elastic modulus, and I being the moment of inertia. θ_G is the global angle of distortion, which is the measurement noted earlier in Table 4.1, and l is the length between the joint location and edge of grip.

Using Equation 6.5, we can determine the total stress concentration effect due to the membrane stress effect and the bending stress effect as:

$$SCF = 1.0 + k_m + k_b \quad (6.5)$$

In the equation, k_m is defined as 0.05, as it was in Equation 6.3 in the linear analytic method. There is no axial misalignment stress concentration effect term in this equation, as the addition it made to the SCF in the linear analytic method was small enough that it was deemed to be insignificant and did not need to be considered for this nonlinear analytic method.

By multiplying the total stress concentration factor in Equation 6.5 by the nominal load for each test, we can determine the nonlinear analytic structural stress for our test data. Figure 6.6 shows a plot of the Master S-N curve results, the linear analytic results from the first method, and the new nonlinear method results.

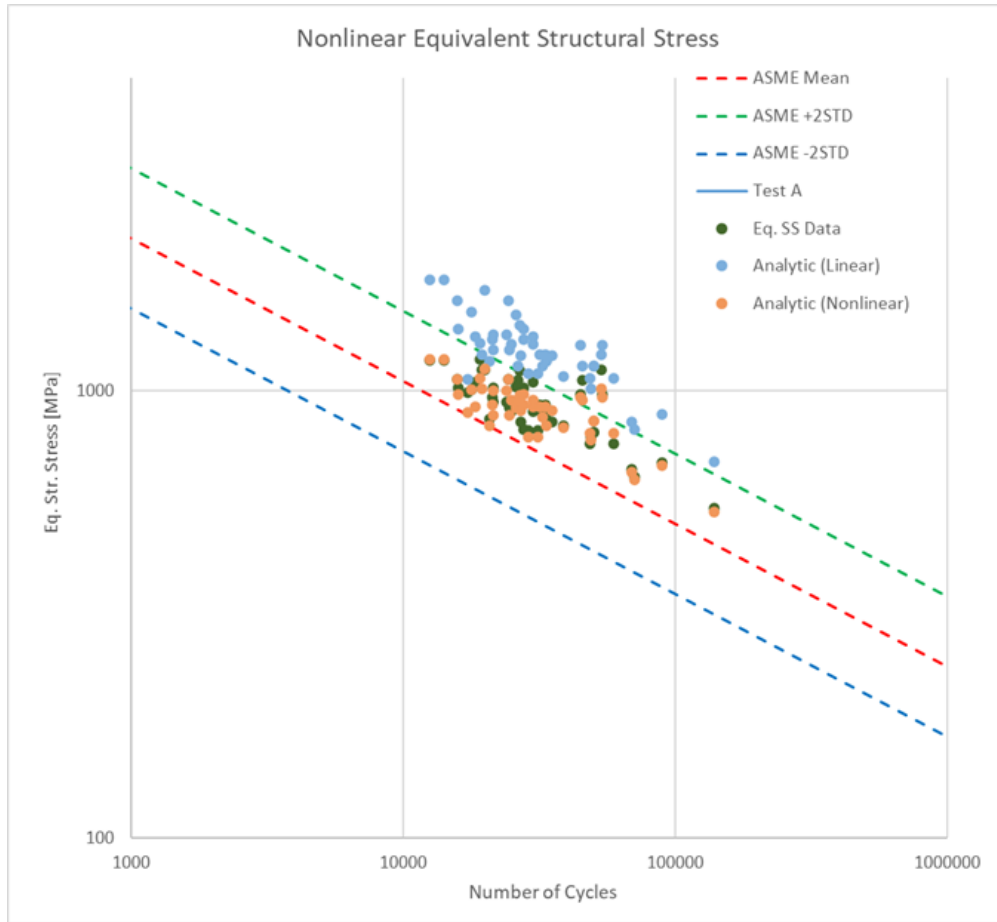


Figure 6.6: The linear analytic, nonlinear analytic, and Master S-N curve method results

From the plot, we can see that the nonlinear analytic method has much better agreement with the Master S-N curve data than the linear approach. While not an exact point-for-point match, the nonlinear analytic results show a remarkably similar mean shift as the Master S-N curve equivalent structural stress data while still having a large majority of points within two standard deviations. In some cases, the nonlinear datapoints are nearly identical to their Master S-N counterparts. The similarity between the Master S-N dataset and the nonlinear dataset gives a lot of confidence that the strip testing and analysis were done properly, and the mean shift of the Master S-N data is not due to the testing or modeling method as a whole. Since the nonlinear analytic and Master S-N curve methods are both predicting a mean shift, something else must be driving the mean shift of the data.

6.2 Finite Element Model Refinement

The analytic approach used on the Master S-N curve dataset is a valuable tool for double checking the Master S-N curve results, but it does not explain the most pressing issue with the data; the presence of a mean shift. The nonlinear analytic method also predicted a mean shift in the data, which helps confirm the original test results, however it does not help explain what caused the mean shift. If, for instance, there were unaccounted for stresses present in the actual test strips during fatigue loading, the analytic methods would not account for them similarly to how the original test data did not account for them. The presence of unknown stresses could be due to a residual stress issue from the poor width-to-thickness ratio of the test specimens or it could be to non-representative clamping in the models that over or under predicts structural stresses.

At the time, it seemed likely that insufficient clamping methods in the finite element models were likely responsible for shifting the data. From the Abaqus model outputs, it was easy to tell that the induced bending stress during clamping in the test models caused a lot of additional stress. If the clamping in the FE was inducing too much bending stress it seemed likely that it would results in increased structural stresses across the board, thus

shifting all of the test data “up” on the Master curve. It was necessary to investigate if the FE model’s clamping method and compare it to the true as-tested conditions in order to see how much of an effect the clamping conditions had on the structural stresses and Master S-N curve results.

The photograph below (Figure 6.7) is of a strip specimen after clamping in the fatigue tester. Using CAD software, the red lines indicate the vertical planes of the outer edges of the lower half of the test specimen while the cyan line indicates the vertical plane of the midpoint of those edges. In theory, if the fatigue tester appropriately bent the test specimen during clamping, then the outer edges of the bottom half should line up perfectly with the outer edges of the top half. From the photo, however, that is clearly not the case.

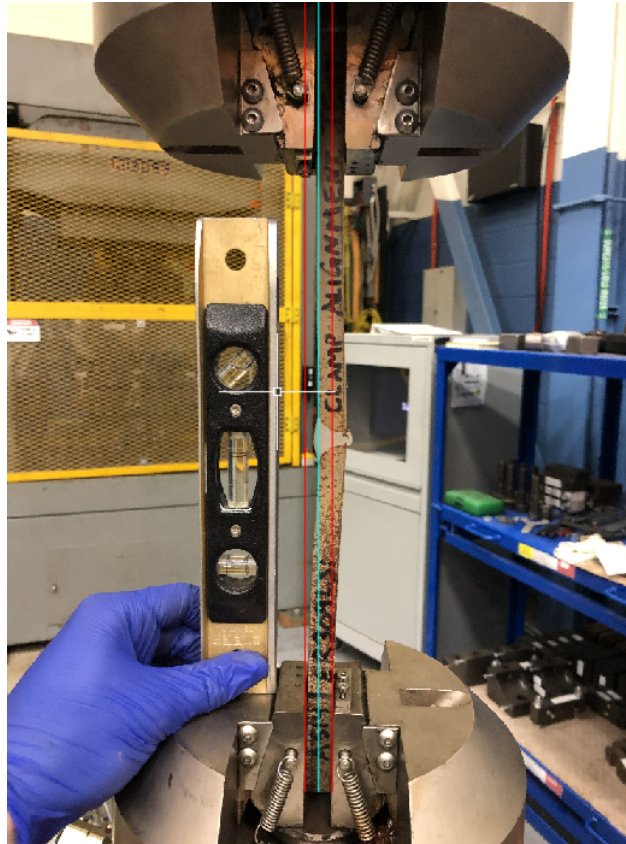


Figure 6.7: Photograph of a clamped test specimen prior to testing. The red lines indicate vertical planes of the upper and lower (outer) edges while the cyan line indicates a midsection. Note how the sample appear to be clamped more than straight.

It appears as though the two halves of the test strips do not become perfectly aligned when they are clamped with the fatigue tester’s grips. Despite their thin dimensions, the strip

specimens are still stiff enough to resist being forced into complete alignment by the grips. In fact, given the orientation of the clamped specimen in the photo above, they appear to be in a condition of being bent further than straight alignment and beyond into misalignment. Visually, it seems as though the strip is being “overclamped” by around half of its thickness. This is a concern, as the finite element models simulate the clamping conditions by using forced displacements on the nodes of the grip contact areas to “clamp” the model into perfect alignment. In order to understand the effect that the imperfect clamping the fatigue tester may have on the test strip, it is necessary to adjust the finite element model to better match it and compare the results to the current test data.

In addition to issues with the as-clamped photograph in Figure 6.7, other concerns were raised over the forced-displacement clamping method of the finite element models. Forcing the grip contact areas into alignment with displacement boundary conditions, as was done in the original model, may be too rigid of a representation and affect the clamping-induced distortion shape of the modeled specimen too much. Rather, it was decided to investigate how changing both how the clamping conditions were enforced in FE as well as how well the clamps became aligned.

Instead of enforcing a clamping condition through the use of boundary conditions like how the finite element model was made originally, a rigid body model of the clamp itself was created. This rigid body clamp, which can be modeled as a simple flat rigid surface in finite element, will be instanced above the side of the strip model that was originally using rigid boundary displacements. The new rigid body clamp can be defined as the master in a surface-to-surface contact interaction, with the corresponding area on the strip model that would be in contact with the grip defined as the slave. Then, by using a displacement boundary condition on the rigid body clamp model, we can simulate a more geometrically similar clamping condition by lowering the rigid body clamp model down into the strip model. Since one end of the clamp model is still fixed in all three degrees of freedom, forcing the rigid clamp down into the other side of the strip model will cause the strip model to deform in a

way that is more similar to the actual fatigue tester than the forced-displacement method. After deforming the model by use a rigid clamp, the clamped end can then be loaded and analyzed in finite element using the same method as the original model.

Figure 6.8 below shows an example comparing the two FE clamping methods.

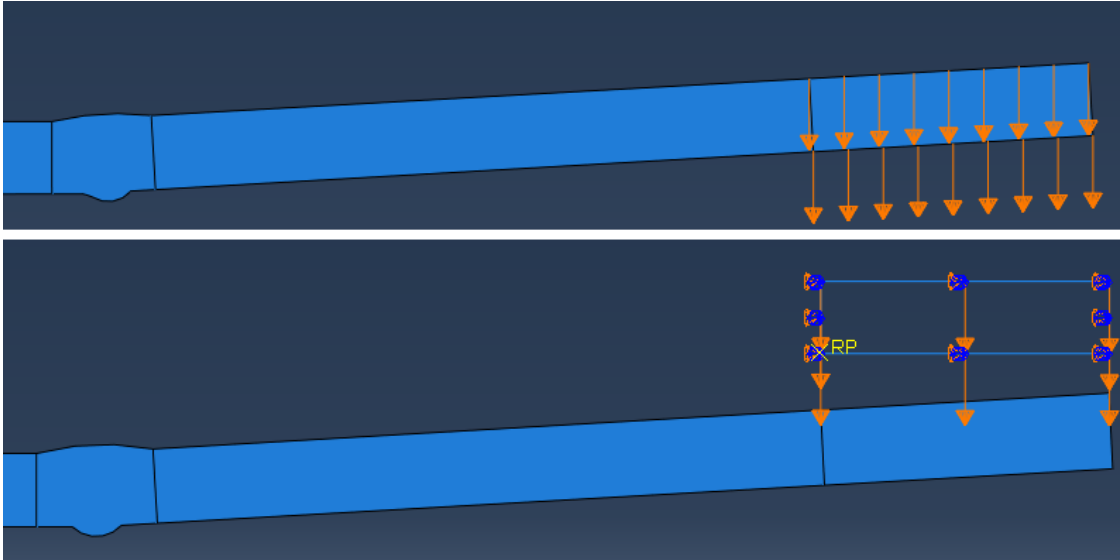


Figure 6.8: Top: A screenshot of the original clamping method using boundary conditions to displace the right (loaded) end. Bottom: A screenshot of the new rigid body clamping method, which forcibly displaces a simulated tester grip into the right end of the deformable strip model.

There was concern that only using a single rigid clamp still was insufficient for appropriately modeling the clamping condition of the fatigue tester. So, in addition to running models with a single rigid clamp, models were run for each test strip using a second rigid clamp underneath the lower surface of the strip model. This second rigid clamp would be instanced the same way as the first, and would be displaced using the same boundary condition method as the first. Figure 6.9 shows a two rigid clamp model as an example.



Figure 6.9: A screenshot of a two rigid clamp finite element model. The rigid body grips only need to exist as a surface, so they are modeled as just a line.

To summarize, there were two primary concerns with the clamping methods used in the finite element models discussed in Chapter 4.3. The first being that the models were being

clamped in such a way that ensured perfect alignment of the two halves of the strip, while in reality the actual test strips were not perfectly aligned when clamped. The second concern was that the process itself used on the finite element models to simulate clamping was too rigid and not representative of how strip specimens underwent clamping in reality. Since finite element models did not require access to GVSC, it was decided to alter the models remotely during the period of testing downtime.

6.2.1 Forced-Displacement Misalignment Test

Testing the first concern, that the perfectly aligned models were not representative of the misaligned clamped models of reality, had a bit of a caveat that made it difficult to investigate: there was only one photo of a clamped specimen. At this time, the coronavirus pandemic still prevented the continued use of the fatigue tester, so it was not possible to go to GVSC and take photos of each test combination in the clamped tester. So in order to test the effect that the misaligned clamp could have in finite element analysis on the output structural stresses, an assumption needed to be made that other test combinations deformed similarly to the one in the photo.

Additionally, it was decided just to model one test combination at first using the same forced-displacement clamping method to see the magnitude of effect that an over-clamped misalignment could have on the data. If one combination showed very little difference in structural stress outputs when comparing the misaligned clamp with the perfectly aligned clamp, it would not be necessary to run the test on all the data points for forced-displacement clamping methods. However, if the one combination showed notable difference when compared to its aligned model, they would all be run. This was mostly to save time, as using a rigid body clamping method was theorized to have a much bigger effect and we wanted the focus to be spent there.

Here is a list of all the assumptions made for to check how much a misaligned forced-displacement clamp would have on the test data:

- The alignment test strip deformed approximately half of its thickness beyond straight alignment from clamping
- All strip tests would deform to approximately the same relative amount of misalignment in the fatigue tester
- All test strips would, therefore, deform approximately half of their thickness beyond straight alignment
- The effect that misalignment would have on one test combination would be relatively similar to the others

These are fairly liberal assumptions, but given the limited data detailing the misaligned clamping and more interest in investigating a different method of modeling clamping entirely, these assumptions were made to speed up the process. The Test F combination was selected for checking the effect of a 50% overbend due to it having the highest number of individual tests and the greatest load range. Test F was remodeled with a 50% overbend in its forced-displacement clamping step, and then loaded normally. Table 6.1 below gives the original Test F structural stresses for the perfectly aligned clamping condition and the 50% overclamped clamping condition.

Table 6.1: Original Straight Clamp Structural Stress vs. 50% Overclamp Structural Stress

Test ID	Straight Alignment Stress (psi)	Misaligned Stress (psi) (50% Overclamp)	% Difference
F1	554.824	562.378	1.36%
F2	588.314	595.952	1.30%
F3	621.734	629.601	1.27%
F4	655.044	663.127	1.23%
F5	688.258	696.541	1.20%
F6	487.440	494.238	1.39%
F7	470.524	477.171	1.41%
F8	453.578	460.343	1.49%
F9	655.044	663.127	1.23%
F10	655.258	696.541	1.20%
F11	385.471	391.335	1.52%

The table suggests that accounting for the misalignments present in the actual fatigue tester clamps has a minimal effect on the total structural stress for a test combination. This is likely because applying loads up to 21,000 pounds on the finite element model has such a massive effect on the structural stress outputs of the model that the change in bending and membrane stresses experienced due to the clamping misalignment are so small that they become essentially negligible. From these results, even though the assumptions taken were rather aggressive, it appears that changing the strip model clamping alignment in the finite element model to better match the as-clamped alignment of the test strips has very little impact on the structural stress outputs from the model when still using the forced-displacement clamping method.

6.2.2 Rigid Body Contact-to-Contact Clamping Method

After analyzing the effect that an overclamped condition had on output stresses of the Abaqus finite element model, the next step was to assess the impact that changing the FE clamping method from a forced-displacement approach to a rigid body grip approach would have. In these cases, it was decided to model the rigid body grip method with both a perfectly aligned model and with the 50% overclamped misaligned model. This allows for a comparison of how both the clamping misalignment and clamping method could affect the stress outputs, hopefully helping to explain the mean shift of the dataset.

As mentioned earlier, it was also decided to make models of each test specimen using a single rigid body to simulate an actual fatigue tester grip as well as two opposite rigid bodies to simulate both sides of a tester grip. Using rigid body surface-to-surface contact interactions is significantly faster to set up than the node by node forced-displacement method, so it was comparatively quick to generate models for the new clamping methods.

In total, four new models were generated for each test combination: a straight-aligned model with one rigid body grip, a 50% misaligned model with one rigid body grip, a straight-aligned model with upper and lower rigid body grips, and a 50% misaligned model with

upper and lower rigid body grips. These models were created in Abaqus and loaded with their corresponding test strips the same way as the original test data.

Figure 6.10 below shows four plots. Each plot shows the original Master S-N curve test data which was modeled with a straight alignment clamping and the forced-displacement method. Each plot also shows a different alignment/rigid body clamping condition for comparison

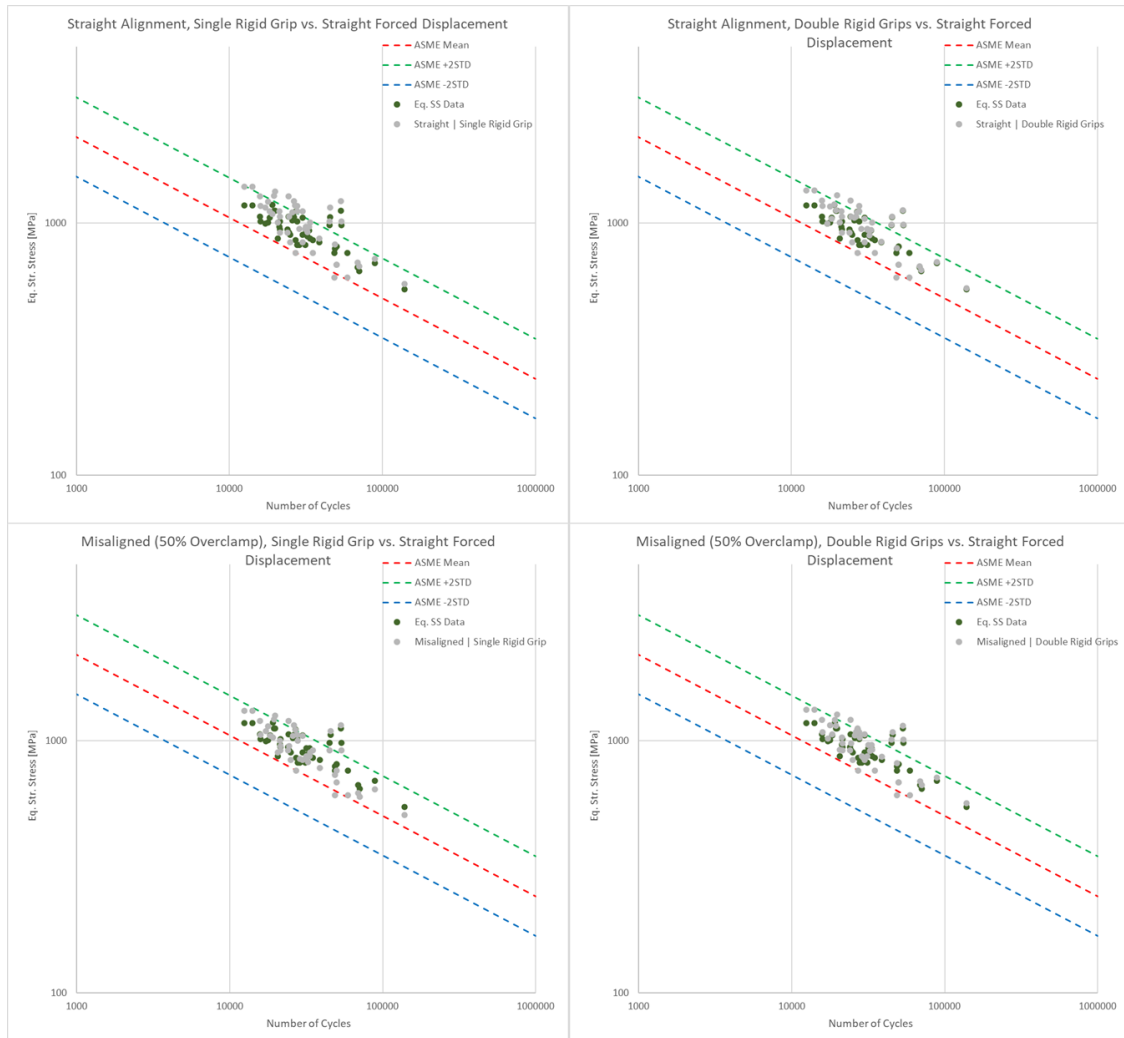


Figure 6.10: Upper left: Straight-alignment, single rigid grip. Upper right: Straight-alignment, double rigid grip. Lower left: 50% thickness misalignment, single rigid grip. Lower right: 50% thickness misalignment, double rigid grip.

Looking at the plots, it is appears that the presence of the mean shift of the Master S-N curve data is present regardless of the finite element clamp alignment or clamping method. Neither the alignment issues due to the imperfect clamping of the fatigue tester nor the

minutia of how exactly the clamping is simulated in the finite element models have any noticeable effect on the overall mean curve of the original test data. While we can pick out differences and irregularities in each of the four different modeling methods, none of them show significant change in any metric.

While it is disappointing that the extensive changes to the finite element models did not explain the mean shift in the original data, these differing modeling methods increase our confidence in the robustness of the Master S-N curve method as a whole. All four different rigid body grip contact methods had similar results and solid agreement with the original Master S-N curve fatigue results, with structural stress differences of only a couple percent for a vast majority of datapoints. Given the relative similarity in all of the outcomes, the exact method of simulating clamping in the finite element models does not have a significant enough effect on the Master S-N curve data to warrant changing away from the original forced-displacement method. Likewise, the minimal effect that incorporating the actual specimen misalignments has on estimated structural stresses also do not suggest any need to change the way the current test data is being analyzed. Again, it is likely that the relatively large loads imposed on the finite element model constitute such a large majority of the structural stress that the small effect of the clamping condition or clamp alignment cannot have a significant impact.

Since neither the analytic methods nor clamping conditions in the finite element models could explain the mean shift of the original test data, the only likely explanation left was experimentally poor width-to-thickness ratio. Understanding how the low width-to-thickness ratio of the strip specimens can provide insight as to why the strip test data could be mean-shifted.

6.3 Residual Stress Effects

The Master S-N curve is based on a large amount of fatigue test data from various joint types, loading modes, and plate thicknesses. [3] These fatigue data are from actual built structures, which still contain various residual stresses from welding and manufacturing processes as has been demonstrated in several papers. [25, 26, 27] Any effort to use the Master S-N curve method for fatigue analysis needs to consider the presence of these residual stresses.

The strip test specimens, as mentioned in Chapter 3.3, are believed to lack any welding induced residual stresses due to their low width-to-thickness ratio of 1.0. In typical fatigue testing, a width-to-thickness ratio of 10:1 is considered sufficient for ensuring residual stresses remain in fatigue test samples. [28] This being the case, the critically low width-to-thickness ratio of strip samples would present a problem when comparing them to the Master S-N curve.

The effect that insufficient width-to-thickness ratios can have on the residual stresses of welded plates is very well understood in academia and industry. Examples of this effect can be seen in a variety of literature. J. Zhang and P. Dong, working for Battelle Memorial Institute, determined a width-to-thickness ratio of at least 6:1 was enough to sufficiently capture the weld residual stresses in butt-welded plates. [29] Liang et al. investigated the effect that the cutting process has on the residual stresses of a welded joint. They determined that as the width of a welded joint decreases, the longitudinal tensile stresses of a fillet-welded cruciform joint continually relax at both the weld groove and toe (Figure 6.11). [30] Liang et al. discovered that peak value residual stresses remained steady at all width-to-thickness ratios above 10:1 and ratios below 5:1 having notably lower peak residual stresses. Altenkirch et al. had similar results with lowering width to thickness ratios in their residual stress determination trials of welded butt plates. [31]

These results would suggest that testing the welded combinations at a width-to-thickness

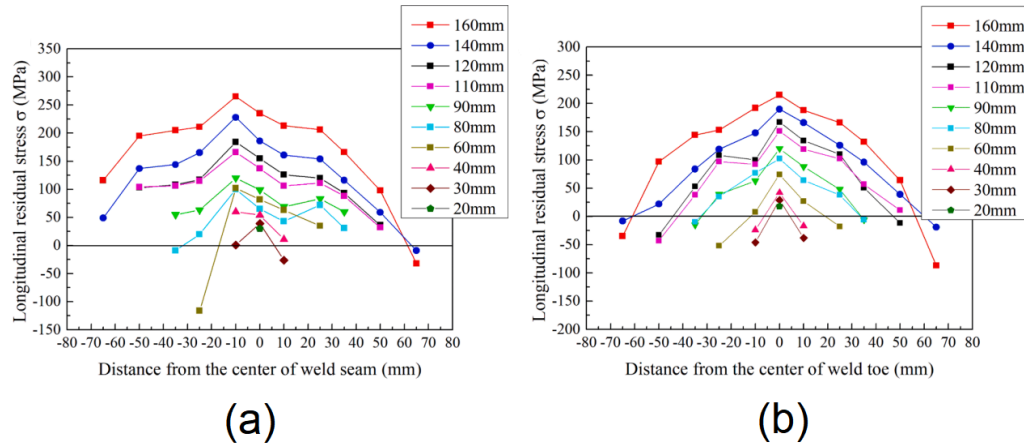


Figure 6.11: Welding residual stresses of an differing width 8mm thick steel cruciform joints at (a) the weld groove and (b) the weld root from Liang et al. [30] Note how the residual stresses continue to relax as the specimen width is reduced.

ratio of at least 5:1 would more sufficiently capture the welding induced residual stresses in the plates. Fortunately, 2 1/2" wide plate specimens with a 5:1 ratio of several of the welded base-filler combinations were already prepared for fatigue testing. However, there were two main issues with testing these wider specimens. The first being that, due to coronavirus pandemic restrictions during 2020, it was not possible to conduct more fatigue tests of larger specimens since GVSC was not allowing contractors access on base.

The second issue was that, even in the event contractors were allowed access, the wider 2 1/2" wide plate specimens could not be feasibly tested with the current fatigue tester. GVSC technicians required that contractors or employees be present to monitor any fatigue tests conducted using the Model 1333 tester. The plate specimens, which were small enough to be tested in the 1333 machine's hydraulic grips, would only be able to be tested at one-fifth of the maximum stress as the strip specimens. An 80% reduction in equivalent structural stress would likely cause a massive increase in the number of cycles to failure for these plate specimens.

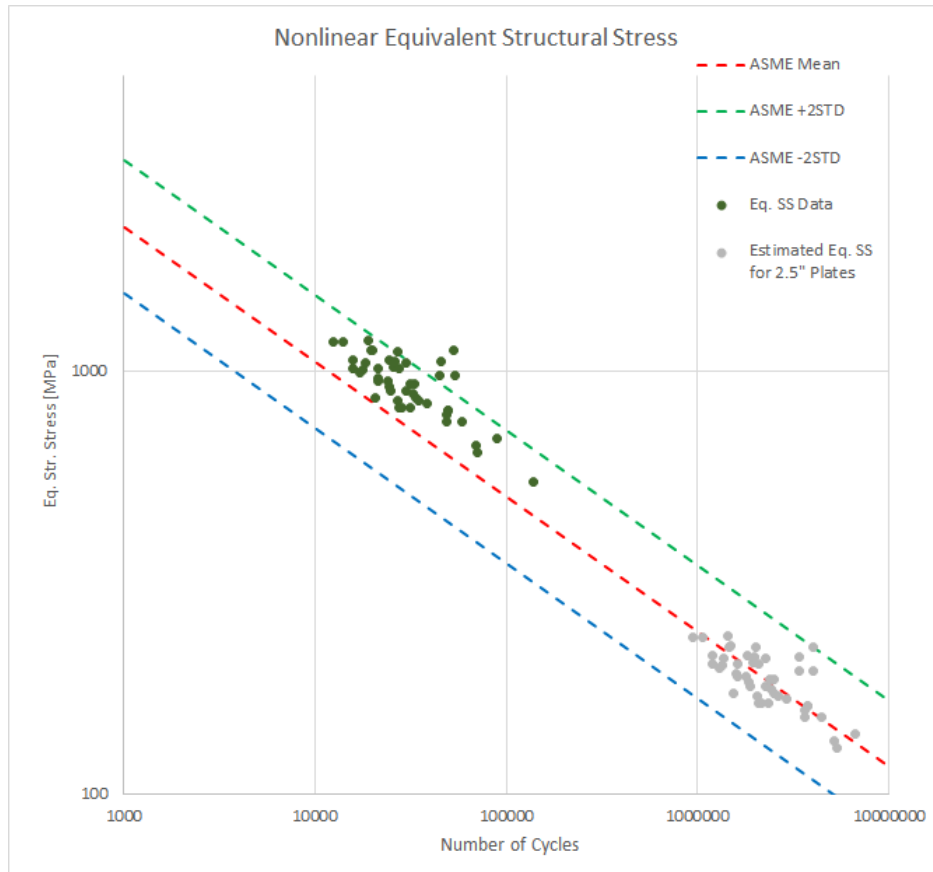


Figure 6.12: Estimate of where the 2 1/2” wide plate specimens would fall on the Master S-N curve if they were fatigue tested at the same loads as the strip specimens.

The current strip test Master S-N curve results can be used to get a rough idea of how long the 2 1/2” plate specimens would take to successfully fatigue test to failure using the Model 1333 tester. Figure 6.12 gives the original Master S-N curve results of the strip tests as well as the estimated position of the 2 1/2” plate tests if they were tested with the Model 1333 tester at the same loads as the strip tests and conformed to the Master S-N curve mean as expected due to their more appropriate width-to-thickness ratio.

From the plot it appears that the plate specimens would likely reach fatigue failure in 1,000,000 to 6,000,000 cycles. Assuming a relatively fast load-cycle rate of 15Hz, this means the plate tests would take anywhere from 18 to 115 hours each. This is a wildly unreasonable amount of time to run fatigue tests involving a specimen of this size, and cannot be monitored during the regular working hours of GVSC. So even in the event GVSC would allow non-

employees on base, the current fatigue tester could not realistically be used to test these wider specimens.

At this point, it seemed very likely that the low width-to-thickness ratio of the strip specimens was the reason for the mean-shift of the strip test data. Neither the nonlinear analytic method nor the clamping condition modeling changes had any appreciable effect on the mean of the strip data, and a significant amount of literature suggested there were notable residual stress issues due to the low 1:1 ratio of the strips. Fatigue testing the wider 2 1/2" plate specimens would prove the residual stress effect, however it would need to wait until contractors were allowed back on base and a fatigue tester with more load capacity was available for use. Since there were no other conceivable explanations for the mean-shift at this point, the focus of the remote research was switched to instead investigate ways to better understand the current strip dataset and see if there were any additional trends or observations to be made.

6.4 Statistical Methods

With a reasonable explanation of what is likely causing the mean shift in the Master S-N curve data, focus could be shifted to move on to investigating a different issue: how to quantify the magnitude that the individual variables of the test strips had on the test results given the fact many variables were coupled together. As discussed in Chapter 5.4, the specimens with the lowest number of cycles to failure and highest equivalent structural stresses were test group B. Group B had both the largest angular deformations as well as the lowest mismatch ratios. In order to better understand the extent to which each variable contributed to higher stresses and lower cycles to failure, statistical analysis would need to be performed.

6.4.1 Regression Analysis

Simple linear regression analyses were first run to see if any large, generic trends could be determined from a line of best fit. Figure 6.13 below shows four linear regressions of strip test data: Angle vs. Eq. Structural Stress, Mismatch Ratio vs. Eq. Structural Stress, Angle vs. Cycles to Failure, and Mismatch Ratio vs. Cycles to Failure. Table 6.2 below gives each regression's R-squared value and rough interpretation.

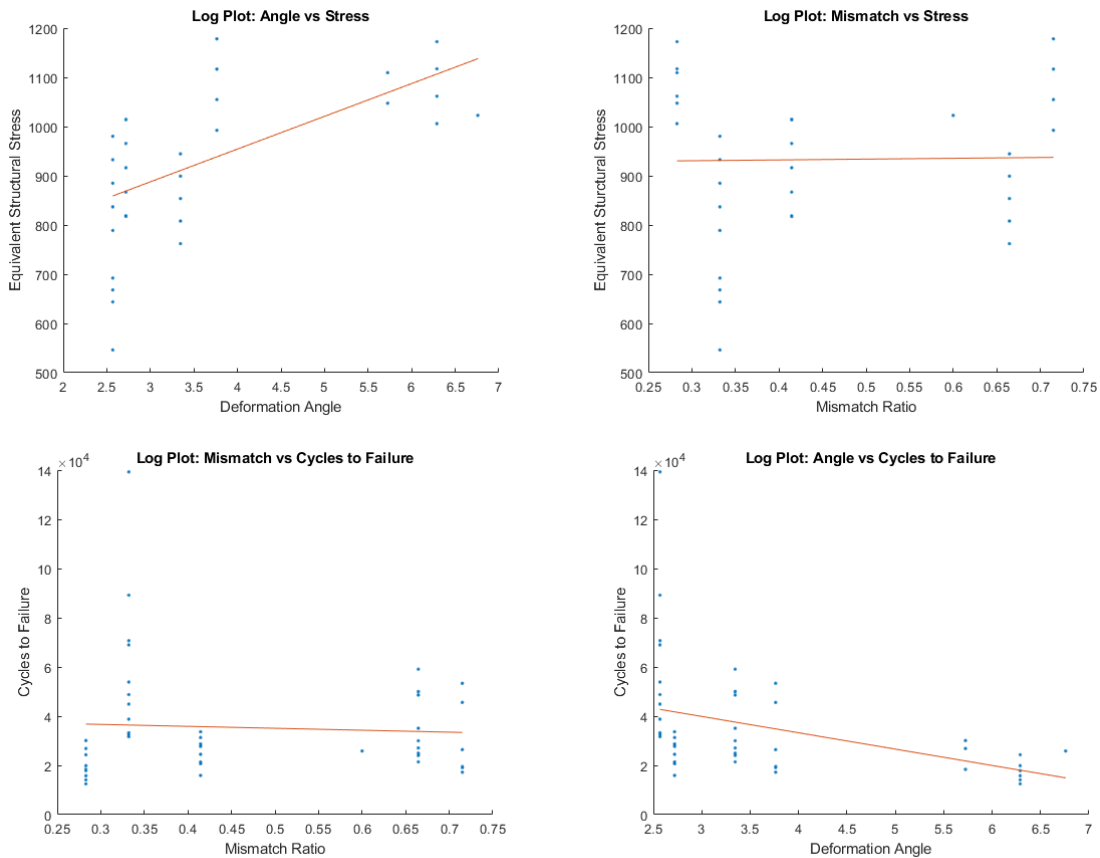


Figure 6.13: Regression lines of best fit plotted against the logarithmic scatterplot data of the test strips.

Table 6.2: Regression Analysis of Strip Test Data

Independent vs. Dependent	R ² Value	Interpretation
Angle vs. Eq.SS	0.3899	Low to moderate impact
Mismatch Ratio vs. Eq.SS	0.0004	No impact
Angle vs. Cycles to Failure	0.1625	Low impact
Mismatch Ratio vs. Cycles to Failure	0.0035	No impact

From the table and figure, we can see that the R^2 value, which is a measure of goodness of fit, is exceedingly low for three of the four comparisons. Only the regression of distortion angle vs. equivalent structural stress has a notable R^2 of 0.3899, which statistically speaking can be interpreted as a low to moderate impact. Even with this result we cannot draw any real conclusions about the relationship of these variables to the number of cycles to failure or final equivalent structural stress.

There are several shortcomings to using a linear regression on the test data set for purposes of statistical analysis. Firstly, an R^2 value of 0.3899 implies that less than half of the variation of the the equivalent structural stress could be contributed to the effect of distortion angle. This means that, at best, the regression analysis still shows distortion angle to have less impact than random chance. Additionally, the equivalent structural stress isn't the main area of interest for this research: the number of cycles to failure is. So even if we could accept such a low goodness of fit for drawing conclusions, this is not the relationship of interest in the first place. The regression of distortion angle vs. cycles to failure is much more relevant for this research, but unfortunately there is even less confidence in its goodness of fit at $R^2 = 0.1625$.

In addition, a linear regression like this ignores any polynomial or higher order relationships that could be present between our independent and dependent variables. There could be a much better fit regression for our dataset, but there just is not a reasonable way of running the high number of regressions to detect one. The limited number of datapoints to use for these regressions itself does not give a lot of confidence in their use, as simple linear regressions in particular are very sensitive to smaller sample sizes.

These above linear regressions do help to corroborate the observations and finite element results that higher distortion angles lead to higher stresses, but currently these linear regression methods are not robust enough to give us any confidence in this analysis. This leads to the question: What statistical methods are available to use that are more appropriate for examining coupled variables in isolation and analyzing the fatigue test data for trends?

Without a background in statistics, finding alternative methods can be difficult. The University of Michigan’s Center for Statistics, Consulting, and Analytics Research (CSCAR) has resources specifically for faculty and students who need help determining what kind of statistical methods are available for them to use. After meeting with CSCAR on a couple of occasions and following up on their suggestions, it was determined that a Cox proportional hazards model would be an appropriate approach for better analyzing the fatigue test strip data.

6.4.2 Cox Proportional Hazards Model

Cox proportional hazards models [32] are a class of survivability models in statistics. While typically used for disease survivability statistics or lifetime estimates, Cox PH models can also be used for analysis of product longevity. They work as a much more robust regression model for adjusting survival rate estimates to quantify the effects a “predictor” variable has on subject lifetime.

In Cox models, “predictor” variables include any independent variables of interest that may affect the “response” or dependent variables. In survival statistics, the response variable is usually duration of survival or longevity. Cox model results are represented in terms of hazard ratio, which can be thought of as an instantaneous percent chance that an event occurs. For example, a hazard ratio of greater than 1.0 represents an increased risk of predictor variable on the response variable, while a hazard ratio of less than 1.0 suggests a smaller or reduced risk of predictor variable on the response. A hazard ratio equal to 1.0 would suggest no association between a predictor variable and a response variable. These hazard ratios are useful for understanding the magnitude of effect that a predictor could have on a response.

With a Cox model, you can load in some type of dependent data denoting “responses” and any number of independent data as “predictors.” The model can then be used to generate hazard ratios for each of the predictors. This is very useful for applications to fatigue

analysis, as we can isolate specific variables of interest and investigate predictor vs. response relationships more robustly than a simple linear regression. Additionally, Cox models allow for the investigation of the predictor vs. response relationships when still considering other predictors in the dataset. The value here is immediately apparent for this research, as with a Cox model we can examine how well the angle or mismatch ratio (predictors) will affect cycles to failure (response), while still considering the other may have an effect in the data.

Creating a working Cox model from scratch could prove difficult, however MATLAB has built-in Cox model functions that are relatively simple to use. For that reason, MATLAB was selected for use in creating Cox proportional hazards models to statistically analyze the strip test data.

6.4.3 Cox Proportional Hazards Model Results

It is important to understand what the Cox model will be generating and how its results can be applied before running models. Primarily, we are interested in generating b-values (coefficient estimates) from running Cox models. These b-values can be used to calculate hazard ratios ($e^b = hr$) for each predictor in a model, which are a measure of instantaneous risk rated on a scale of positive numbers. As an example, a hazard ratio of 1.5 would imply: “as the predictor variable goes up by a unit value of 1, the hazard of failure increases by 50%.” For this research, various specimen variables discussed in Chapter 5.4 such as mismatch ratio, distortion angle, and input load will be used as predictors, and the cycles to failure of each test will be the response. This will allow us to see the instantaneous risk associated with each specimen variable on the longevity of each fatigue test.

The null hypothesis, which in statistics is the hypothesis that there is no significant difference between our test populations, is what the Cox models from MATLAB will test against. The p-value, or evidence against the null hypothesis rated on a scale of 0 to 1, is what we used to reject the it. A p-value of 0.50 implies that 50% of the time you could expect to see a set of predictor data and response data occur randomly. In statistics, a

p-value of 0.05 is considered statistically significant, thus if any of the Cox models we run on the fatigue data on result in a p-value below 0.05, we can reject the null hypothesis that there is no relationship between the predictor and response.

If a Cox model suggests a predictor-response pairing is statistically significant, the model’s hazard ratio for that pairing can be used to get a rough idea of the magnitude of the effect a predictor variable is expected to have on the instantaneous risk of breaking of a strip fatigue test. One other important statistic we need from the Cox model is the confidence interval, which we can calculate from the b-value and standard error of a Cox model’s outputs. A confidence interval is a range of plausible values for the data, e.g. a 95% confidence interval would be interpreted as “we are 95% confident that the true hazard lies between [lowerbound] and [upperbound].” While p-values are useful for determining statistical significance, they can be misleading at times due to issues with sample size. Confidence intervals are more reliable. If a model suggests a confidence interval that passes the value of the null hypothesis (i.e. contains the value of 1), there is insufficient evidence to conclude there is any statistically significant difference between groups. Even in cases where the p-value suggests a statistically significant relationship between a predictor and response, a relationship can not be concluded if the confidence interval still contains the value of 1.

Table 6.3 below is a quick summary of the important output variables from the MATLAB Cox functions and how they are used.

Table 6.3: Cox Model Outputs and Uses

Cox Model Predictor Variable Output	Use Case
b-value	$e^b = \text{hazard ratio}$
p-value	Statistically significant if $p < 0.05$
SE (standard error)	$b \pm SE = 95\% \text{ confidence interval}$

Several Cox models were run, both with single predictors passed in and with several predictors passed into the model. Running a model with a single predictor would give us an idea of if, in isolation, one of the predictors could have a significant impact on response. The main advantage of Cox’s method was the ability to pass multiple predictors into the model

at the same time, as this allows us to compare different predictors' effects to each other.

Table 6.4 below contains the MATLAB outputs and statistical calculations of the Cox PH models. A total of four Cox models were run for the strip test data, three of which can be seen in the figure. The first proportional hazards model run passed in angular deformation as a predictor and uses the cycles to failure as the response.

Table 6.4: MATLAB outputs from the Cox PH models and calculated statistics for the first two Cox models

Variable		Model #:	1	2
		Time Data:	Cycles	Cycles
		Predictors:	Angle	Mismatch
		Focus:	Angle	Mismatch
b	Coefficient Estimates	0.547	0.3105	
logl	Loglikelihood	-128.629	-136.747	
hr	-Hazard ratio	1.728	1.3641	
se	-Standard errors of coefficient estimates, b	0.1262	0.9263	
z	-Z-statistics for b (b divided by standard error)	4.3354	0.3352	
p	-p-values for b	1.46E-05	0.7375	
covb	-Estimated covariance matrix for b (diagonals)	0.159	0.858	
r2	-Coefficient of determination	0.165	0.0035	
-2 σ	-95% confidence interval (- two std)	0.2946	-1.5421	
+2 σ	-95% confidence interval (+ two std)	0.7994	2.1631	
-	- confidence interval includes 1?	No	Yes	

From the table, we can see that the Model #1 took angular distortion as a predictor and cycles to failure as the response. This Cox model generated a hazard ratio for distortion angle of 1.728. This implies that for every 1 unit (degree) increase in distortion angle, we would expect a 72.8% increase risk of a test specimen failing or breaking. This result, while fairly drastic, makes sense. We would anticipate that the more deformed a test specimen is, the more bending forces are induced during clamping and cyclic loading. This would lead to higher the structural stresses, which would result in a shorter specimen fatigue life. The p-value of 0.000014 gives a lot of confidence to this observation, as it is statistically significant. The confidence interval of 0.2946 to 0.7994 does not contain the null hypothesis value of 1, therefore we can reject the null hypothesis that there is no relation between distortion angle and cycles to failure for the strip fatigue tests in isolation. The hazard ratio implies that even a relatively small increase in distortion angle has a significant effect on the fatigue life

of these strip test specimens.

Model #2 passed in mismatch ratio as the sole predictor with cycles to failure as the response again. As we can see from the figure, mismatch ratio as a predictor has a hazard ratio of 1.3641 at a p-value of 0.7375. This would imply that for every unit increase to the mismatch ratio would result in a 36.41% increased risk of test specimen breaking. This is the opposite of what we hypothesized, as the original theory was that particularly small mismatch ratios (low weld material yield strength and high base material yield strength) would have resulted in higher hazards. According to this model, as you increase the yield strength of the weld material relative to the yield of the base, the hazard of breaking also increases. The p-value of 0.7375 helps elucidate this outcome. This p-value implies there is a 73.75% chance of the relationship between mismatch ratio and cycles to failure to occur randomly. This data is not at all statistically significant, so we cannot reject the null hypothesis that mismatch ratio has any significant relationship with the number of cycles to failure. Additionally, the confidence interval for the second model contains 1, again concluding that we cannot reject the null.

These first two models alone appear to show that presence of angular deformation has a major impact on fatigue life. On the contrary, the model doesn't suggest any relationship between mismatch ratio and fatigue life even exists. These observations are incredibly valuable for understanding the fatigue of these welded armor samples, but it is necessary to look at both predictors in tandem, not just isolation, as these two variables were highly coupled in the results of Chapter 5. The test cases with the highest angular deformations also had lowest mismatch ratios, so both variables need to be passed in as predictors in the same Cox model in order to see their effects relative to each other.

Table 6.5: MATLAB Cox outputs for Model #3

Variable		Model #:	3	
		Time Data:	Cycles	
		Predictors:	Angle, Mismatch	
		Output	Angle	Mismatch
b		Coefficient Estimates	3.6971	-0.0067
logl		Loglikelihood	-128.6285	
hr		-Hazard ratio	40.3318	0.9934
se	-Standard errors of coefficient estimates, b		0.8529	0.6379
z	-Z-statistics for b (b divided by standard error		4.3346	-0.0104
p	-p-values for b		0	0.9917
covb	-Estimated covariance matrix for b (diagonals)		0.7275	0.407
r2	-Coefficient of determination		-	-
-2 σ	-95% confidence interval (- two std)		1.9913	-1.2825
+2 σ	-95% confidence interval (+ two std)		5.4029	1.2691
-	- confidence interval includes 1?		No	Yes

Model #3, shown in Table 6.5, had both distortion angle and mismatch ratio passed in as predictors. In this model, we can see that the hazard ratio of distortion angle is relatively unchanged at 1.728 compared to Model #1. However, the hazard ratio corresponding to the mismatch ratio predictor has shrunk to nearly 1 in the joint Cox model. This appears to show that when considering both predictors in the Cox proportional model, the distortion angle is much more hazardous to fatigue life than mismatch ratio which has nearly no effect.

When looking at the p-values and confidence intervals, the distortion angle has a p-value of about 0 and a confidence interval that does not contain the null while mismatch ratio has a p-value of nearly 1 and a confidence interval which contains 1. From these, we are 95% confident that a relationship between distortion angle and the number of cycles to failure exists with a nearly nonexistent chance that the data could have occurred randomly. We are not confident any relation exists between mismatch ratio and fatigue life, as we would expect the mismatch data to have a 99.17% of occurring randomly.

The statistics from the third model are very important, as it mathematically demonstrates that the ratio of weld yield strength to base yield strength is likely not a driver of fatigue. Instead, the weld quality (by metric of the amount of angular deformation in the test

samples) cannot be ruled out as having a significant effect on fatigue life of a specimen. The ability of Cox PH models to decouple variables from each other and compare their relative impacts is an incredible tool for fatigue research.

It is important to note that all the models discussed thus far take the raw data from the fatigue specimens and tests. So, while we can examine their individual hazard ratios, they can be hard to interpret and compare to each other. This can be remedied by standardizing all of our input predictor data, making their hazard ratios and confidence intervals more directly comparable. Since the goal of using Cox models was simply to decouple variables and see if we can reject the idea that predictors have no relation to the response, it was decided that standardizing all the predictors was unnecessary. Running models with the untouched data is sufficient for the purposes of these tests. Standardizing the data in a Cox model does not change the p-values or change presence of the null in a confidence interval, so there is no risk in outcomes being different.

The primary use of the Cox models was to decouple variables, but the method can be used more to understand other variables as well. A fourth model for the strip tests was run to determine how the distortion angle and mismatch ratio statistics would be affected with the inclusion of the input load as a predictor. Table 6.6 lists of the statistics of the fourth model.

Table 6.6: MATLAB Cox outputs for Model #4

Variable		Model #:	4		
		Time Data:	Cycles		
		Predictors:	Load range, Angle, Mismatch		
		Focus:	Load	Angle	Mismatch
b	Coefficient Estimates		0.0106	0.5761	-0.4732
logl	Loglikelihood			-112.7457	
hr	-Hazard ratio		1.0107	1.7791	0.623
se	-Standard errors of coefficient estimates, b		0.0048	0.1494	1.0448
z	-Z-statistics for b (b divided by standard error		2.2268	3.857	-0.4529
p	-p-values for b		0.026	0.0001	0.6506
covb	-Estimated covariance matrix for b (diagonals)		0	0.0223	1.0917
r2	-Coefficient of determination		-	-	-
-2 σ	-95% confidence interval (- two std)		0.001	0.2773	-2.5628
+2 σ	-95% confidence interval (+ two std)		0.0202	0.8749	1.6164
-	- confidence interval includes 1?		No	No	Yes

From the table, we can see that once again the mismatch ratio confidence interval contains 1, therefore we can rule it out immediately as having no any relation to the response. Both input load and distortion angle do not contain 1 in their confidence intervals, and their p-values are 0.26 and 0.001 respectively. When considering what are likely the three most significant variables in our Cox model, both load and angle are shown to be statistically significant. This makes sense, as we expect both input load and distortion angle have a large effect on the equivalent structural stress range in each loading cycle, thus lowering the number of cycles to failure. The hazard ratio of the distortion angle is relatively unchanged at 1.7791 and the hazard ratio of the input load is 1.0107. As a reminder, in a Cox model we would associate a hazard ratio of 1 with no actual association between predictor and response. Figure 6.14 below can help explain why no association is reasonable for input load.

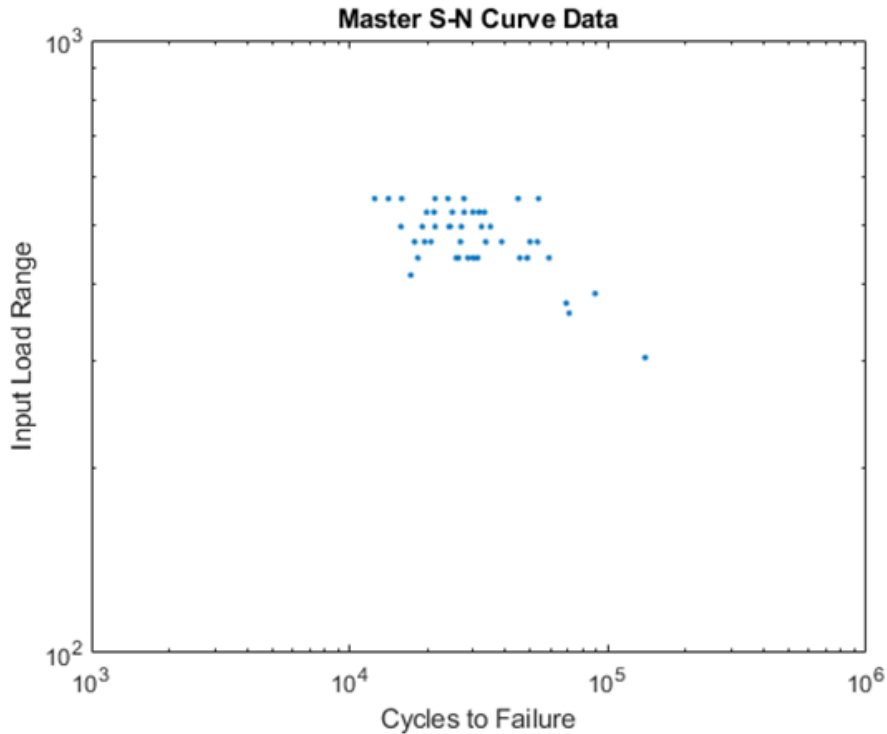


Figure 6.14: MATLAB Scatterplot of Input Loads vs. Cycles to Failure for the Fatigue Tests

The above figure gives the input load range in kips for each strip specimen fatigue test. Nearly all of the fatigue specimens failed in the 20,000 to 60,000 cycle range, except for a few group F samples that were deliberately tested to exceed 60,000 cycles. In addition, these specimens were fatigued at the exact same load ranges. Looking at the plot, it is understandable how the Cox model could predict very little to no association between input load range and the number of cycles to failure. The data appears to have no correlation at all. This is consistent with our understanding of these fatigue tests. The input load is only the source of the stress in each fatigue test. The structural stresses experienced by the test specimens during a fatigue loading cycle are scaled-up input load stresses due to the effect of specimen geometry, any microscopic deformations, and angular/eccentric distortions. Without accounting for those stress concentration effects in the model, it makes sense that the input load is essentially irrelevant to the number of cycles to failure. The vastly different stress concentration factors of the various test groups gives the data its appropriate-fitting slope on the Master S-N curve, so input loads are not as significant in

the fatigue life outcome for these samples.

Cox proportional hazards models are very useful in this line of research for situations where variables need to be separated from each other for analysis without isolating each other's potential effects. In the strip test samples, the Cox models show how significant of an impact the welding-induced angular deformations have on our test data. After fatigue testing the cut down 2 1/2" wide plate specimens, it will be important to run their fatigue data through Cox models as well in order to see if the effect of the angular deformation is as significant for the wider specimens. If not, they can be used to investigate the effects of mismatch ratio or other variables on the fatigue life of the welded plate specimens.

6.5 Remote Research Conclusions

While the switch to remote research efforts was mostly due to the inability to test, the remote projects were still valuable for understanding the dataset.

The analytic methods investigated during the pandemic lockdowns were useful for confirming that the results of the Master S-N curve were valid, even if they did not explain the mean shift of the test strip data.

The alternative clamping conditions and methods that were modeled during the remote research period were useful in determining how sensitive the Master S-N curve method was to modeling changes. While changing specimen alignment and gripping method can affect the output stresses, they ultimately were not significant enough to explain either the data mean shift or fall outside the expected variance of the Master curve. In conjunction with the nonlinear analysis agreement with the dataset, the changes made to the Abaqus models helped show that the mean shift is not a result of our testing or analysis processes but likely a consequence of the test specimens themselves.

With the analytic and finite element approaches both failing to explain the mean-shift of the strip data, the low width-to-thickness ratio of the strips was the most likely culprit.

Extensive study of how residual stresses can change due to the width-to-thickness ratio lend credence to the theory that testing the wider 2 1/2" plates would solve the mean-shift problem. The inability to access the GVSC lab due to coronavirus restrictions and the limitations of the available fatigue tester made it impossible to prove the residual stress effect until conditions changed and new equipment was available.

The Cox proportional hazards models that were investigated and developed remotely are extremely valuable as a post-processing analysis method. Their ability to decouple angular deformation and mismatch ratio alone makes them useful for this research in particular, but their ubiquity in examining multi-variate survivability data has extensive value in any type of fatigue research. Cox models were an unexpected but welcome discovery during this remote research.

CHAPTER 7

Welded Armor Plate Testing

This Chapter details the return to fatigue testing at GVSC. In order to test the larger plate specimens, alterations to the test plan, testing process, and modeling needed to be made.

7.1 Plate Specimen Test Plan

The two main issues that delayed the testing of the 2 1/2" wide plate specimens were, as mentioned in Chapter 6.3, the COVID-19 pandemic and the lack of appropriate testing equipment. From the start of the pandemic in March of 2020, no contractors were allowed on base at GVSC. This restriction was in place until late fall of that same year. The inability to test during that period led to the remote research of statistical methods, alternative analytic approaches, and modeling adjustments for the strip test data.

Additionally, the lack of sufficient testing equipment to fatigue test the wider specimens was another problem. Specifically, while the Model 1333 fatigue tester had a large enough frame to handle higher load fatigue tests, it did not have sufficiently large hydraulic grips. The hydraulic grips on the tester used for the strip specimens could only sustain a maximum tensile load of 22.4 kips, even though the tester and frame themselves could handle much larger loads. As shown in Figure 6.12, testing the 2 1/2" wide plates on the original fatigue

tester would massively increase the fatigue life of the specimens beyond the point of being reasonable.

This was a significant problem. Fortunately, GVSC had plans to purchase and install another fatigue tester. This new tester would have larger hydraulic grips with more capacity to allow for higher load tensile fatigue tests. In addition, the tester was to be installed in a private room for the express purpose of letting it run unattended overnight. GVSC also indicated that this research would have priority in using this new tester, so once it was installed fatigue testing the plate specimens could begin immediately. However, by the time contractors could come back on base in December 2020, the tester had still yet to be ordered. By February 2021, the new tester had been ordered and was awaiting delivery. By midsummer, the tester was delivered and being installed while a private room was being constructed for it. At end of September 2021, GVSC finally gave the all clear for contractors to use the fatigue tester with some specific restrictions regarding when testing could be conducted and how tests would be set up. These restrictions would not hinder the research, as we still were given control to determine and program the testing parameters for these fatigue tests, so there was no issue with GVSC's requests to continue testing.

A new test plan was developed for the 2 1/2" wide plate specimens. As discussed in Chapter 3.3, there were a total of 12 available 14" x 5" x 1/2" plate specimens of three base-filler combinations that were shipped from Pacific Northwest Laboratory in Richland, Washington. In order to reduce the cross-sectional area of the welded specimens and increase the number of available specimens, these 5" wide specimens were water-jet cut in half at GVSC during the summer of 2019. This left 24 total 2 1/2" width plate specimens for testing. At the time, it was believed that these limited number of plates could be tested first, and then more could be requested for additional testing if necessary. When the coronavirus pandemic hit, it was no longer feasible to have more plates shipped out of Washington and cut down, so these 24 ended up being the only plates available for fatigue testing. Table 7.1 below gives the base and filler combinations for these available plate specimens.

Table 7.1: Selected base-filler combinations for plate testing

Test ID	Base-Filler Combination	Equivalent Strip Combo?	# Available	# Tested
G	46100 with ER316LSi	Same as Test B	8	7
H	12560 with E110C-G H4	Same as Test C	8	6
I	12560 with ER70S-6	Same as Test D	8	6

These test group combinations were selected for plate testing after consulting with GVSC because they represented the most likely combinations that the US Army could see in armored vehicles. These three combinations allow for fatigue testing with a high hardness base and stainless steel filler (Test G), the largest mismatch ratio with an armor steel base material (Test H), and a base-filler combination that is frequently used in armored vehicles (Test I). Welded combinations of A514 steel were intentionally avoided, as again they were not high priority for Army purposes. Due to the limited number of plates that could be shipped, it was decided to focus on Army relevant combinations as opposed to the strip samples which were easily available at GVSC.

Eight specimens for each group were available for testing, however only six tests were planned for each combination. After consulting with the committee, 18 tests were considered sufficient for testing. This would also leave two unused plate specimens for each group in the event more data was deemed necessary or a test needed to be redone.

7.2 Plate Specimen Procedure Adjustments

Due to the differences between testing the strips with the old fatigue tester compared to testing the plates with the new one, there were a number of adjustments that needed to be made to the testing process in order to assure GVSC that their new equipment was being used properly.

The biggest change in testing procedure was the inability to run tests by ourselves. After some internal discussions, GVSC stated that contractors would not be allowed to setup or operate the new fatigue tester by themselves. Instead, they required that one of the employees who was trained by Instron, the machine's manufacturer, be the only person to

operate the new tester. Contractors would still be allowed to select which tests to run, what parameters to choose, and determine how to conduct the tests with the stipulation that every test be approved and started by their materials science engineer. While this made the process slower, as testing was limited to the availability of an already busy employee, this was not a large concession to have to make.

Another big difference in testing the plate specimens was the introduction of specimen flattening. After meeting with and discussing the test plan with Ian Toppler, the materials engineer who would be operating and monitoring the fatigue tests, it was discovered that the angular deformations of the welded plates were too large. The deformed 2 1/2" wide test specimens were too distorted to fit in the new fatigue tester. In addition, GVSC had concerns that even if the distorted plates could fit, the counter-bending forces induced into the fatigue tester frame during clamping would potentially be damage the new tester. This is an understandable concern, as a far larger counter-moment would be induced into the testing apparatus with the wider plate specimens than the thinner strip specimens with the old tester. After some discussion and approval by the committee, it was decided to use a hydraulic press to manually flatten the bent plate specimens to be straight and level. This would allow them to be used in the new fatigue tester. Figure 7.1 on the next page is a photo demonstrating how plate specimens were flattened for testing.

A method of straightening the plate specimens was developed by using a hydraulic press and a couple of steel blocks to create a four-point bending machine. A single plate specimen would be flipped upside-down and placed on top of two large support blocks on the hydraulic press frame. Using calipers, the specimen would be centered with respect to the hydraulic piston in the specimen length and width directions. Then, the portions of the specimen that hung over the support blocks would be measured in all four corners and adjusted as necessary to be equal. When the overhang distance in each corner was equal, the specimen was symmetrically spaced and perfectly perpendicular to the support blocks it rested on. Afterwards, a nearby steel wedge that was dubbed a "boot" was turned upside-down and

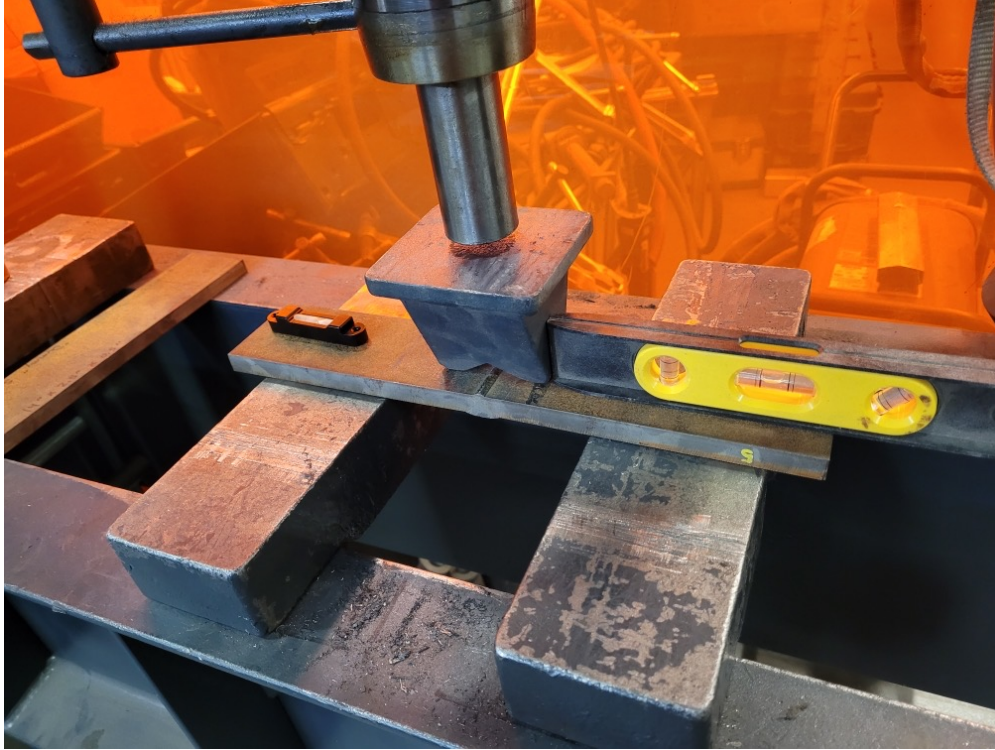


Figure 7.1: Flattening a plate specimen with a hydraulic press

centered above the root of the flipped plate specimen. The boot was necessary to distribute the bending force away from the weld root, as we did not want to alter the root or HAZ during hydraulic pressing. The hydraulic piston was then slowly lowered until it made full but light contact with the bottom of the boot. Using calipers, more checks were made to ensure the upside-down boot and flipped specimen were both correctly centered with respect to the hydraulic piston.

Once the positioning and centering of the hydraulic press setup was ready, the steel blocks were both checked to ensure they were level. Then, a small level was placed on one of the edges of the plate specimen. This was done to allow for checking how level the specimen was during straightening. Hydraulic pressure was slowly increased, causing the piston to press down on the boot, which in turn began to bend the specimen back to being straight. This jerry rigged four-point bending machine proved to be a very effective method for straightening the plate samples. Plate samples were pressed until they were determined to be level. Then, after confirming this by checking the four corners of the plate, the press

was left to sit for a couple minutes. This was to let the bending-induced residual stresses have time to settle. Just pressing the plates to be level was not enough to sufficiently straighten these plates, however. If the hydraulic cylinder was lifted just at this point, the plate would spring back into a deformed state. It was necessary to force plastic deformation into the plate such elastic response of the plate after removing the hydraulic piston would spring the plate into a flat, undeformed shape. Thus, the hydraulic load on the boot would be increased further on the visually flat specimen, causing it to become bent in the opposite direction, before reducing the load and checking the elastic response. If the plate was able to spring back into a level shape as determined by checking its corners, then the specimen was sufficiently flattened. If the plate was not level after applying plastic deformation and allowing it to spring back, the process would be repeated until it was level. Typically, the plate would be successfully straightened the first try, with a few specimens requiring two or three attempts to achieve the proper amount of plastic deformation. These four-point bends were sufficiently low in number that they do not need to be considered low-cycle fatigue.



Figure 7.2: A successfully flattened specimen

Each specimen was flattened using this bending method before testing. After flattening, each specimen was manually wire-brushed to remove surface rust from the areas that would be clamped by the fatigue tester grips. At this point, specimens were examined for any damage or irregularities and sketches of the newly flattened specimens were made for future use in CAD.

The new fatigue tester, as detailed in Chapter 2.3, had wedges with a 4" x 4" gripping zone, so care had to be taken that the 2 1/2" wide specimens were properly seated and centered relative to the grip zones before clamping. A tilted or offset specimen could invalidate test results and damage the machine, so centering brackets were used to ensure every specimen was appropriately aligned with the grips.

Flattening the specimen to fit in the new fatigue tester has major implications on the fatigue tests themselves. In the strip specimens, bending was induced while clamping in the grips. This bending contained both elastic and plastic deformation. During a fatigue cycle, tensile loads would axially pull the strips. If the strips had unresolved bending stresses and deformations from being clamped, additional bending stresses would be introduced while loading. While this effect is accounted for in the finite element models, it is not present in the 2.5" wide plate specimen tests due to the fact that they are straightened. Thus, it is necessary to adjust how the finite element models simulate the new grip clamping condition of the plate tests.

7.3 Finite Element Model Adjustments

As mentioned in Chapter 4, the strip fatigue tests were modeled in Abaqus. The first step of their analysis, which was investigated further in Chapter 6.2, involved using a displacement boundary condition to simulate the forced bending of the strip model during the clamping step of the analysis. Since the plate specimens were required to be straightened before testing, the clamping step of the finite element model needed to be adjusted to account for

this.

Fortunately, this change made running the finite element models easier, as it required less work to model and clamp a straight specimen than a distorted one. Figure 7.3 below is a screenshot of the new finite element model clamping step.

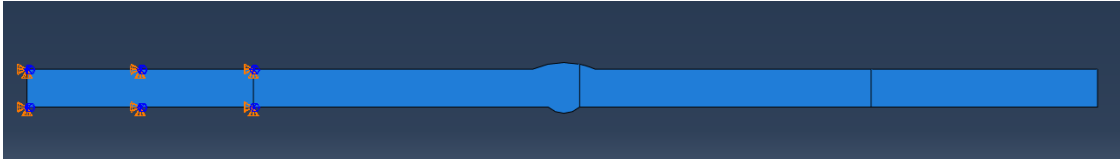


Figure 7.3: Screenshot of the simplified clamping condition. The left end is fixed in all three degrees of freedom on its grip contact surfaces. The right end does not need to be fixed, it only needs to be loaded at its contact surfaces.

Sketches of the plate specimens were taken before flattening and testing. Only a few sketches of plate specimens were taken after flattening. These sketches were taken and imported into CAD software and were shown to have an inconsequential amount of angular deformation. This means that the four-point bending method used to flatten the samples was successful.

Similar to how the strip specimens were modeled in Abaqus using a median strip sketch to represent their entire Test ID group, pre-flattened plate specimen sketches were also compared in CAD to see if they were approximately equivalent. For the plate specimens, all three test groups again showed less than 1% variation between specimens in their group, so it was determined to be appropriate to select one median plate specimen sketch to again represent the entire group. Since not every flattened specimen was sketched, the median sketches for each test group needed to be redrawn to be straight in CAD before being imported into Abaqus.

After examining the two straightened sketches of plates in CAD and comparing them to their pre-flattened counterparts, three main observations were made, the first being that the length of the flattened specimens remained at approximately 14" long, so none of the welding, bending, or straightening of the specimens had any effect on total length. The second observation was that the radius of the weld cap of the straightened sketches and their

pre-flattened counterparts were also nearly identical. This meant that, during straightening, the weld caps would increase in arc length but not change radius. The final observation was that roots of the weld, where the filler metal would collect and form a droplet-like shape, was unchanged between straightened and pre-flattened sketches. This implies that during the straightening process the root acts as the center of rotation, and thus any displacements or rotations around it are very small.

With those three observations, the distorted sketches of the median test number from each group could be approximately flattened so long as the overall length was kept at 14", the weld cap maintained the same radius, and the root remained unchanged. Figure 7.4 below offers examples of these observations and how they were implemented to make straightened sketches for the plate specimens.

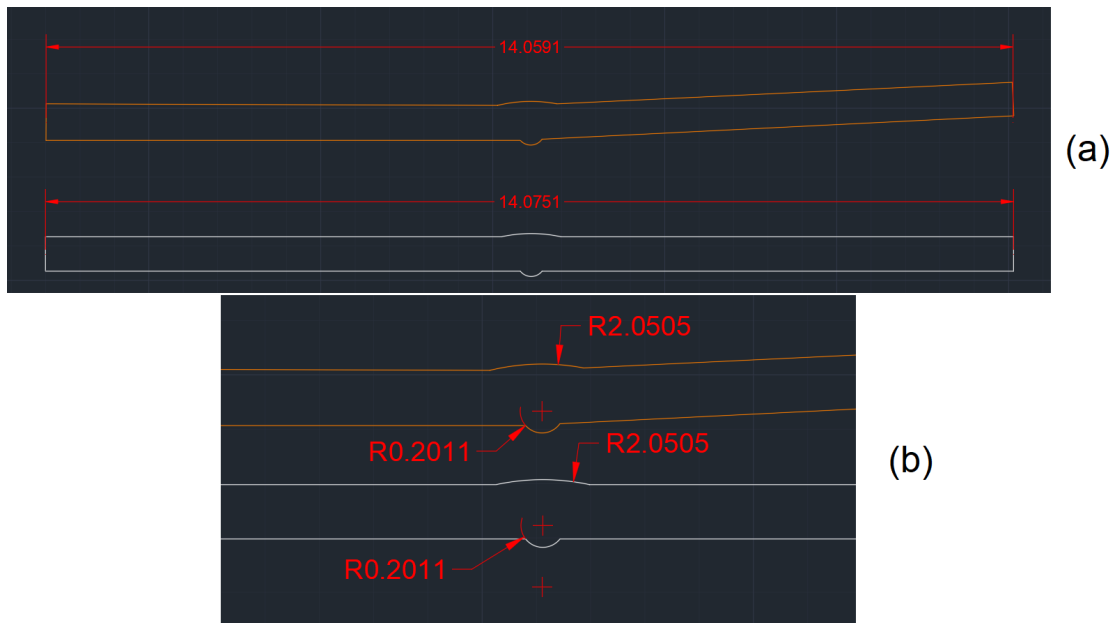


Figure 7.4: AutoCAD screenshots showing examples of: (a) equivalent OAL between deformed and straightened sketch, (b) equivalent weld cap radius and identical root radius of deformed and straightened sketch

With the straightened sketches complete, each of the plate fatigue test groups could be properly modeled in Abaqus without needing to simulate the clamping-induced bending.

7.3.1 Root-cracking Revisited

Before discussing the final Master S-N curve results for the plate tests, a few adjustments needed to be made to account for how the plate specimens were failing during fatigue tests. During the strip specimen tests, there were a handful of irregular cracking cases detailed in Chapter 5.2 that we considered to be faulty. In those cases, the fatigue crack did not initiate at the groove as it did in the large majority of strip specimens, they instead initiated at the root of the weld.

At the time, it was decided to remove these root cracking cases from analysis. That option was not available for the plate specimens that had crack initiation at the root, however, as about halfway through testing every single plate fatigue test had root cracking. (See Figure 7.5) A different approach than avoiding the root cracking cases needed to be developed due to the limited supply of plate samples and the ubiquity of root cracking.

Previously, it was theorized that there was a lack of fusion during welding in those particular strip samples with root cracking. Insufficient fusion would lead to a gap between the weld material and base material at the root. This gap would act as a pre-crack, and fatigue damage would propagate from this location due to stress concentrations being higher than at the groove. Due to the small number of strip samples that experienced this, it was acceptable to ignore these cases entirely. Halfway through testing plate samples, however, and it was becoming clear that root cracking was present in all of the plates regardless, so it was necessary to develop a better understanding of what was occurring in these plate specimens.

The simplest explanation for root cracking would be that there was some sort of pre-crack in all of the plate samples. If these plates all had pre-cracks at their weld roots, it would explain why fatigue cracking kept initiating from there. These samples sat idle for a number of years before testing, and their non-stainless base materials and filler metals were covered in a layer of rust. If there was a pre-crack present in these plate samples, we would then expect to see rust covering the pre-crack on their fracture surface. Therefore, we can check



Figure 7.5: Root cracking in a plate specimen

for a pre-crack by examining the fracture surfaces for any signs of rust.

Several plate specimens were broken open after their fatigue testing using the hydraulic press in order to get a better view of their fracture surface. These fracture surfaces were digitally photographed, and these photographs were imported into both CAD and photo editor software in order to examine them closely. For the plate test groups that did not have stainless steel filler metals (Test H and Test I), we would expect rust in a pre-crack to be present on either the filler or base metal. Test G, which had a stainless steel filler, we would

still expect to see rust on its base metal fracture surface, however there may not be any on the stainless steel side due to its corrosion resistance.

After visually inspecting the fracture surfaces and digitally examining the photographs of the fracture surfaces of all three test groups, the presence of any rust was not detected in any test group. Figure 7.6 below shows the fracture surface of Test 3H, which appears to not only lack any rust but doesn't suggest visible presence of a pre-crack at all. Other samples that were broken open after testing had the same issue of no visible pre-crack or rust. This was puzzling, as the existence of a pre-crack was the most likely cause of fatigue initiation at the root. While it was possible that a pre-crack was too small to detect in digital photographs, we did not have the ability to microscopically examine the fracture surfaces at GVSC. Fortunately, they did have a dye penetrant test kit that we were given permission to use.

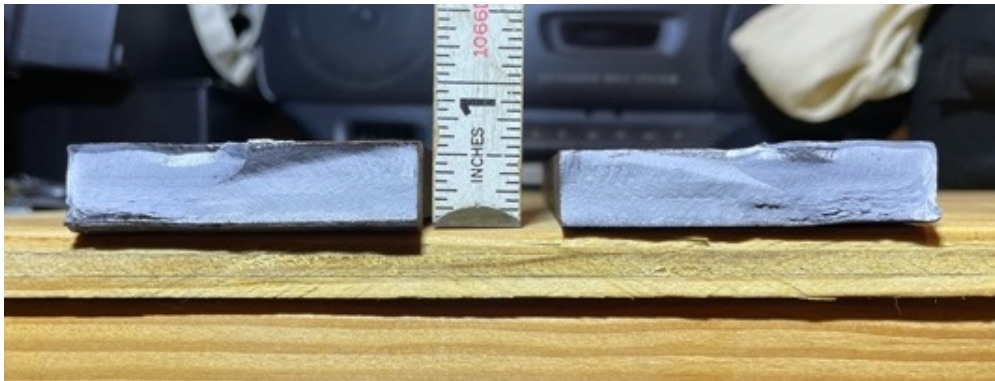


Figure 7.6: Test Group H specimen fracture surface. There does not appear to be any evidence of rust

Using a dye penetrant test, we could forcibly dye the root of an untested fatigue sample. Then, after fatiguing it to failure, we could break it open and examine the fracture surface for the presence of dye. The dye would be visually much easier to see than rust, plus it would be likely to help us better identify the depth and location of pre-cracks as well. So, a seventh Test G plate specimen was planned during testing for use in a dye penetrant test. Before fatigue testing, it was hit with surface sample cleaner, dye penetrant, and developer and let to sit for 20 minutes. Photos taken before and after letting the developer sit can be seen in Figure 7.7.



Figure 7.7: Dye penetrant testing for Test G before (left) and after (right) letting the developer sit. Note that there does not appear to be any obvious cracks at the root in either photo as expected for dye penetrant tests.

After taking photos, the surface of the dye penetrant specimen was wiped down to stop any dye or developer from shaking off the sample during a fatigue test and making a mess. Wiping the surface would not have any effect on dye that worked its way down into any cracks, so cleaning the specimen is acceptable. After wiping, the sample was fatigue tested to failure. Once it was successfully tested to fatigue failure, the dyed specimen was cracked open using the hydraulic press and photographed for examination in CAD. Figure 7.8 on the next page is a photograph of the dye-pen test G specimen's fracture surface.

From the figure, there is no red dye anywhere along the fatigue cracking of the specimen. If there was a pre-crack in the stainless steel filler Test G plate samples, dye penetrant would have seeped through during application and it would be visible on the fracture surface. This appears to show fairly conclusively that there was no pre-crack in these root cracking cases for the plate specimens, despite the presence of crack initiation at the root. In order to check this, another dye penetrant test was performed on a yet-to-be tested test group H sample. This test group H specimen is the one shown in Figure 43 above, and it also did not show

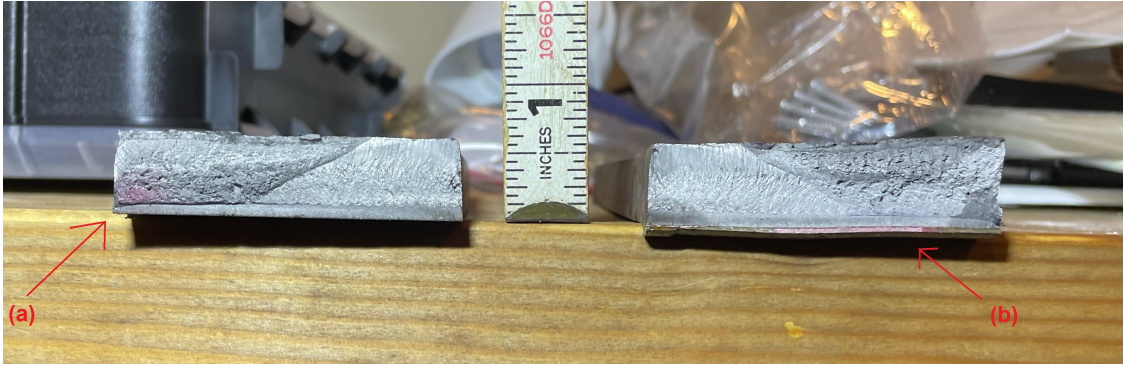


Figure 7.8: Test 6G, which was dye penetrant tested before fatiguing. (a) small amount of dye in the unstable fracture zone from after fatigue testing; (b) a small amount of dye is present on the external part of root. Neither (a) nor (b) are indicative of penetrant seeping through a pre-crack

any dye staining on its fracture surface, nor did it show the presence of rust after testing.

For both dye penetrant tests, the lack of rust or dye penetrant anywhere on their fracture surfaces is sufficient to conclude a pre-crack was not present. For the test G case in particular, however, there does appear to be an odd band of texture at the bottom of the fracture surfaces that was initially believed to be a pre-crack (circled in Figure 7.9). Since it did not contain any dye or rust, it could not be a pre-crack, but it was obviously different than the other areas of the fracture surface.

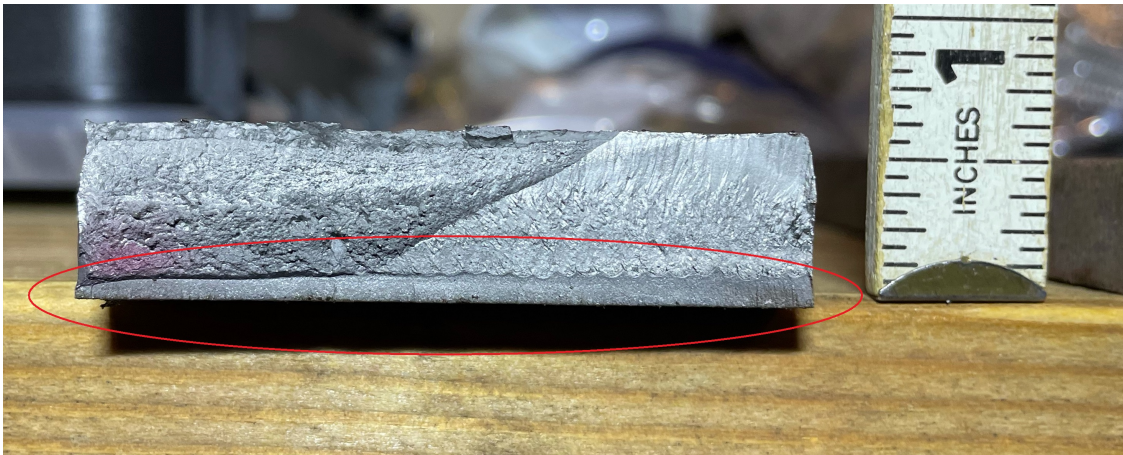


Figure 7.9: Test G dye penetrant fracture surface. Note the narrow band at the root. The lack of dye penetrant in the band suggests sufficient fusion and thus not a pre-existing crack.

After sharing these various results and photos with the committee, we believe this narrow band where the fracture surface texture appears different is not evidence of a pre-crack but rather the result of a poor weld that led to brazing at the root. With brazing, a leak-proof

seal is made between the filler metal and a base metal. Since brazing is still fusion, it would not cause the development of a pre-crack as well as prevent any dye penetrant from seeping through. However, brazing at the root is not as strong as a full fusion weld, making the root a local weakness compared to the sufficiently fused weld cap. Given that we were explicitly warned that the welds of all of our specimens were likely poor, it is reasonable to assume that instead of complete lack of fusion at the weld root the base metals instead were brazed together. This would explain why crack initiation occurred in the weld roots of the plate samples even if finite element models predicted stress concentration at the groove.

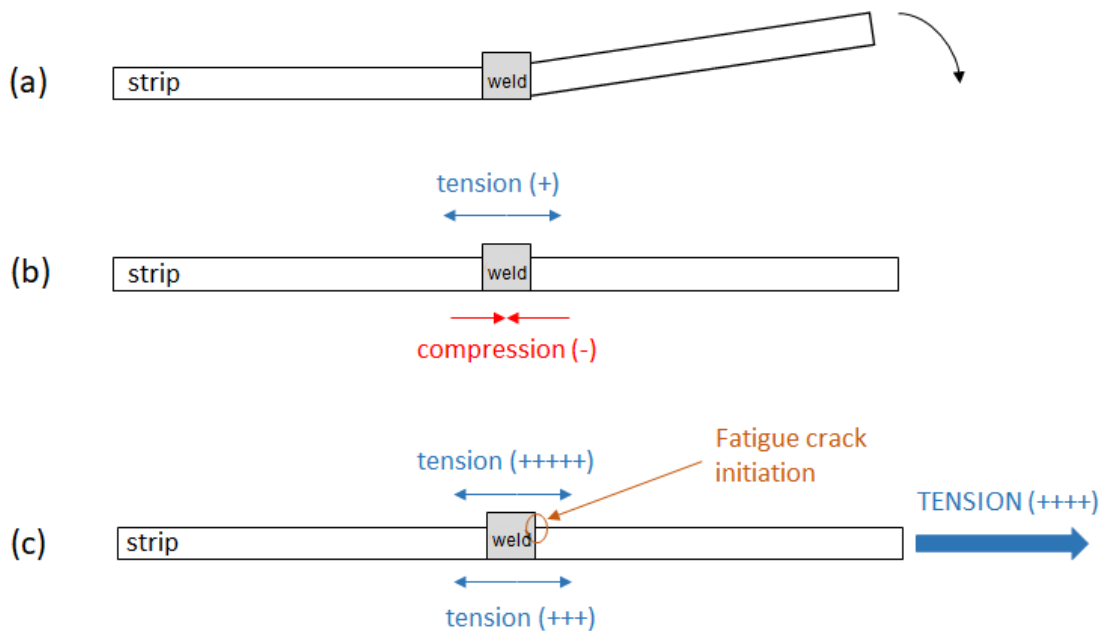


Figure 7.10: (a) Strip specimen being clamped in fatigue tester. (b) Strip specimen while clamped to straight, with tension at its weld cap and compression at weld root. (c) Strip specimen after loading with tension at the cap being significantly higher than at the root, leading to fatigue crack initiation.

If brazing was present in the roots of all of the welded specimens, it begs the question: why was groove cracking more common in the strip samples? During the forced clamping of the strip samples while in the fatigue tester, very large bending forces are introduced due to the forced clamping of the grips onto the strip specimen. These induced bending forces add compression at the bottom of the specimen (root) and tension at the top of the specimen (groove). This additional tension at the top of the strip specimen, in conjunction with the axial tensile loads of a fatigue test, cause the weld groove to have the highest stress

concentration during fatigue loading. This clamping-induced increase in stress concentration is significant enough to cause fatigue crack initiation at the groove instead of the brazed root, as is demonstrated in Figure 7.10.

On the contrary, the plate samples are flattened before testing and their bending-induced residual stresses are able to settle before axially loading. This means groove does not have any additional stress concentration effects during test clamping or fatigue loading. Even though the weld groove does have a slightly higher stress concentration due to the difference local geometry of the weld groove compared to the root, without the additional bending stresses from clamping the stresses at the groove are no longer greater enough to cause crack initiation compared to the weaker brazed area at the root (See Figure 7.11. This would explain why the strip samples were overwhelmingly groove cracking cases while the flattened plate samples were all root cracking. The cases of test group A strip specimens that had 5 of 6 still experience root cracking are likely the result of group A having a particularly weak brazen root.

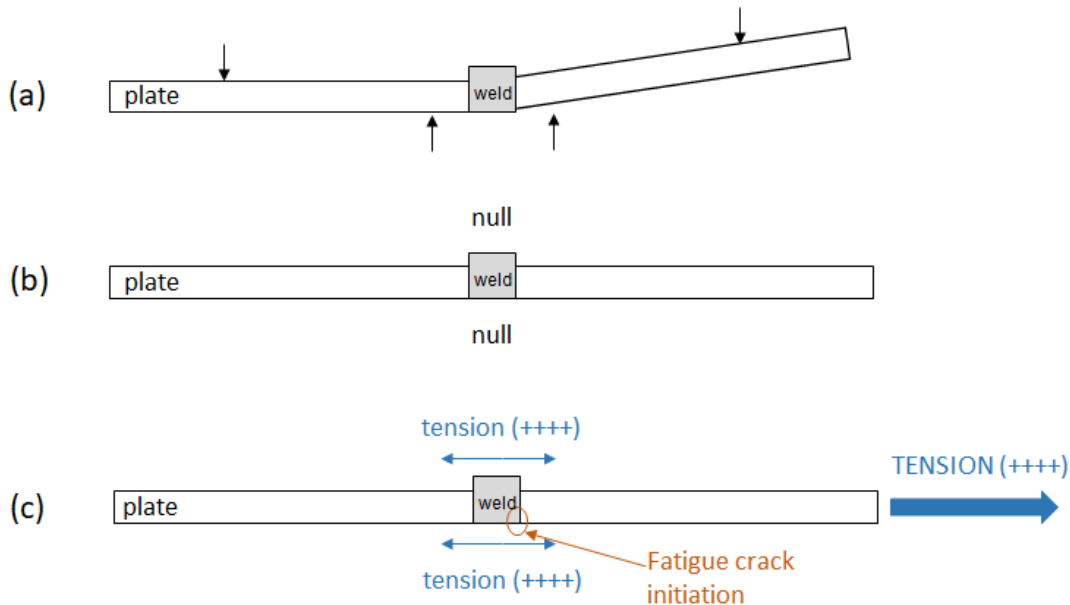


Figure 7.11: (a) Plate specimen experiences four-point bending beyond straight alignment. Four-point bending load is removed, allowing residual stresses to resolve and plate elastically deforms to straight. (b) Plate specimen after being clamped in fatigue tester, with no additional bending stresses due to plate being straight. (c) Plate specimen after loading, weld cap tension being equivalent to weld root tension. In this case, the relative weakness of the brazen root ("kissing bond") leads to fatigue crack initiation.

With the issue of root crack in the plate specimens appropriately addressed, all the remaining tests could be finished and analysis could begin on the fatigue test results.

CHAPTER 8

Analysis of Fatigue Test Plate Data

This chapter details the Master S-N curve results when including the 2.5” wide plate specimen fatigue test results.

8.1 Updated Master S-N Curve

Figure 8.1 on the next page is a plot of all of the Master S-N curve data from both the strip tests and the plate tests.

As can be seen in the figure, the plate tests have a nearly perfect fit to the Master S-N curve. Of the 19 total plate tests, 18 of them are within two standard deviations of the mean. In addition, the plate tests have significantly improved agreement with Master S-N mean curve line. From this data, it is likely that the low width-to-thickness ratio of the strip specimens was almost certainly the primary reason the test data had a shift away from the expected mean. These wider plate specimens, with a ratio of 5:1, are much better samples for fatigue testing than the strips.

There is one notable irregularity with the new plate data that needs to be addressed; the Test G and Test I data do not share a slope with the Master S-N curve. Visually, they both appear to have fatigue life values that are almost independent of the equivalent structural stress. This is primarily an issue with the relatively small range of structural stress values

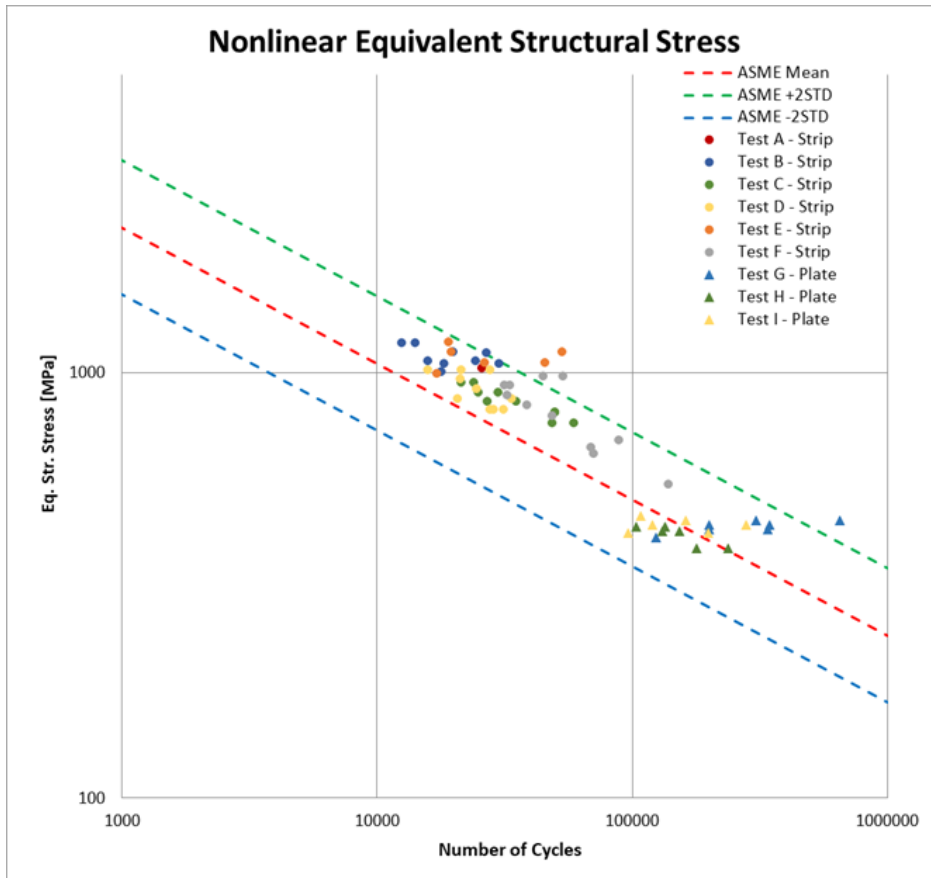


Figure 8.1: The updated Master S-N curve with both strip tests (circles) and plate tests (triangles). Test groups with the same color are of the same combination.

present in these tests. The highest and lowest equivalent structural stresses of Test G were only different by about 40 equivalent MPa. By comparison Test B, which was the strip test data of the same base-filler combination, had a range of nearly 200 equivalent MPa. This significantly narrows the vertical band of datapoints. Combined with the fact that these plate samples had a much larger range of cycles to failure (125k to 600k) than their strip counterparts (12k to 30k), the outcome of the relatively small amount of plate tests ends up with a dataset for Test G and Test I that looks to have a slope of zero. Had there been the opportunity to test dozens more plate combinations at a larger range of input loads, it is likely the Test G and Test I data would fill in more appropriately and mimic the slope of the Master S-N curve more closely.

Aside from that, the plate results are in agreement with the Master S-N curve method. From these results, it appears that there are no unique fatigue characteristics of welded armor materials, since they follow the Master S-N curve well with a more appropriate width-to-thickness ratio.

8.2 Trends and Cox PH Results

With the curve updated, we can look for any obvious signs of trends in the data. The two most critical variables of interest in the strip tests, angular deformation and mismatch ratio, were prioritized due to their importance during the strip test analysis.

8.2.1 Angular Deformation

As discussed in Chapter 7.2, the 2.5” wide plate specimens needed to be flattened in order to be fatigue tested per GVSC’s request. Since the plate specimens were all essentially perfectly straight after flattening, they no longer contained any angular deformation. These flattened specimens were all fatigue tested with no welding-induced distortion.

This in essence means that angular deformation was controlled for in these plate tests, and therefore could not be examined for trends. Since both the strip test results and statistical model outputs suggested that welding-induced distortions had a significant impact on fatigue characteristics already, controlling for their effect in the plate tests is acceptable. Mismatch ratio, however, was still present in the plate samples and could be examined.

8.2.2 Mismatch Ratio

Figure 8.2 shows the strip and plate test data when organized by their mismatch ratios. When only the strip tests were considered, excessively low mismatch ratios were observed to be among the lowest cycles to failure and highest equivalent structural stress. This relationship was shown with the Cox PH models to be a result of the high distortion of the low mismatch ratio pairs and not due to the yield strength of the base and filler metals

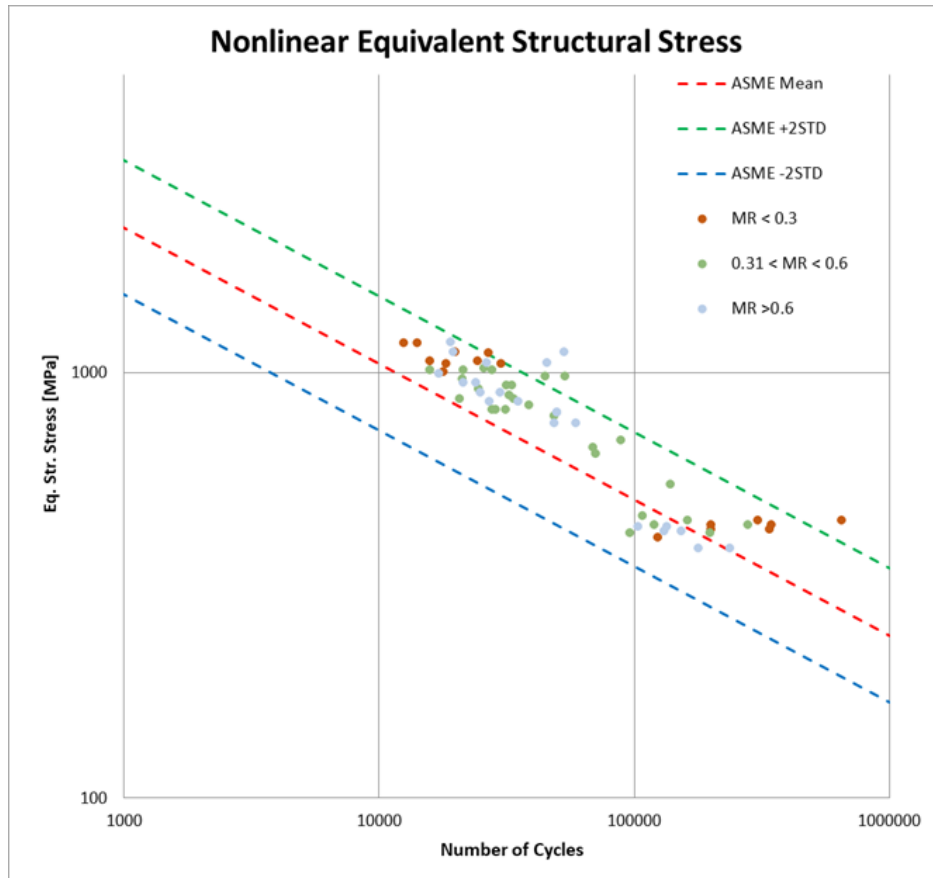


Figure 8.2: Comparison of mismatch ratios

themselves. When looking at the plate data, there does not appear to be any semblance of trend with mismatch ratio that can be seen in the plate tests. This helps lend more credence to the Cox model results for the strip data that suggested distortion drove fatigue life, not mismatch ratio.

A new Cox proportional hazards model was generated as well to test the predictor effect of mismatch ratio on just the plate test results (Table 8.1). When passing in mismatch ratio as the predictor and number of cycles to failure as the response, the model suggests a hazard ratio of 41.4577 with a p-value of 0.0223. This p-value would suggest that mismatch ratio has a massive effect on cycles to failure. However, the confidence interval of 0.4647 to 6.9847 contains the value of one, so we cannot conclude there is any relationship between mismatch ratio and cycles to failure. This is in agreement with the results from running the Cox model on the strip tests, where the Cox method also could not determine there was any

relationship. From both the plot and Cox PH model, mismatch ratio does not appear to have any effect or relationship to fatigue life of our welded specimens.

Table 8.1: Outputs from the 5th Cox PH Model, which took in mismatch ratio as the predictor

Variable	Model #: Time Data: Predictors: Output	5 Cycles Mismatch Mismatch
b	Coefficient Estimates	3.7247
logl	Loglikelihood	-36.728
hr	-Hazard ratio	41.4577
se	-Standard errors of coefficient estimates, b	1.63
z	-Z-statistics for b (b divided by standard error	2.2851
p	-p-values for b	0.0223
covb	-Estimated covariance matrix for b (diagonals)	2.6568
-2 σ	-95% confidence interval (- two std)	0.4647
+2 σ	-95% confidence interval (+ two std)	6.9847
-	- confidence interval includes 1?	Yes

8.2.3 Stainless vs. Non-stainless Weld Filament

Figure 8.3 on the next page splits the data into stainless steel filler wires vs. carbon steel filler wires. Again, we see the same outcome as with mismatch ratio, namely that what appeared to be a trend in the scatterplot of the strip tests instead does not appear in the plate tests. The angular deformation of the strip tests was the primary culprit behind most of the trends that we could observe in the first round of strip testing. Given the higher difficulty associated with welding stainless steels, it seems reasonable to assume our specimens with stainless steel fillers were likely welded more poorly than the specimens with carbon steel fillers. Poorer quality welds likely lead to more plate deformation, which would cause additional structural stresses during testing, thus lowering fatigue life. This also explains why the mismatch ratio appeared to have an effect on the strip samples, as combinations with stainless steel fillers would have the lowest mismatch ratio due to the comparatively low yield strength of stainless steels.

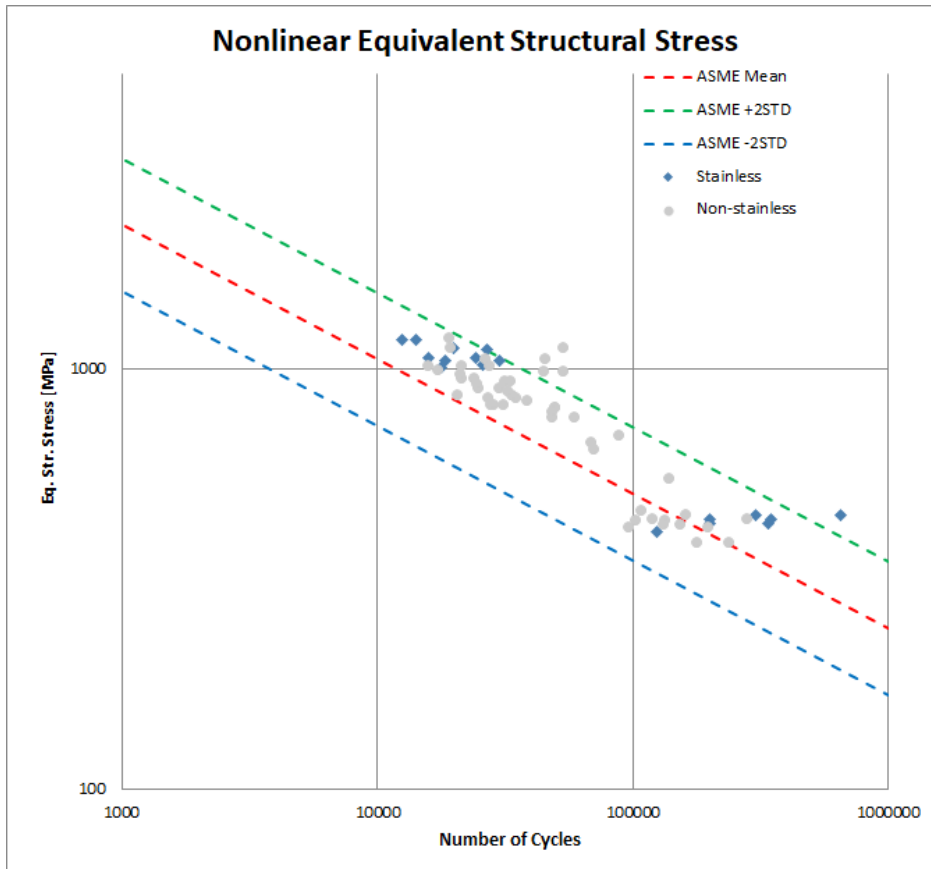


Figure 8.3: Updated comparison of stainless vs. non-stainless weld wires

Based on this plot and the mismatch ratio plot, it appears that angular deformation was such a strong driver of fatigue life that any other variable with close association to angular deformation also appeared to have a strong effect on fatigue life. When angular deformation was normalized in the plate tests by having them become flattened before testing, any relationship that mismatch ratio or stainless steel weld wire appeared to have on fatigue life essentially vanished. It seems likely that the presence of stainless steel weld wires lead to both lower mismatch ratios and higher angular deformations for the cutdown strip samples.

A 6th Cox PH model was created to better examine the effect a stainless steel filler wire could have on the number of cycles to failure for the plate test. Binary variables can be used as predictors in Cox models by assigning one of the variable states to be “1” and the other to be “0”. Here, the presence of a stainless steel filler metal was defined as equaling 1. Passing in stainless steel presence as the predictor and number of cycles to failure as the

Table 8.2: Cox PH Model #6 and #7, which both use the presence of stainless steel filler as a predictor.

Variable		Model #:	6	7
		Time Data:	Cycles	Cycles
		Predictors:	Stain	Stain
		Output	Stain	Stain
b	Coefficient Estimates		-1.7028	-1.5028
logl	Loglikelihood		-35.2103	-33.2104
hr	-Hazard ratio		0.1822	0.2225
se	-Standard errors of coefficient estimates, b		0.6659	0.6637
z	-Z-statistics for b (b divided by standard error		-2.557	-2.2642
p	-p-values for b		0.0106	0.0236
covb	-Estimated covariance matrix for b (diagonals)		0.4434	0.4405
-2σ	-95% confidence interval (- two std)		-3.0346	-2.8302
$+2\sigma$	-95% confidence interval (+ two std)		-0.371	-0.1754
-	- confidence interval includes 1?		No	No

response, the model suggests a hazard ratio of 0.1822 with a p-value of 0.0106. This would suggest that the presence of stainless steel as a filler metal has a negative effect on the fatigue life of a welded plate, with the presence of stainless steel reducing the risk of a specimen breaking per cycle by 81.78%. The confidence interval of -3.0346 to -0.371 does not contain 1, therefore from this model we are 95% confident that the presence of a stainless steel weld filler metal has a beneficial effect on the fatigue life of a welded plate. These results can be seen above in Table 8.2.

This is unexpected, as one would not anticipate this relationship existing. The presence of the single large outlier in the plate data could possibly be throwing the model off. To test this, a 7th Cox model was run on the plate data with stainless steel filament as the predictor and the outlier data point ignored. That model's results can also be seen in Table 8.2.

Interestingly, omitting the outlier did not significantly change the outputs of the Cox model. The p-value remained under 0.05 and the confidence interval still did not contain 1. The hazard ratio was slightly larger, implying the instantaneous risk of breaking is not as reduced as it was with the outlier, however it still implies a 77.5% reduction in break risk. There is nothing inherent about the presence of a stainless steel filament that would be expected to lead to such a significant reduction in break risk, so these results are puzzling.

In the plate tests, only test group G contained a stainless steel filler material, with groups H and I containing non-stainless carbon filler material. If group G was, for some reason, unrepresentative of the population of plate tests as a whole, it may explain why the presence of stainless steel was so drastic in the Cox PH model. For this reason, it was decided to run a Kruskal-Wallis test on the plate data.

Kruskal-Wallis Test

The Kruskal-Wallis test is a non-parametric method for testing if samples originate from the same distribution. [33] Typically, Kruskal-Wallis (K-W) tests are used for comparing two or more independent samples of similar or different sample sizes. For the plate research, the K-W test can be used to determine if the three test groups (G, H, and I) all come from the same distribution.

Test groups G, H, and I are not from the same distribution given they consist of different base metal and weld filler material combinations and were cutdown from different welded plates. However, the K-W test can be used as a metric to see if all three test groups could be expected to be from the same population. Then, that result can be compared to another K-W test consisting only of test groups H and I. If the K-W test determines that groups H and I could be from the same distribution but groups G, H, and I cannot be determined to be from the same distribution, that would give significant evidence to the theory that group G is unique from H and I. If group G is unique from H and I, this would help explain why the Cox PH model for stainless steel filament suggests such a significant hazard ratio with a small p-value.

Kruskal-Wallis tests need single-variable data, while the Master S-N curve plate data is multi-variate (cycles and equivalent structural stress). In order to run a K-W test with this plate data, we need to control for either cycles to failure or equivalent structural stress. Since cycles to failure is of interest, all the plate data needs to be standardized to a single stress value.

$$\Delta S_{range} = C \cdot N^{-h} \quad (8.1)$$

Equation 8.1, originally taken from the Master S-N curve formulation table in Figure 5.2, shows how the mean and standard deviation Master S-N curves are calculated. For each plate test, the N number of cycles to failure and ΔS_{range} are already known from the Master S-N curve scatterplot data, and the value of the curve slope h is constant at 0.3195 for ferritic and stainless steels. This means that the scaling constant C can be found for each test plate. Once determined, these C constants can be used in conjunction with a pre-selected stress value and $h = 0.3195$ to standardize the equivalent structural stresses of each plate test. In essence, this will allow for all the plate tests to be set at the same equivalent structural stress by “riding” along the slope of the Master S-N curve. Standardizing the equivalent structural stresses of all the plate tests will adjust their corresponding number of cycles to failure as well. These adjusted cycles to failure all lie on the same stress level, which turns the plate data into single-variable.

Single-variable plate data would be able to be used in a Kruskal-Wallis test. The average equivalent structural stress for the plate data test was 429MPa, so the plate tests were standardized to 425MPa using Equation 8.1. Figure 8.4 on the next page shows the original plate test data and the newly standardized plate test data on the Master S-N curve.

MATLAB has a built-in Kruskal-Wallis function that was used to run K-W tests on the standardized plate test data. This function takes in an array or matrix of numbers and returns the p-value for the null hypothesis that the input data comes from the same distribution. For the purpose of this research, the adjusted number of cycles to failure data from the stress-standardized plate data would be the input. Each index of the input array can be assigned a category in the MATLAB script, so each adjusted number of cycles to failure data point could be labeled according to which test group it originated from. This allows the MATLAB Kruskal-Wallis function to automatically organize the inputs into their

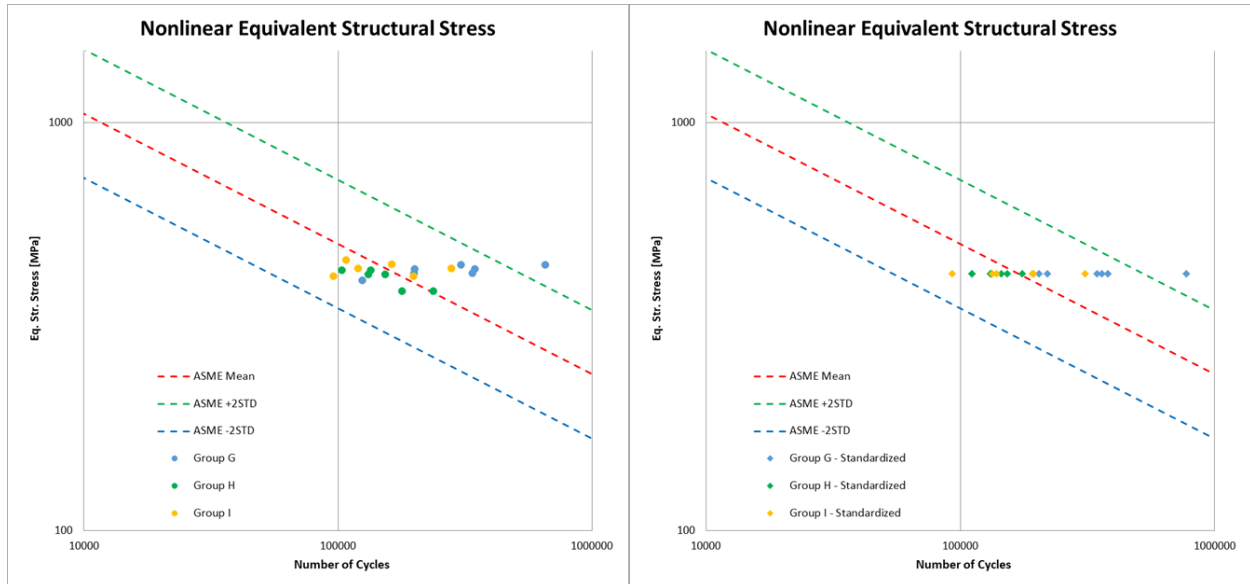


Figure 8.4: Left: The original Master S-N curve plate data. Right: The plate data if each test was shifted along the $-h = -0.3195$ slope to be standardized at an equivalent structural stress of 425MPa.

appropriate test groups to check if the test groups all come from the same population.

Two Kruskal-Wallis tests were run using this MATLAB script. The first took in the adjusted cycles to failure from test groups G, H and I. This was done to test the K-W null hypothesis that the three groups all came from the same distribution. The second K-W test run took in the adjusted cycles to failure from just test groups H and I. This was to compare the K-W results without including the test G data, which was believed to be throwing off the Cox PH models. Figure 8.5 on the following page gives the MATLAB boxplots and outputs of both Kruskal-Wallis tests.

The most important output from the figure are values labeled “ $Prob > Chi - sq.$ ” These outputs are the p-values of the two K-W tests, where again a p-value of 0.05 is considered statistically significant. The K-W tests generate p-values of 0.0397 for the three test groups and 0.3367 for just test groups H and I. The K-W test rejects the null hypothesis that all three test groups (G, H, and I) come from the same distribution at the 4% significance level while it cannot reject the null hypothesis that just groups H and I come from the same distribution. This suggests that the group G tests are inherently distinct from H and I groups. Any statistical analysis performed on the plate data that would separate the data

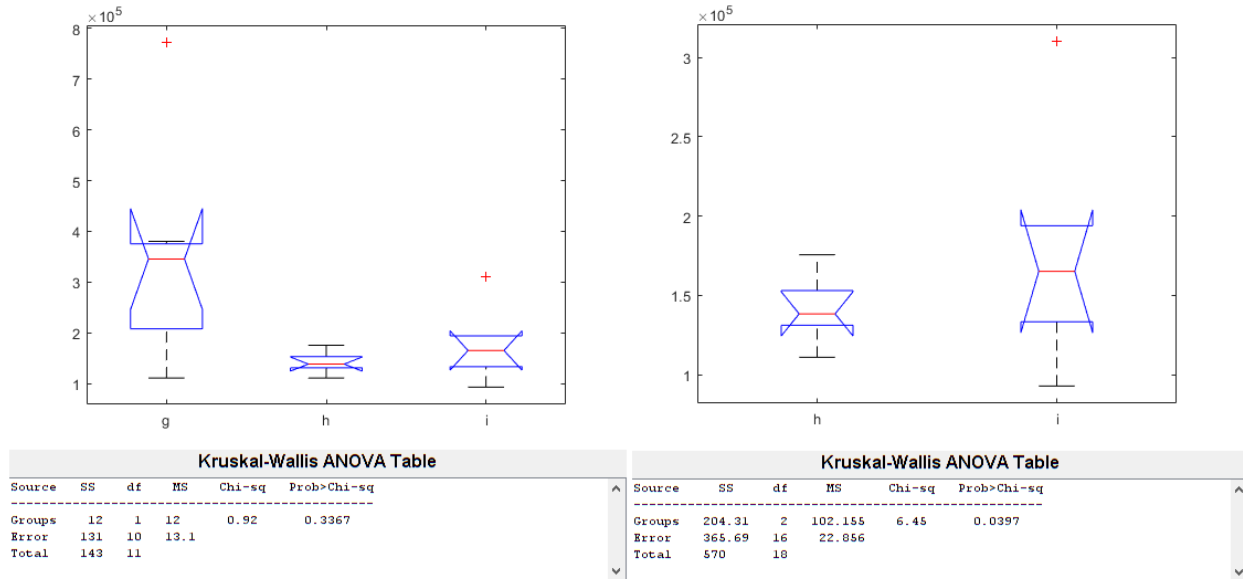


Figure 8.5: Left: Kruskal-Wallis boxplots and outputs for tests G, H, and I. Right: Kruskal-Wallis boxplots and outputs for just tests H and I.

into group G vs. group H and I would have very drastic results, as it appears that the group G data is wildly distinct on its own.

This helps explain why the stainless steel predictor Cox PH models had such an unexpected result. Since test group G was the only plate data that had a stainless steel filament, the Cox model ended up regressing the data as group G vs. groups H and I. With group G being so significantly different as show in the Kruskal-Wallis tests, the Cox model is possible picking up on distinctions in just the group G data itself as opposed to differences due to a stainless steel filament.

In order to examine the effect, if any, that the presence of stainless steel had on the fatigue life of the 2.5" wide plate specimens, more fatigue tests would need to be conducted with a stainless steel filament. There does not appear to be enough test data to run a binary Cox PH model due to the amount of range and variability in the current group G data. Any non-binary Cox models that do not distinctly divide the data into group G vs. group H and I are still valid for analysis purposes, however.

These Kruskal-Wallis tests beg the question: what about test group G has made it so

distinctly unique compared to test groups H and I? While the presence of stainless steel is the most obvious difference in the test groups, it is more likely that an unaccounted for effect or variable is present in the test group G data. One possibility is that the test group G specimens undergo materialistic nonlinear effects due to the relatively low yield strength of the ER316LSi stainless steel wire compared to the higher equivalent structural stresses they undergo during a fatigue cycle. ER316LSi weld wire has a rated yield strength of 58ksi. On some of the group G fatigue tests equivalent structural stress range can be as high as 65ksi in tension, easily exceeding the yield strength of the wire. Test group I, which has the next lowest filament yield strength, has a filler yield of 68.1ksi. This would suggest that group I likely never experiences any plastic strain as the equivalent structural stresses do not exceed the yield of the ER70S-6 wire. It is possible that the nonlinear effects associated with plastic strain in a tensile fatigue test of the group G specimens could be affecting the outcomes of the fatigue tests. The presence of these materialistic nonlinear effects, in addition to the relatively small sample size and narrow stress range of test group G, could have had a large enough impact on the tests to make group G more distinct when compared to groups H and I. This is why more fatigue test data with additional stainless steel filament specimens is necessary, as fatigue tests could be run at a wider range of lower tensile loads to better fill out the Master S-N curve and avoid any potential plastic effects.

8.2.4 Weld Filament Yield Strength

The primary relevant difference between the stainless steel filler metals and the carbon steel filler metals is their yield strengths, since they share the same elastic modulus. Since there is not enough plate data to analyze the effect of stainless steel filaments on fatigue life, examining the effect of filament yield strength is another way to see the effect of filament selection on fatigue life. This also acts as a method to investigate how the weld filament selection could have an impact on the fatigue parameters of welded armored structures. Figure 8.6 shows a plot of the test data organized by filler metal yield strength.

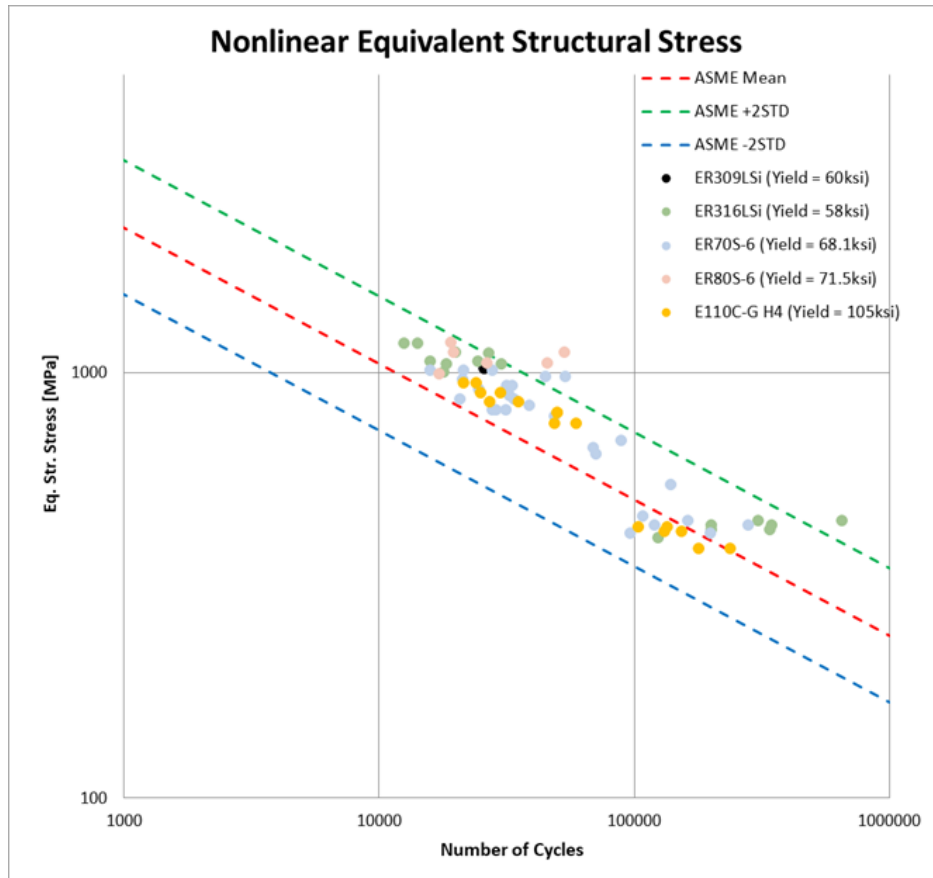


Figure 8.6: Comparison of filler materials

From the figure, there does not appear to be any visible or discernable pattern for the plate tests with regards to filler metal yield, which was also visibly the case with the stainless vs. non-stainless plot. Another Cox PH model (Table 8.3) was created with filler yield strength passed in as the predictor and cycles to failure as the response. This model generates a hazard ratio of 1.0254 with a p-value of 0.0453 and a confidence interval that contains 1. This would imply that for every 1ksi increase in the yield strength of the filler material, the Cox model anticipates a 2.54% increase in instantaneous risk of breaking. Cox model hazard ratios sufficiently close to 1.0 are usually interpreted as showing no relationship between predictor and response. In this case, a reduction effect of 2.54% is likely small enough to be considered inconsequential for purposes of statistical analysis, and therefore would suggest that the yield strength of the weld filament does not have any significant effect on the fatigue life of welded specimens.

Table 8.3: Outputs of Cox PH Model #8 with filler yield strength is passed in as the predictor.

Variable	Model #: Time Data: Predictors: Output	8 Cycles F. Yield F. Yield
b	Coefficient Estimates	0.251
logl	Loglikelihood	-37.419
hr	-Hazard ratio	1.0254
se	-Standard errors of coefficient estimates, b	0.0125
z	-Z-statistics for b (b divided by standard error)	2.0022
p	-p-values for b	0.0453
covb	-Estimated covariance matrix for b (diagonals)	0.001565
-2 σ	-95% confidence interval (- two std)	0.226
+2 σ	-95% confidence interval (+ two std)	0.276
-	- confidence interval includes 1?	No

This suggests a discrepancy between the stainless steel Cox models and the filler yield Cox model. The stainless Cox model, which essentially was a regression of just test group G vs. test groups H and I, would imply that increasing the yield strength of the filler metal will likely reduce the fatigue life of the welded plate slightly. This is likely due to the fact that the lowest yield test combination (Test group G) undergoes some plastic deformation during cyclic loading. Test group G, which is the only group with a stainless steel filament in the plate tests, has a filler yield strength of 58ksi. On some of the tests, the equivalent structural stress range can be as high as 65ksi while being solely in tension, easily exceeding the yield strength. The next lowest filler yield in the plate tests, test group I, has a filler yield of 68.1ksi and thus likely never experiences any plastic strain. Any nonlinear effects associated with plastic strain in a tensile fatigue test could likely explain the unexpected effect that a lower yield weld filament could lead to reduced risk of fatigue failure. The presence of materialistic nonlinear effects, in addition to the relatively small sample size and narrow stress range of test group G, likely have a notable impact on the Cox results for stainless steel filaments. While the survival models imply that a lower filament yield strength would slightly reduce hazard and improve fatigue life, this outcome would likely change if we were able to fatigue test significantly more welded plate samples. In turn, the

results of the stainless steel Cox models would also likely change with the addition of more tests and a wider stress range.

8.2.5 Base Material Yield Strength

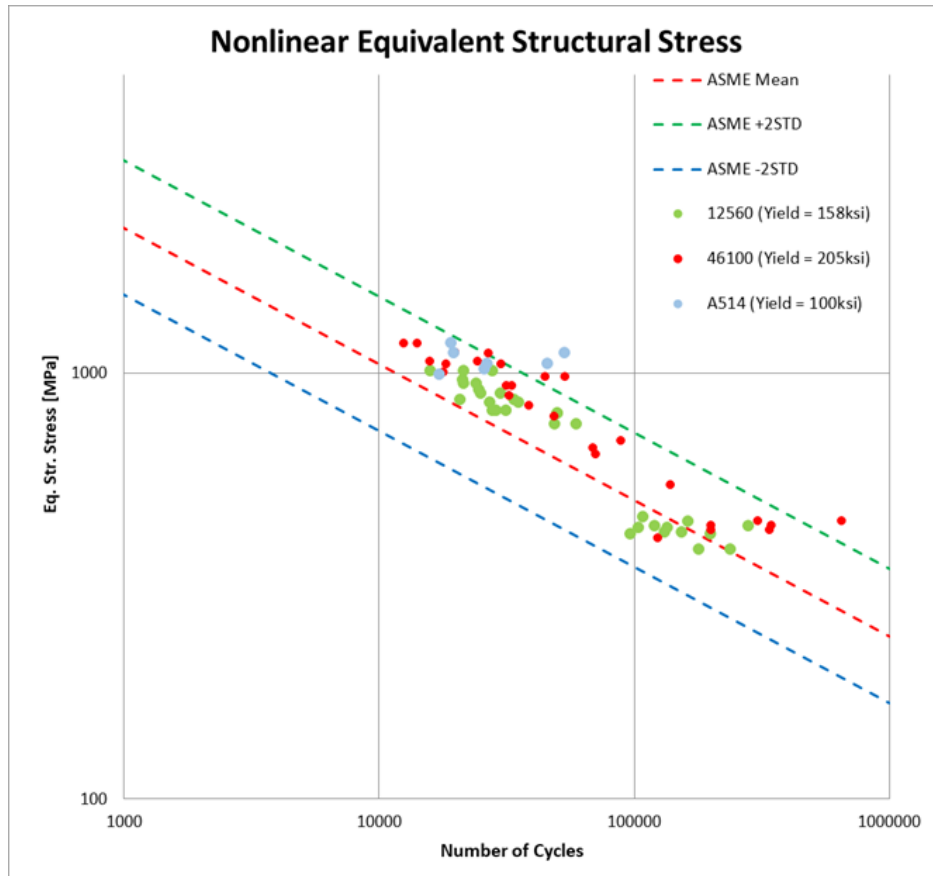


Figure 8.7: Updated comparison of base metals

After examining the effect of the filler metal yield strength, the effect of the base metal yield strength was next. Again, since the yield strengths are the only relevant difference in terms of fatigue between the base steels of interest, examining the yield strength effects acts as a method to examine base metal selection as a whole. Figure 8.7 shows the updated Master S-N curve data as categorized by base material. As a reminder, due to limited testing time and low interest, ASTM A514 combinations were not tested during the plate tests. In the plot, there doesn't appear to be any significant trend or differences between 12560 and 46100 steel for the base metal of the plate tests. 46100 does appear to have more variability in cycles to failure compared to 12560 but this is more likely a consequence of the smaller

sample size and presence of a large outlier. 12560 and 46100 have the same elastic modulus (30,457ksi) and Poisson ratio (0.25). In fact, the only major difference between the two is 12560 has a yield strength of 150,800psi and 46100 has a yield of 200,500psi. There does not appear to be any notable difference in fatigue properties between 12560 and 46100 when examining the plot.

A 9th Cox PH model (Table 8.4) with base material yield strength as the predictor was run with cycles to failure as the response. This model suggests a hazard ratio of 0.9644 with a p-value of 0.0106. This would suggest that for every 1ksi increase in base metal yield strength the model predicts a reduction in instantaneous hazard by 3.56%. With a confidence interval of -0.0646 to -0.0078, we are 95% confidence that increasing the yield strength of the base material will improve the fatigue life of the welded plate. This is the opposite result of the filler material yield model, which implied that increasing the yield strength of the filler would lower the fatigue life of the welded plate. We expect a stronger yield strength on the base material would improve fatigue characteristics, and given the irregularities discussed with the filler metal model we are confident in the base material Cox results.

Table 8.4: Outputs of Cox PH Model #9 with base material yield strength is passed in as the predictor.

Variable	Output	9 Cycles B. Yield B. Yield
b	Coefficient Estimates	-0.0362
logl	Loglikelihood	-35.2103
hr	-Hazard ratio	0.9644
se	-Standard errors of coefficient estimates, b	0.0142
z	-Z-statistics for b (b divided by standard error	-2.557
p	-p-values for b	0.0106
covb	-Estimated covariance matrix for b (diagonals)	0.000201
-2σ	-95% confidence interval (- two std)	-0.0646
+2σ	-95% confidence interval (+ two std)	-0.0078
-	- confidence interval includes 1?	No

CHAPTER 9

Observations and Conclusions

The most significant conclusion that can be drawn from this research regarding the fatigue of welded armor vehicle structures is that there does not appear to be anything novel or unique about the fatigue characteristics of welded armor steels when applied to the Master S-N curve. When controlling for the amount of distortion and ensuring an experimentally-acceptable width-to-thickness ratio, there is nothing about welded armor steels in particular that falls outside of the expected parameters of the Master S-N curve for ferritic and stainless steels. Even cases with distorted samples and low width to thickness ratios still proved to be overwhelmingly in agreement with the Master S-N curve despite their non-ideal geometries and distortions.

Most of the distinct trends and relationships that were observed from the results of the strip fatigue tests can be reasonably explained by their poor weld quality and were appropriately simulated using finite element models. These trends all but vanish when test specimens were of appropriate width-to-thickness to ensure the welding-induced residual stresses remained and were flattened to eliminate welding induced angular deformation. Disparate relationships between specimens and test variables cannot be proven to even exist when applying survivability models to the test data. Welded armor steels do not behave outside of the expectations of the Master S-N curve for ferritic and stainless steels. The

unexpected results in the statistical analysis of stainless steel filament and weld filler yield strength are likely the result of small sample sizes and limited testing range and not a consequence of filament selection.

While the coronavirus pandemic delayed this research, pivoting to remote-capable research topics helped to better flesh out the strengths of the nodal force mesh-insensitive method as well as lead to the novel application of survivability statistics to fatigue tests. These efforts can be valuable for future applications of the Master S-N curve.

A focus on proper welding procedures, proper welding technique, and consistent weld quality will have a much more significant impact on the expected fatigue life of a welded armor structure than the selection of the base armor metal and weld wire material.

CHAPTER 10

Future Work

Several additional points of interest are still open to study further with the conclusion of this research. The biggest opportunity for future study would be in continuing to test welded plate specimens for the purpose of deepening the dataset of stainless steel weld filaments as well as increasing the sample size. While future research will likely prove the suspicion that stainless steel weld filaments do not behave any differently in welded armor samples, an interested party may still wish to confirm this with additional testing. Typically, a sample size of at least 30 is considered sufficiently large according to the central limit theorem, so adding in additional plate tests of stainless steel filament would help better flesh out the plate data by getting the sample size closer to 30 as well.

Another avenue of further study would be the development of a residual stress estimate adjustment for use in fatigue cases with insufficient width-to-thickness ratios. An analytic or regression-based approach that would allow a research to roughly anticipate how much residual stresses they could expect to be missing with particularly low width-to-thickness fatigue samples. In this research, attempts were made at simulating welding induced residual stresses by use of a shrinkage-strain approach in finite element, but never came to fruition. Even then, a finite element estimate would only work to prove the losses of welding induced residual stresses; it could not be used to get any sort of meaningful estimate as to the mag-

nitude of losses. While there are a significant number of variables that could impact the magnitude of residual stresses in a welded plate, a metadata analysis looking at thousands of fatigue tests of varying width-to-thickness ratios would likely show the rough trend that width-to-thickness could have on residual stresses. Even though it could not be used conclusively, a rough residual stress adjustment developed from this metadata would be valuable for fatigue analysis.

Continued application of Cox proportional hazards models to fatigue tests is another area of future study that would be highly recommended. While survival statistics are already used in analyzing fatigue, the use of Cox models appears to be novel for purposes of structural fatigue. The ability to decouple and compare relative hazards of structural variables has significant potential for design, construction, and maintenance applications. What was originally a side project undertaken due to pandemic restrictions has led to the realization of a massive opportunity to broaden the field of fatigue analysis and may prove very useful in academia and industry.

Appendix

This Appendix contains resources that were unnecessary to include in the body of the text but may be of interest.

A.1 Cox Proportional Hazards Model - Script

The following attachment is a printout of the simple MATLAB scrip written for generating and running Cox PH models for use in data analysis of the strip and plate tests.

```

% Cox Plotter
% Daniel Sinnott
% Last update 2/16/22

% This code was written to pass in data from the master excel file of
% fatigue tests into the coxph MATLAB function to generate
% cox proportional hazards models and outputs.
% Sections of code were commented/uncommented as needed to run models

data = xlsread('Test Data v7 Plot Data and Cox PH Model
  Outputs.xlsx', 'D5:AT70');
close all

cycles = data(1:47,11);
eqss = data(1:47,23);
angle = data(1:47,29);
MR = data(1:47,6);
loadrange = data(1:47,9);

% [b4,logl4,H4,stats4] = coxphfit(angle,cycles);
% [b5,logl5,H5,stats5] = coxphfit(MR,cycles);
%
%
% hr4 = exp(b4);
% hr5 = exp(b5);

cycles_plate = data(48:end,11);
MR_plate = data(48:end,6);
stain_plate = data(48:end,24);
stain_plate2 = stain_plate(2:end);
cycles_plate2 = cycles_plate(2:end);
filler_plate = data(48:end,5);
base_plate = data(48:end,4);

[b5,logl5,H5,stats5] = coxphfit(MR_plate,cycles_plate);
hr5 = exp(b5);

set1 = [angle,MR];
[set1b,set1logl,set1H,set1stats] = coxphfit(set1,cycles);
set1hr = exp(set1b);

[b6,logl6,H6,stats6] = coxphfit(stain_plate,cycles_plate);
hr6 = exp(b6);

[b8,logl8,H8,stats8] = coxphfit(filler_plate,cycles_plate);
hr8 = exp(b8);

[b9,logl9,H9,stats9] = coxphfit(base_plate,cycles_plate);
hr9 = exp(b9);

```

```
%
% set2 = [MR,angle];
% [set2b,set2logl,set2H,set2stats] = coxphfit(set2,cycles);
% set2hr = exp(set2b);
%
% set3 = [loadrange,angle,MR];
% [set3b,set3logl,set3H,set3stats] = coxphfit(set3,cycles);
% set3hr = exp(set3b);
%
% set4 = [loadrange,stain,angle,MR];
% [set4b,set4logl,set4H,set4stats] = coxphfit(set4,cycles);
% set4hr = exp(set4b);

% % Normalized (or scaled) predictors for cox model UNUSED
%
% normalset1 = [angle_scale,MR_scale];
% [nor1b,nor1logl,nor1H,nor1stats] = coxphfit(normalset1,cycles);
% nor1hr = exp(nor1b);
%
% normalset2= [LR_scale,angle_scale,MR_scale];
% [nor2b,nor2logl,nor2H,nor2stats] = coxphfit(normalset2,cycles);
% nor2hr = exp(nor2b);
%
% normalset3= [LR_scale,stain,angle_scale,MR_scale];
% [nor3b,nor3logl,nor3H,nor3stats] = coxphfit(normalset3,cycles);
% nor3hr = exp(nor3b);
```

Published with MATLAB® R2019b

A.2 Cox Proportional Hazards Model - Function

The following attachment is a printout of the built-in MATLAB Cox PH function for making hazards models. This printout does not contain any inputs, it is only an example of the function code itself.

```

function [b,logL,H,stats] = coxphfit(X,y,varargin)
%COXPHFIT Cox proportional hazards regression.
% B=COXPHFIT(X,Y) fits Cox's proportional hazards regression model
to the
% data in the vector or 2-column matrix Y, using the columns of the
% matrix X as predictors. Y is typically a vector providing the
event
% time of right censored time-to-event data. X and Y must have the
same
% number of rows, and X should not contain a column of ones. The
result B
% is a vector of coefficient estimates. This model states that the
hazard
% rate for the distribution of Y can be written as  $h(t)*exp(X*B)$ 
where
%  $h(t)$  is a common baseline hazard function.
%
% For data with time-dependent covariates, Y is specified as a 2-
column
% matrix. Each individual appears in multiple rows, with one row for
each
% of the distinct values of the time-dependent variables. The
% corresponding row of Y provides the (start,stop] time interval.
This is
% the counting process form as described in reference [1]. For
example:
%
%           Age  Med           Time0 Time1           Censor = [0
%   X = [ 20 false           Y = [ 0     5           1
%         30 true            0    12           1
%         30 false]         12   20]           1]
%
% This represents two patients. The age 20 patient was not taking
% medication for the interval from week 0 to 5. The age 30 patient
was
% taking medication for the interval from week 0 to 12, but not for
the
% interval from week 12 to 20. The value of the 'Censoring'
parameter
% (see below) is 0 if the event (death) was observed at the end of
the
% interval, and 1 if it was not. In this example, Med is considered
to be
% a time dependent covariate while Age is not.
%
% [...] = COXPHFIT(X,Y,'PARAM1',VALUE1,'PARAM2',VALUE2,...)
specifies
% additional parameter name/value pairs chosen from the following:
%
%           Name           Value
%           'B0'           A vector containing initial values for the
estimated

```

```

%           coefficients B. Default is 0.01/SD where SD
represents
%           the standard deviation of each predictor in X.
%           'Baseline' The X values at which the baseline hazard is to
be
%           computed. Default is mean(X), so the hazard at X
is
%            $h(t)*\exp((X-\text{mean}(X))*B)$ . Enter 0 to compute the
%           baseline relative to 0, so the hazard at X is
%            $h(t)*\exp(X*B)$ .
%           'Censoring' A boolean array of the same size as Y that is 1
for
%           observations that are right-censored and 0 for
%           observations that are observed exactly. Default
is
%           all observations observed exactly.
%           'Frequency' An array of the same size as Y containing non-
negative
%           frequencies
%           for the corresponding observations, but may
%           contain any
%           non-integer values which represent observation
%           weights.
%           Default is 1 per row of X and Y.
%           'Options' A structure specifying control parameters for the
%           iterative algorithm used to estimate B. This
argument
%           can be created by a call to STATSET. For
parameter
%           names and default values, type
STATSET('coxphfit').
%           'Strata' An array of the same number of rows as Y
containing the
%           stratification
%           stratification
%           variables. The values of the
%           variables must be real numbers. Observations are
grouped
%           into strata based on the different combinations
%           of values
%           in the stratification variables. Each stratum
%           defines
%           a set of observations having a common baseline
%           hazard.
%           'Ties' A string specifying the method to handle tied
failure
%           times. The methods are equivalent if there are no
%           ties.
%           Two methods are available:
%           'breslow' Breslow's approximation to the
%           partial
%           likelihood. It is the default.
%           'efron' Efron's approximation to the partial
%           likelihood.

```

```

%
% [B,LOGL,H,STATS]=COXPHFIT(...) returns additional results. LOGL
% is the log likelihood. For unstratified model, H is a two-column
matrix
% containing y values in column 1 and the estimated baseline
cumulative
% hazard evaluated at those values in column 2. For stratified
model, H
% is a (2+K)-column matrix with the last K columns being the K
% stratification variables in the same order as in STRATA array.
STATS is
% a structure containing the following fields:
%   'beta'      coefficient estimates (same as B output)
%   'se'        standard errors of coefficient estimates
%   'z'         z statistics for B (B divided by standard
error)
%   'p'         p-values for B
%   'covb'      estimated covariance matrix for B
%   'csres'     Cox-Snell residuals
%   'devres'    deviance residuals
%   'martres'   martingale residuals
%   'schres'    Schoenfeld residuals
%   'sschres'   scaled Schoenfeld residuals
%   'scores'    score residuals
%   'sscores'   scaled score residuals
%
% For Cox-Snell, martingale and deviance residuals, the result is a
column
% vector with one row per observation. For (scaled) Schoenfeld and
(scaled)
% score residuals, the result is a matrix of the same size as X.
(scaled)
% Schoenfeld residuals of censored observations are defined to be
NaNs.
% Residuals obtained from models with time-dependent covariates have
the
% same number of rows as Y.
%
% Example:
%   % Generate Weibull data with A depending on predictor X
%   x = 4*rand(100,1); A = 50*exp(-0.5*x); B = 2;
%   y = wblrnd(A,B);
%
%   % Fit Cox model
%   [b,logL,H,st] = coxphfit(x,y);
%
%   % Show Cox estimate of baseline survivor and known Weibull
function
%   figure;
%   stairs(H(:,1),exp(-H(:,2)))
%   xx = linspace(0,100);
%   line(xx,1-wblcdf(xx,50*exp(-0.5*mean(x)),B),'color','r')
%   title(sprintf('Baseline survivor function for X=%g',mean(x)));
%

```

```

%       % Assess model adequacy by residual plots
%
load(fullfile(matlabroot,'examples','stats','readmissiontimes.mat'))
%       [b1,logL1,H1,st1] = coxphfit([Age Sex Weight
Smoker],ReadmissionTime,...
%                               'censoring','Censored','ties','efron');
%
%       % Draw a deviance residual plot
%       Deviance = st1.devres;
%       SmokerDev = Deviance(Smoker==1);
%       NonsmokerDev = Deviance(Smoker==0);
%       figure;
%       plot((1:length(SmokerDev)),SmokerDev,'ro',...
%            (1:length(NonsmokerDev)),NonsmokerDev,'b*')
%       % Add a horizontal reference line with intercept 0
%       hline = reffline([0,0]);
%       hline.Color = 'k';
%       legend('Smoker','Non-smoker','Location','Best')
%       xlabel('Observation number')
%       ylabel('Deviance residuals')
%
%       % Draw a martingale residual plot
%       Schres = st1.schres(:,4);
%       figure;
%       plot(ReadmissionTime(Smoker==1),Schres(Smoker==1),'ro',...
%            ReadmissionTime(Smoker==0),Schres(Smoker==0),'b*')
%       hline = reffline([0,0]);
%       hline.Color = 'k';
%       legend('Smoker','Non-smoker','Location','Best')
%       xlabel('Time')
%       ylabel('Schoenfeld residuals')
%
%       % Refit the model by stratifying a covariate
%       [b2,logL2,H2,st2] = coxphfit([Age Sex Weight],
ReadmissionTime,...
%
%       'censoring','Censored','ties','efron','strata',Smoker);
%
%       See also ECDF, STATSET, WBLFIT.
%
% References:
% [1] Therneau, Terry M., and Patricia M. Grambsch, Modeling
survival
%       data: extending the Cox model. Springer Science & Business
Media, 2000.

if nargin > 2
    [varargin{:}] = convertStringsToChars(varargin{:});
end

narginchk(2,inf);

```

```

% Check the required data arguments
if ndims(X)>2 || ~isreal(X)
    error(message('stats:coxphfit:BadX'));
end
if ~(isvector(y) || size(y,2)==2) || ~isreal(y)
    error(message('stats:coxphfit:BadY'));
end
if size(y,2)==2
    if any(y(:,1) >= y(:,2))
        error(message('stats:coxphfit:BadY2'));
    end
end

% Process the optional arguments
okargs = {'baseline' 'censoring' 'frequency' {'init' 'b0'}
         'strata' 'ties' 'options' };
defaults = {[[] [] [] [] []]
            'breslow' [[]]};
[baseX, cens, freq, init, strata, ties, options] = ...

internal.stats.parseArgs(okargs,defaults,varargin{:});

if ~isempty(cens) && (~isvector(cens) || ~all(ismember(cens,0:1)))
    error(message('stats:coxphfit:BadCensoring'));
end
if ~isempty(freq) && (~isvector(freq) || ~isreal(freq) || any(freq<0))
    error(message('stats:coxphfit:BadFrequency'));
end
if ~isempty(baseX) && ~(isnumeric(baseX) && (isscalar(baseX) || ...
        (isvector(baseX) &&
        length(baseX)==size(X,2))))
    error(message('stats:coxphfit:BadBaseline'));
elseif isscalar(baseX)
    baseX = repmat(baseX,1,size(X,2));
end
strataFlag = 0; % Default is no strata
if ~isempty(strata)
    strataFlag = 1;
    if ~isreal(strata)
        error(message('stats:coxphfit:BadStrata'));
    end
end
ties = lower(ties);
if isempty(ties)
    ties = 'breslow';
elseif ~ischar(ties)
    error(message('stats:coxphfit:BadTies'));
elseif ~ismember(ties,{'breslow', 'efron'})
    error(message('stats:coxphfit:BadTiesName',ties));
end

% Make sure the inputs agree in size, and remove NaNs
freq(freq==0) = NaN; % easiest way to deal with zero-frequency
observations

```

```

[badin,~,y,X,cens,freq,strata]=statremovenan(y,X,cens,freq,strata);
if badin>0
    whichbad = {'Y' 'X' ''censoring'' ''frequency'' ''strata''};
    error(message('stats:coxphfit:InputSizeMismatch',
    whichbad{ badin }));
end

% Default values of cens and frequency
[n,p] = size(X);
if isempty(cens)
    cens = false(n,1);
end
if isempty(freq)
    freq = ones(n,1);
end

% Data pre-processing before fitting
if ~strataFlag
    [X,sorty,cens,freq,atrisk,tied,lastloc,tiedygrps,idx] = ...

    dataProcessing(X,y,cens,freq,ties);
else
    ndeath = sum(~cens);
    nStrataVar = size(strata,2);

    % Find groups according to distinct combinations of values in
    strata
    [group,~,~,~,ngroups] = mgrp2idx(strata,n);
    groups = cell(1,ngroups);
    for gnum = 1:ngroups
        groups{gnum} = find(group==gnum);
    end

    % Pre-process data within each stratum
    grpdata = cell(ngroups,1); % Store preprocessed data in grpdata
    for j = 1:ngroups
        gX = X(groups{j},:);
        gy = y(groups{j},:);
        gcens = cens(groups{j},:);
        gfreq = freq(groups{j},:);
        gstrata = strata(groups{j},:);
        [gX,gsorty,gcens,gfreq,gatrisk,gtied,glastloc,gtiedgrps,gyidx]
    = ...

    dataProcessing(gX,gy,gcens,gfreq,ties);
        gX = Xcentering(gX,gfreq,baseX);
        % Save grouped data
        grpdata{j} =
        {gX,gfreq,gcens,gatrisk,gtied,gsorty,gtiedgrps,...
        glastloc,gstrata,gyidx};
    end
end

X = Xcentering(X,freq,baseX);

```

```

% Try to diagnose some potential problems
try
    if rank([ones(n,1), X]) < (p+1)
        if n>1 && any(all(diff(X,1)==0,1))
            warning(message('stats:coxphfit:DisallowedContantTerm'));
        else
            warning(message('stats:coxphfit:RankDeficient'));
        end
    end
end
catch ME
    if isequal(ME.identifier, 'MATLAB:svd:matrixWithNaNInf')
        warning(message('stats:coxphfit:XorFreqWithInf'));
    end
end

% Get starting values of coefficients b
sumf = max(1, sum(freq));
if isempty(init)
    stdX = sqrt((freq'*X.^2)/sumf);
    b0 = zeros(size(stdX),class(X));
    t = (stdX ~= 0);
    b0(t) = 0.01 ./ stdX(t);
elseif isvector(init) && numel(init)==p && isreal(p) && isnumeric(p)
    b0 = init(:);
else
    error(message('stats:coxphfit:BadInit', p));
end

% Perform the fit
unboundwng = false;
if p==0
    b = zeros(0,1,class(X));
else
    % The default options include turning statsfminbx's display off.
    This
    % function gives its own warning/error messages, and the caller
    can
    % turn display on to get the text output from statsfminbx if
    desired.
    options = statset(statset('coxphfit'),options);
    options = optimset(options);
    dflts = struct('DerivativeCheck','off', 'HessMult',[], ...
        'HessPattern',ones(p), 'PrecondBandWidth',Inf, ...
        'TypicalX',ones(p,1), 'MaxPCGIter',1, 'TolPCG',0.1);

    % Maximize the log-likelihood
    if ~strataFlag
        funfcn = {'fungradhess' 'coxphfit' @(b)negloglike(b) [] []};
    else
        funfcn = {'fungradhess' 'coxphfit' @(b)negloglikeStrata(b) []
[]};
    end
    lastb = [];
try

```

```

[b, ~, ~, err, output] = ...
    statsfminbx(funcfn, b0, [], [], options, dflts, 1);
if (err == 0)
    % Check for convergence failure
    if output.funcCount >= options.MaxFunEvals
        warning(message('stats:coxphfit:EvalLimit'));
    else
        warning(message('stats:coxphfit:IterLimit'));
    end
    unboundwng = true;
elseif (err < 0)
    error(message('stats:coxphfit:NoSolution'));
end

catch ME
    if
isequal(ME.identifier, 'stats:statsfminbx:BadFunctionOutput') || ...
isequal(ME.identifier, 'MATLAB:eig:matrixWithNaNInf')
        warning(message('stats:coxphfit:EvalWarning'));
        b = lastb;
        unboundwng = true;
    else
        m = message('stats:coxphfit:FitError');

throw(addCause(MException(m.Identifier, '%s', getString(m)), ME));
    end
end
end

% Compute log likelihood at the solution, incl. baseline hazard
if ~strataFlag
    [logL,~,ddl,H,mlflag,resid] =
LogL(X,b,freq,cens,atrisk,lastloc,tied,...
        sorty,ties,tiedygrps,idx);

    % Try to diagnose a likelihood with no local maximum
    if ~unboundwng && mlflag
        warning(message('stats:coxphfit:FitWarning'));
    end

    if nargout>=4
        % Compute standard errors, etc.
        [covb,se,z,pval] = statscov(b,ddl);
        stats.covb = covb;
        stats.beta = b;
        stats.se = se;
        stats.z = z;
        stats.p = pval;

        stats.csres = resid.csres;
        stats.devres = resid.devres;
        stats.martres = resid.martres;
        stats.schres = resid.schres;

```

```

        stats.sschres = sum(~cens)*stats.schres*covb +
    repmat(b',size(cens));
        stats.scores = resid.scores;
        stats.sscores = stats.scores*covb;
    end
else
    [logL,~,ddl,H,res] =
    LogLstrata(ngroups,grpdata,b,ties,p,nStrataVar,ndearth,groups);

    % Compute standard errors, etc.
    if nargin>=4
        [covb,se,z,pval] = statscov(b,ddl);
        stats.covb = covb;
        stats.beta = b;
        stats.se = se;
        stats.z = z;
        stats.p = pval;

        stats.csres = res.csres;
        stats.devres = res.devres;
        stats.martres = res.martres;
        stats.schres = res.schres;
        stats.sschres = sum(~cens)*stats.schres*covb +
    repmat(b',size(cens));
        stats.scores = res.scores;
        stats.sscores = stats.scores*covb;
    end
end

% -----
function [L,dl,ddl] = negloglike(b)
    % Compute negative log likelihood
    [L,dl,ddl] =
    LogL(X,b,freq,cens,atrisk,lastloc,tied,sorty,ties,tiedygrps,idx);
    L = -L;
    dl = -dl;
    ddl = -ddl;
    lastb = b;
end

function [L,dl,ddl] = negloglikeStrata(b)
    % Compute negative log likelihood for stratified model
    [L,dl,ddl] =
    LogLstrata(ngroups,grpdata,b,ties,p,nStrataVar,ndearth,groups);
    L = -L;
    dl = -dl;
    ddl = -ddl;
    lastb = b;
end

function [X,sorty,cens,freq,atrisk,tied,lastloc,tiedygrps,idx] =
    dataProcessing(X,y,cens,freq,ties)
    % Sort by increasing time

```

```

if size(y,2)==1
    [sorty,idx] = sort(y);
else
    [~,idx] = sort(y(:,2));
    sorty = y(idx,:);
end
X = X(idx,:);
cens = cens(idx);
freq = freq(idx);

% Determine the observations at risk at each time
if size(y,2)==1
    [~,atrisk] = ismember(sorty,flipud(sorty), 'legacy');
    atrisk = length(sorty) + 1 - atrisk;
    % Determine the last location of distinct values in sorty
    [~,lastloc] = ismember(sorty,sorty, 'legacy');
    tied = diff(sorty) == 0;
else
    atrisk = grp2idx(sorty(:,2));
    [~,lastloc] = ismember(atrisk, atrisk, 'legacy');
    tied = diff(sorty(:,2)) == 0;
end
tied = [false;tied] | [tied>false];

% Find observation indices of tied noncensored sorty values
if strcmp(ties,'breslow')
    tiedygrps = [];
else
    uy = unique(sorty(:,end));
    ngrp = length(uy);
    tiedygrps = cell(ngrp,1);
    for i = 1:ngrp
        tiedygrps{i} = find(sorty(:,end)==uy(i) & ~cens);
    end
end
end

function X = Xcentering(X,freq,baseX)
    % Recenter X to make it better conditioned; does not affect
    coefficients
    n = size(X,1);
    sumf = max(1, sum(freq));
    if ~isempty(X)
        if isempty(baseX)
            baseX = (freq'*X) / sumf;
        end
        X = X - repmat(baseX,n,1);
    end
end

function cums = timeDependentRiskset(sorty,Q,atrisk)
    %Compute quantities at risk for Cox model with time varying
    covariates.

```

```

    % sorty is the 2-column sorted matrix whose first and second
    columns represent
    % the starting and ending points of intervals in the counting
    process syntax.
    % Q is a matrix representing the quantity that need to be
    calculated for the
    % risk sets. atrisk is a column vector of the index indicating
    % observations at risk.

    uystop = unique(sorty(:,2));
    len = length(uystop);
    cums = zeros(len,size(Q,2));
    for k = 1:len
        cums(k,:) = sum( Q((uystop(k)>sorty(:,1) &
    (uystop(k)<=sorty(:,2))),:),1 );
    end
    cums = cums(atrisk,:);
end

function H = cumhazest(obsfreq, risksum, sorty)
    %Compute estimate of baseline cumulative hazard
    terms = obsfreq ./ risksum;
    cumbh = cumsum(terms);
    H = [sorty(:,end), cumbh];
    H = H(obsfreq>0,:);
    if ~isempty(H)
        H = [H(1,1), 0; H];
    end
end

function [covb,se,z,p] = statscov(b,ddl)
    % Compute cov, standard error, z score and p value

    covb = cast(-inv(ddl),class(b));
    varb = diag(covb);
    % In cases where we did not converge to a maximum, the 2nd
    derivative
    % matrix may not be negative definite. It's likely a warning was
    % displayed and that varb has -Inf values. We'll give infinite
    % variances for parameters affected by this.
    se = Inf(size(varb),class(b));
    se(varb>0) = sqrt(varb(varb>0));
    % se may be empty, we need a column vector
    se = se(:);
    z = b ./ se;
    p = 2*normcdf(-abs(z));
end

function [L,d1,ddl,H,res] =
    LogLstrata(ngroups,grpdata,b,ties,p,nStrataVar,nddeath,groupidx)
    % Compute log-likelihood, first derivative and second derivative
    of each stratum.
    L = 0;
    d1 = zeros(1,p);

```

```

    ddl = zeros(p,p);
    if nargout>=4
        % Used to store cumulative hazards of each stratum; the
baseline
        % hazards are along the sorted y within each stratum. For each
        % stratum, the baseline hazards starts from a zero.
        len = 0;
        H = zeros(ngroups+ndeath,2+nStrataVar);
    end

    for j = 1:ngroups
        gX = grpdata{j}{1};
        gfreq = grpdata{j}{2};
        gcens = grpdata{j}{3};
        gatrisk = grpdata{j}{4};
        gtied = grpdata{j}{5};
        gsorty = grpdata{j}{6};
        gtiedgrps = grpdata{j}{7};
        glastloc = grpdata{j}{8};
        gstrata = grpdata{j}{9};
        gyidx = grpdata{j}{10};
        [gL,gdl,gddl,gH,~,gresid] =
LogL(gX,b,gfreq,gcens,gatrisk,glastloc,...

gtied,gsorty,ties,gtiedgrps,gyidx);
        if nargout>=4
            glen = size(gH,1);
            H(len+1:len+glen,:) = [gH repmat(gstrata(1,:),glen,1)];
            len = len+glen;
        end
        if nargout>=5
            res.csres(groupidx{j},:) = gresid.csres;
            res.devres(groupidx{j},:) = gresid.devres;
            res.martres(groupidx{j},:) = gresid.martres;
            res.scores(groupidx{j},:) = gresid.scores;
            res.schres(groupidx{j},:) = gresid.schres;
        end
        L = L + gL;
        dl = dl + gdl;
        ddl = ddl + gddl;
    end
end

function
[L,dl,ddl,H,mlflag,res]=LogL(X,b,freq,cens,atrisk,lastloc,tied,sorty,ties,tiedygr
% Compute log likelihood L
obsfreq = freq .* ~cens;
Xb = X*b;
r = exp(Xb);
rfull = freq.*r;
if size(sorty,2)==1
    risksum = cumsum(rfull, 'reverse');
    risksum = risksum(atrisk);
else

```

```

        risksum = timeDependentRiskset(sorty,rfull,atrisk);
end

if strcmpi(ties,'breslow')
    L = obsfreq'*(Xb - log(risksum));

    % Compute first derivative dL/db
    [n,p] = size(X);
    Xr = X .* repmat(rfull,1,p);
    if size(sorty,2)==1
        Xrsum = cumsum(Xr, 'reverse');
        Xrsum = Xrsum(atrisk,:);
    else
        Xrsum = timeDependentRiskset(sorty,Xr,atrisk);
    end
    A = Xrsum ./ repmat(risksum,1,p);
    dl = obsfreq' * (X-A);
    if nargout>=5
        % Set the mlflag (monotone likelihood flag) to indicate if
the
        % likelihood appears to be monotone, not at an optimum.
This
        % can happen if, at each of the sorted failure times, the
        % specified linear combination of the X's is larger than
that
        % of all other observations at risk.
        if n>2
            mlflag = all(cens(1:end-1) | (diff(Xb)<0 &
~tied(1:end-1)));
        else
            mlflag = true;
        end
    end
end

% Compute second derivative d2L/db2
t1 = repmat(1:p,1,p);
t2 = sort(t1);
XXr = X(:,t1) .* X(:,t2) .* repmat(r.*freq,1,p^2);
if size(sorty,2)==1
    XXrsum = cumsum(XXr, 1, 'reverse');
    XXrsum = XXrsum(atrisk,:,:)./ repmat(risksum,[1,p^2]);
else
    XXrsum = timeDependentRiskset(sorty,XXr,atrisk)./
repmat(risksum,[1,p^2]);
end
ddl = reshape(-obsfreq'*XXrsum, [p,p]);
ddl = ddl + A'*(A.*repmat(obsfreq,1,p));

if nargout>=4
    % Compute estimate of baseline cumulative hazard
    H = cumhazest(obsfreq, risksum, sorty);
end
if nargout>=6

```

```

                                % Baseline hazards are defined at distinct failure times:
for                                % tied data set, they share the value of the last obs of
each                                % tied group; thus, to calculate residuals, set all obs of
each                                % tied group to have that value(the last one of each tied
group).
                                cumbh = cumsum(obsfreq ./ risksum);
                                cumbh = cumbh(lastloc);

                                % Cox-Snell residuals
                                csres = cumbh.*r;
                                res.csres(yidx,:) = csres;

                                % Martingale residuals
                                if size(sorty,2)==1
                                    martres = (~cens) - csres;
                                else
                                    tempres =
internal.stats.coxmresmex(~cens', sorty(:,1)', sorty(:,2)', freq', r', 0);
                                    martres = (~cens) - tempres';
                                end
                                res.martres(yidx,:) = martres;

                                % Deviance residuals
                                devres = sign(martres).*sqrt(-2*(martres +
(~cens).*log((~cens)-martres)));
                                % When martingale residual is zero, deviance residual is
defined as zero
                                devres(martres==0) = 0;
                                res.devres(yidx,:) = devres;

                                % Schoenfeld residuals
                                schres = (~cens) .* (X-A);
                                schrescopy = schres;
                                % Schoenfeld residuals are undefined at censored times,
set them to be NaNs
                                schres(cens==1,:) = NaN;
                                res.schres(yidx,:) = schres;

                                % Score residuals
                                if size(X,1)>1
                                    diffH = [cumbh(1);cumbh(2:end)-cumbh(1:end-1)];
                                else
                                    diffH = cumbh;
                                end
                                if size(sorty,2)==1
                                    res.scores(yidx,:) = schrescopy - X.*r.*cumbh +
r.*cumsum(A.*diffH);
                                else
                                    tempres = internal.stats.coxsresmex(~cens', X',
sorty(:,1)', sorty(:,2)', freq', r' ,0);
                                    res.scores(yidx,:) = schrescopy - tempres';

```

```

        end
    end
else
    % Efron's method
    [n,p] = size(X);
    fr = freq.*r;
    Xr = X .* repmat(fr,1,p);
    if size(sorty,2)==1
        Xrsum = cumsum(Xr, 'reverse');
        Xrsum = Xrsum(atrisk,:);
    else
        Xrsum = timeDependentRiskset(sorty,Xr,atrisk);
    end
    A = Xrsum ./ repmat(risksum,1,p);

    t1 = repmat(1:p,1,p);
    t2 = sort(t1);
    XXr = X(:,t1) .* X(:,t2) .* repmat(fr,1,p^2);
    if size(sorty,2)==1
        XXrsum = cumsum(XXr, 1, 'reverse');
        XXrsum = XXrsum(atrisk,:,:);
    else
        XXrsum = timeDependentRiskset(sorty,XXr,atrisk);
    end
    B = XXrsum ./ repmat(risksum,[1,p^2]);

    wtrisksum = risksum; % Weighted version of risksum
    wtfreq = freq; % Weighted version of freq

    % Average within tied groups
    for j = 1:length(tiedygrps)
        idxDeath = tiedygrps{j};
        len = numel(idxDeath);
        wtfreq(idxDeath(:)) = sum(freq(idxDeath(:)))./len;
        if len>1
            idxDeath = idxDeath(:);
            avgrisksum = risksum(idxDeath(2:end)) -
(1:len-1)' .* ...
                sum(fr(idxDeath(:)))./len;
            wtrisksum(idxDeath(2:end)) = avgrisksum;
            A(idxDeath(2:end),:) = ( Xrsum(idxDeath(2:end),:) - ...
                (1:len-1)' .* sum(Xr(idxDeath(:),:))./len ) ./
avgrisksum;
            B(idxDeath(2:end),:) = ( XXrsum(idxDeath(2:end),:)
- ...
                (1:len-1)' .* sum(XXr(idxDeath(:),:))./len ) ./
avgrisksum;
        end
    end

    % Compute log-likelihood, first derivative, and second
    derivative
    wtobsfreq = wtfreq.*(~cens);
    L = obsfreq'* Xb - wtobsfreq'*log(wtrisksum) ;

```

```

dl = obsfreq'*X - wtobsfreq'*A;
ddl = reshape(-wtobsfreq'*B, [p,p]) +
A'*(A.*repmat(wtobsfreq,1,p));

if nargout>=4
    % Compute estimate of baseline cumulative hazard
    H = cumhazest(obsfreq, risksum, sorty);
end

if nargout>=5
    % Set the mlflag (monotone likelihood flag) to indicate if
the
    % likelihood appears to be monotone, not at an optimum.
This
    % can happen if, at each of the sorted failure times, the
that
    % specified linear combination of the X's is larger than
    % of all other observations at risk.
    if n>2
        mlflag = all(cens(1:end-1) | (diff(Xb)<0 &
~tied(1:end-1)));
    else
        mlflag = true;
    end
end

if nargout>=6
    % Residuals of Efron's method
    % Cox-Snell residuals
    csterms = cumsum( obsfreq./risksum );
    csres = csterms(lastloc).*r;
    res.csres(yidx,:) = csres;

    % For martingale, Schoenfeld, and score residuals, reset
values
    % at tied times
    terms = wtobsfreq ./ wtrisksum;
    cumbh = cumsum(terms);
    cumbhmart = cumbh(lastloc);
    hazard = wtfreq./wtrisksum;
    cumAh = cumsum(terms.*A);
    cumAhsco = cumAh(lastloc,:);
    for j = 1:length(tiedygrps)
        idxDeath = tiedygrps{j};
        len = numel(idxDeath);
        if len>1
are
            % For martingale residuals: the baseline hazards
cumulative
            % averaged within each tied group, and the
one
            % baseline hazards have the same value as the last
            % of that group
            idxDeath = idxDeath(:);

```

```

        frac = (1:len-1)'./len;
        tiedbh = wtfreq(idxDeath(2:end)).*(1-frac)./
wtrisksum(idxDeath(2:end));
        tiedcumbh = cumsum([cumbh(idxDeath(1));tiedbh]);
        cumbhmart(idxDeath) =
        repmat(tiedcumbh(end),len,1);

        % For Schoenfeld residuals
        tiedA = ( Xrsum(idxDeath(2:end),:)-
frac.*sum(Xr(idxDeath,:)) )./...
        ( risksum(idxDeath(2:end)) -
        frac.*sum(fr(idxDeath(:))) );
        tiedcumA = cumsum([A(idxDeath(1),:);tiedA]);
        A(idxDeath,:) = repmat(tiedcumA(end,:),len,1)./
len;

        % For score residuals
        tiedcumAh = cumsum([cumAh(idxDeath(1),:);
        tiedA.*(1-
frac).*hazard(idxDeath(2:end))]);
        cumAhsco(idxDeath,:) =
        repmat(tiedcumAh(end,:),len,1);
        end
    end

    % Martingale residuals
    if size(sorty,2)==1
        resid = cumbhmart.*r;
        resid = (~cens) - resid;
    else
        resid =
internal.stats.coxmresmex(~cens',sorty(:,1)',sorty(:,2)',freq',r',1);
        resid = (~cens) - resid';
    end
    res.martres(yidx,:) = resid;

    % Deviance residuals
    devres = sign(resid).*sqrt(-2*(resid +
(~cens).*log((~cens)-resid)));
    devres(resid==0) = 0;
    res.devres(yidx,:) = devres;

    % Schoenfeld residuals
    schres = (~cens) .* (X-A);
    schrescopy = schres;
    schres(cens==1,:) = NaN;
    res.schres(yidx,:) = schres;

    % Score residuals
    if size(sorty,2)==1
        res.scores(yidx,:) = schrescopy - X.*r.*cumbhmart +
r.*cumAhsco;
    else

```

```
        tempres = internal.stats.coxsresmex(~cens', X',
sorty(:,1)', sorty(:,2)', freq', r', 1);
        res.scores(yidx,:) = schrescopy - tempres';
    end
end
end

    if nargout>1 && any(isnan(dl(:)))
        % If we ran in to problems in computing the derivatives and
got a
        % NaN result, this will cause problems in statsfminbx. Best
to set
        % the objective function to infinity, causing statsfminbx to
back
        % up.
        L = -Inf;
    end
end
```

*Error using coxphfit (line 159)
Not enough input arguments.*

*Copyright 2005-2018 The MathWorks, Inc.
Published with MATLAB® R2019b*

A.3 Kruskal-Wallis - Script

The following attachment is a printout of the simple MATLAB scrip written for generating and running Kruskal-Wallis tests for use in data analysis of the strip and plate tests.

```

% Kruskal Wallis Test
% Daniel Sinnott
% Last update 2/16/22

% This code was written to pass in data from the master excel file of
% fatigue tests into the kruskal wallis MATLAB function
% for the purpose of running KW tests on the G H I plate data

close all
kw_data = xlsread('Test Data v7 Plot Data and Cox PH Model Outputs
  1-25-22.xlsx', 'Kruskal Wallis', 'Q50:S68');

Gcycles = kw_data(1:7,1);
Gstress = kw_data(1:7,3);

Hcycles = kw_data(8:13,1);
Hstress = kw_data(8:13,3);

Icycles = kw_data(14:end,1);
Istress = kw_data(14:end,3);

cycles = [Gcycles;Hcycles;Icycles]';
group = {'g','g','g','g','g','g','g',...
         'h','h','h','h','h','h',...
         'i','i','i','i','i','i'};

p = kruskalwallis(cycles,group)

cyclesHI = [Hcycles;Icycles];
group2 = {'h','h','h','h','h','h',...
          'i','i','i','i','i','i'};
p2 = kruskalwallis(cyclesHI,group2)

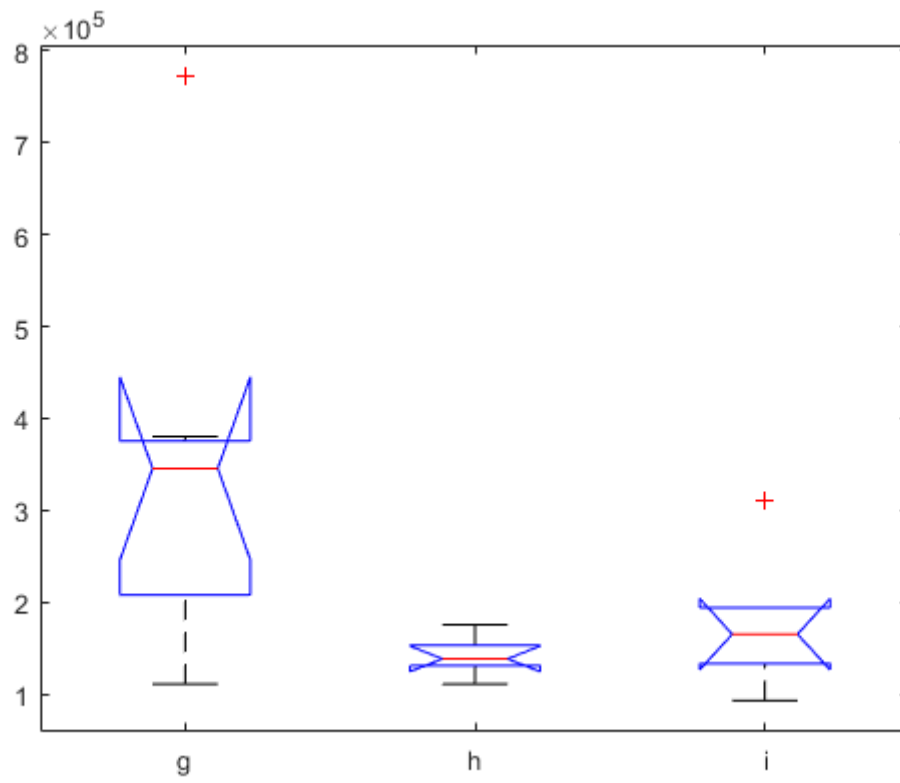
p =

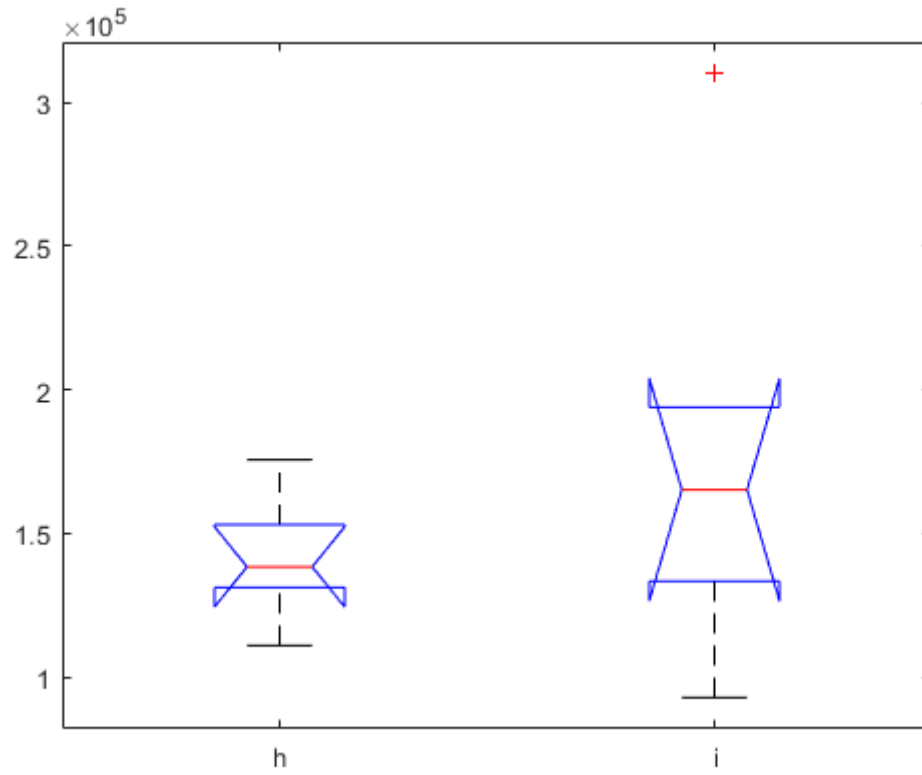
    0.0397

p2 =

    0.3367

```



Published with MATLAB® R2019b

A.4 Kruskal-Wallis - Function

This attachment is a printout of the built-in MATLAB Kruskal-Wallis function for running Kruskal-Wallis tests. This printout does not contain any inputs, it is only an example of the function code itself.

```

function [p,anovatab,stats] = kruskalwallis(varargin)
%KRUSKALWALLIS Nonparametric one-way analysis of variance (ANOVA).
% P = KRUSKALWALLIS(X,GROUP,DISPLAYOPT) performs a non-parametric
one-way
% ANOVA to test the null hypothesis that independent samples from
two or
% more groups come from distributions with equal medians, and
returns the
% p-value for that test. The data are assumed to come from
continuous
% distributions that are identical except possibly for location
shifts
% due to group effects, but are otherwise arbitrary.
%
% If X is a matrix, KRUSKALWALLIS treats each column as coming from
a
% separate group. This form of input is appropriate when each
sample
% has the same number of elements (balanced). GROUP can be a
string
% array, character array or a cell array of strings, with one row
per
% column of X, containing the group names. Enter an empty array
([])
% or omit this argument if you do not want to specify group names.
% If X is a vector, GROUP must be a categorical variable, vector,
% string array, or cell array of strings with one row for each
element
% of X. X values corresponding to the same value of GROUP are
placed
% in the same group.
%
% DISPLAYOPT can be 'on' (the default) to display figures containing
a
% boxplot and the Kruskal-Wallis version of a one-way ANOVA table,
or
% 'off' to omit these displays.
%
% [P,ANOVATAB] = KRUSKALWALLIS(...) returns the ANOVA table values
as the
% cell array ANOVATAB.
%
% [P,ANOVATAB,STATS] = KRUSKALWALLIS(...) returns an additional
structure
% of statistics useful for performing a multiple comparison of group
% medians with the MULTCOMPARE function.
%
% See also ANOVA1, BOXPLOT, FRIEDMAN, MULTCOMPARE, RANKSUM.
%
% References:
% [1] Hollander, M. and D. A. Wolfe. Nonparametric Statistical
% Methods. Wiley, 1973.

```

```
%      [2] Gibbons, J.D.  Nonparametric Statistical Inference,  
%      2nd ed.  M. Dekker, 1985.
```

```
if nargin > 0  
    [varargin{:}] = convertStringsToChars(varargin{:});  
end  
  
narginchk(1,3);  
[p,anovatab,stats] = anova('kruskalwallis', varargin{:});
```

```
Error using kruskalwallis (line 47)  
Not enough input arguments.
```

```
Copyright 1993-2006 The MathWorks, Inc.  
Published with MATLAB® R2019b
```

Bibliography

- [1] Hong Tae Kang, Pingsha Dong, and J.K.Hong
Fatigue analysis of spot welds using a mesh-insensitive structural stress approach
International Journal of Fatigue, Volume 29, Issue 8, August 2007, Pages 1546-1553.
<https://www.sciencedirect.com/science/article/pii/S0142112306003173>
- [2] P. Dong, J. K. Hong, Z. Cao
A Mesh-Insensitive Structural Stress Procedure for Fatigue Evaluation of Welded Structures
International Institute of Welding, IIW Doc. XIII-1902-01/XV-1089-01, July 2000.
- [3] P. Dong, M. Prager, and D. Osage
The Design of the Master S-N Curve in ASME Div 2 Rewrite and its Validations
<https://link.springer.com/content/pdf/10.1007/BF03266573.pdf>
- [4] P. Dong, J. K. Hong, D. Osage, M. Prager
Master S-N Curve Method for Fatigue Evaluation of Welded Components
WRC Bulletin, No. 474, August 2002
- [5] P. Dong *NAVARCH 514 - Fatigue of Structures*
Lecture 5: Fatigue Behaviors of Welded Joints University of Michigan, 2021. Reference images taken from course with permission.
- [6] P. Dong, J.K. Hong, D.A. Osage, D.J. Dewees, and M. Prager
The Master S-N Curve Method an Implementation for Fatigue Evaluation of Welded Components in the ASME BP&V Code, Section VIII, Division 2 and API 579-1/ASME FFS-1
Welding Research Council Bulletin Shaker Heights, OH. 2010
- [7] Aleksander Cabrilo and Miroslav Cvetinovic
Fatigue Crack Propagation and Charpy Impact Properties in Armor Steel Welds.
Materiale Plastice, December 2017.
- [8] Aleksandere Cabrilo and Katarina Geric
Weldability of High Hardness Steel.
<https://www.scientific.net/AMR.1138.79>, July 2016.
- [9] Tekin Ozdemir
Mechanical & Microstructural Analysis of Armor Steel Welded Joints.

https://www.researchgate.net/publication/338952241_Mechanical_Microstructural_Analysis_Of_Armor_Steel_Welded_Joints, January 2020.

- [10] G. Magudeeswaran, V. Balasubramaniang, and G. Madhusudhan Reddy
Effect of welding processes and consumables on fatigue crack growth behaviour of armour grade quenched and tempered steel joints
Defense Technology, January 2014.
- [11] Aleksander Cabrilo, A. Sedmak, Zijah Burzic, and Srdja Perkovic
Fracture Mechanics and Fatigue Crack Propagation in Armor Steel Welds.
Engineering Failure Analysis, August 2019.
- [12] DNV
Fatigue Strength Analysis of Offshore Steel Structures
DNV RP-C203, May 2000, Oslo, Norway
- [13] European Committee for Standardization
European Standard
CEN (2002), EN 13445:2003, Unfired Pressure Vessels
European Standard
- [14] Neimi, E.
Stress Determination for Fatigue Analysis of Welded Components
IIS/IIW 1221-93
Abington Publishing, Abington Cambridge, 1993.
- [15] Hobbacher, A., ed.
Fatigue Design of Welded Joints and Components
Recommendations of IIS/IIW Joint Working Group XIII-XV (XIII-1539-96,XV-845-96),
1996.
- [16] P. Selkvakumar and J.K. Hong
Robust Mesh Insensitive Structural Stress Method for Fatigue Analysis of Welded Structures
<https://www.sciencedirect.com/science/article/pii/S187770581300622X>
- [17] P. Dong
A Robust Structural Stress Method for Fatigue Analysis of Offshore/Marine Structure
J. Offshore Mech. Arct. Eng. Feb 2005, 127(1): 68-74 (7 pages). March 23, 2005
https://asmedigitalcollection.asme.org/offshoremechanics/article/127/1/68/463302/A-Robust-Structural-Stress-Method-for-Fatigue?casa_token=Fmbb7A2Cv3kAAAAA:YGZ6R43ryJS6SCrCYImyemZeijAhv3jOez9l1E6Gu0
- [18] Oguzhan Mulkoglu, Alireza Seyedi, Mehmet Ali Guler, and Bora Yildirim
Mesh Insensitive Structural Stress Method for Fatigue Analysis of Welded Joints Using the Finite Element Method
https://www.researchgate.net/publication/326742504_Mesh_Insensitive_Structural-Stress_Method_for_Fatigue_Analysis_of_Welded_Joints_Using_the_Finite_Element_Method

- [19] P. Dong
The Master S-N Curve Approach to Fatigue of Piping and Vessel Welds
 Weld World 48, Pages 28-36 (2004).
<https://doi.org/10.1007/BF03266411>
- [20] S. Xing and P. Dong
Fatigue of titanium weldments: SN testing and analysis for data transferability among different joint types
 Marine Structures 53, Pages 1-19 (2017).
https://www.researchgate.net/publication/312205072_Fatigue_of_titanium_weldments_S-N_testing_and_analysis_for_data_transferability_among_different_joint_types
- [21] Dassault Systems
Abaqus 6.11 Theory Manual
 Accessible at http://130.149.89.49:2080/v6.11/pdf_books/THEORY.pdf
- [22] David A. Osage, Pingsha Dong, Daniel Spring
Fatigue assessment of welded joints in API 579-1/ASME FFS-1 2016 - existing methods and new developments
 Procedia Engineering, Volume 213, 2018, Pages 497-538, ISSN 1877-7058,
<https://doi.org/10.1016/j.proeng.2018.02.049>.
 (<https://www.sciencedirect.com/science/article/pii/S1877705818302807>)
- [23] Shizhu Xing and Pingsha Dong
An analytical SCF solution method for joint misalignments and application in fatigue test data interpretation
<https://www.sciencedirect.com/science/article/abs/pii/S0951833916301435>
 Marine Structures, November 2016.
- [24] Wenqing Zhou, Pingsha Dong, Ingrid Lillemaeb, and Heikki Remesb.
Analytical treatment of distortion effects on fatigue behaviors of lightweight shipboard structures
<https://www.sciencedirect.com/science/article/abs/pii/S0142112319303901>
 International Journal of Fatigue
- [25] P. Dong and J. Zhang
Residual stresses in strength-mismatched welds and implications on fracture behavior
 Engineering Fracture Mechanics, 1 November 1999
<https://www.scinapse.io/papers/2058539537>
- [26] P. Dong and F.W. Brust
Welding Residual Stresses and Effects on Fracture in Pressure Vessel and Piping Components: A Millennium Review and Beyond
 Journal of Pressure Vessel Technology, 10 April 2000
<https://asmedigitalcollection.asme.org/pressurevesseltech/article/122/3/329/449668/Welding-Residual-Stresses-and-Effects-on-Fracture>

- [27] P. Dong
Residual stresses and distortions in welded structures: a perspective for engineering applications
 Science and Technology of Welding and Joining, 04 December 2013
<https://www.tandfonline.com/doi/abs/10.1179/174329305X29465>
- [28] T.R. Gurney
Fatigue of Welded Structures
 Cambridge University Press, Cambridge (1968)
https://www.google.com/books/edition/Fatigue_of_Welded_Structures/tD89AAAIAAJ?hl=en&gbpv=1&pg=PR11&printsec=frontcover
- [29] J. Zhang and P. Dong
Residual Stresses in Welded Moment Frames and Implications for Structural Performance
 ASCE Library
[https://ascelibrary.org/doi/abs/10.1061/\(ASCE\)0733-9445\(2000\)126:3\(306\)](https://ascelibrary.org/doi/abs/10.1061/(ASCE)0733-9445(2000)126:3(306))
- [30] Hang Liang, Ying Kan, Huaning Chen, Rui Zhan, Xiuguo Liu, and Dongpo Wang.
Effect of cutting process on the residual stress and fatigue life of the welded joint treated by ultrasonic impact treatment
 International Journal of Fatigue
<https://www.sciencedirect.com/science/article/pii/S0142112320305302>
- [31] J. Altenkirch, A. Steuwer, M.J. Peel, and P.J. Withers.
The extent of relaxation of weld residual stresses on cutting out cross-weld test pieces
 Cambridge University Press (March 2012)
<https://www.cambridge.org/core/journals/powder-diffraction/article/extent-of-relaxation-of-weld-residual-stresses-on-cutting-out-crossweld-testpieces/8F7A687D1C731256D07AE3C27CD940B0>
- [32] Stanford University.
Cox's Proportional Hazards Model
<https://web.stanford.edu/lutian/coursepdf/unitcox1.pdf>
- [33] National Institute of Standards and Technology
KRUSKAL WALLIS
<https://www.itl.nist.gov/div898/software/dataplot/refman1/auxillar/kruskwal.htm>